Investigation of mycolic acids and biosurfactants from wastewater-foaming-associated bacteria

Héctor de las Heras Prieto

A thesis submitted in partial fulfilment of the requirements of Sheffield Hallam University for the degree of Doctor of Philosophy

January 2026

Candidate Declaration

I hereby declare that:

1. I have not been enrolled for another award of the University, or other academic or professional organisation, whilst undertaking my research degree.

2. None of the material contained in the thesis has been used in any other submission for an academic award.

3. I certify that this thesis is my own work. The use of all published or other sources of material consulted have been properly and fully acknowledged.

   I used AI at AITS 2 (AI for Shaping) of the Artificial Intelligence Transparency Scale (AITS). I acknowledge the use of ChatGPT https://chatgpt.com/ to check the spelling and grammar in some sections of my thesis. No AI was used for generation, analysis, interpretation or discussion of results. AI was only utilised as spelling and grammar support, all thesis content is on my own.

4. The work undertaken towards the thesis has been conducted in accordance with the SHU Principles of Integrity in Research and the SHU Research Ethics Policy, and ethics approval has been granted for all research studies in the thesis, as shown in the table below.

Ethics review reference number	Title of research study	Approval date
ER42058973	Lipidomic Characterisation of Activated Sludge Wastewater Reactors	11/04/2022

5. The word count of the thesis is 31,162.

Name	*Héctor de las Heras Prieto*
Date	*January 2026*
Award	*PhD*
College	*Health, Wellbeing and Life Sciences*
Director(s) of Studies	*Dr Rachel Schwartz-Narbonne*

Acknowledgements

The last four years have been a real rollercoaster. But, like any good rollercoaster, I have enjoyed the ride a lot. Everything I have learned, and especially all the amazing people I have met along the way, is truly priceless.

First of all, I would like to say a huge thank you to my DoS, Dr Rachel Schwartz-Narbonne, for all the support over the years and for showing me the way when I felt completely lost. I know how stubborn I can be, especially when things are not progressing the way I was expecting, and I am well aware that it has not always been easy. But thank you for everything, Rachel. I truly hope I can give something back one day for all the help you have given me.

I would also like to thank my supervisors, Dr Laura Cole and Dr Sarah Forbes, for their support and patience throughout this journey. Without your guidance, this would not have been possible.

Within the academic world, I would also like to thank the technical team at Sheffield Hallam University, especially Mick, Jonathan and Jef (although you now wear a red lab coat...). I have lost count of how many times I asked for help or bothered you about absolutely everything. Thank you for everything you have taught me and for all the support you have given me over the years.

Travelling a little further north, to Glasgow, I would like to thank Dr Moyra McNaughtan and Dr Joanne Roberts for introducing me to the wonderful (although sometimes frustrating) world of research. Joanne, thank you from the bottom of my heart for all your support, for keeping in touch and for always being there. I genuinely believe that without you, this would not have been possible either.

In Scotland, I would also like to thank Dr Philippa Rickard, Dr Ryan Pereira and Dr Juliane Bischoff for hosting me during the fantastic (although very intense) placement at Heriot-Watt University. Thank you for your time, your support and for all the knowledge you shared with me, which made it possible to obtain such excellent polarographic data. I would also like to thank Emma literally saving my fingers, and Nair (soon to be Dr Nair) for all the good moments and for the constant support throughout my time in Edinburgh.

I had an incredible experience from this PhD, not only because of what I have learned, but also because of everything I have lived through: conferences, trips and memories that I will always cherish. Of course, I cannot forget to thank my colleagues at the BMRC. What an amazing bunch of people! Having you around made my time in Sheffield and my PhD experience so much better. From those who have been there since the very beginning to the new (and not so new) starters who joined along the way, thank you for all the support, kindness and great memories.

If there are two people who have seen me both laughing and getting angry, it is Veronika and Liv. Liv, thank goodness I met you during my first year. The happiness you have brought into my life during this time is indescribable. Sheila, Niall, Sarah and you were there when I needed it the most and made my first year (and not just the first) so much easier, because it really was not an easy one. Veronika, I never thought I would find someone so supportive in everything and who shared so many of my interests. I take away from you an incredible friend whom I know I will always be able to count on.

Andrea, you were my main source of support throughout the entire PhD, and especially during my first year. I cannot thank you enough for the constant support and kindness you gave me, and for being someone I truly admire. I hope to see you in Switzerland very soon.

Marta (formerly Mirecka), thank you for always being there, for giving me strength when I needed it most, and for that incredibly positive attitude that managed to lift everyone's spirits even during difficult times (or at least make everyone dance bachata with you).

Sheffield has also been a place where I met many wonderful people outside the university, who became my support system and almost my family. There are so many people who helped make Sheffield a place I will always carry in my heart that it would be impossible to name them all, even though they were a fundamental part of my life here. In particular, I would like to thank Maider, my Basque sister, who has always been there for me and has patiently listened to all my drama over the years; Moya, one of the most fascinating and crazy people I have met here, who has given me lots of love and left a lasting mark on me; Mori and Iago, with whom I formed a small family and learned how to support each other to make life in England better; Ane, for always caring about everyone, for giving so much of yourself to help and bring out the best in us; and Javi and Emma, what an incredible pair. Even though we only shared six months in Sheffield, from day one you gave me unconditional support and kindness that made my final year here so much better. And, of course, all my Greek and Mexican friends! Thank you for the great time we had together, you will definitely be missed.

From Spain, I want to thank all my friends for their constant support. In particular, Marcos and Jorge, thank you for believing in me, for supporting me every step of the way and for always being there despite the distance. Paula, for all the affection, unforgettable moments, hours of supportive conversations and endless laughter. And Nico, for being that person who always welcomed me in Glasgow and wherever you were; although we could only see each other once a year, it feels like no time has passed at all. Thank you for being chill and tropical, and for sharing that much-needed life mood with me during this stage.

Finally, my biggest thanks go to my family, and especially to Lola and Lucía. You both know better than anyone how hard this journey has been, not only professionally, but also mentally. Lola, thank you for always being there for me, for your unconditional love, for

believing in me even when I struggled to believe in myself, and for never letting me give up. Lucía, thank you for walking this path with me, for your patience, your strength and your constant support, especially during the moments when everything felt overwhelming. This PhD would not have been possible without you by my side, and I will always be grateful for that.

Now the same but in Spanish. Ahora o mismo pero en español:

Todos los que me conocéis, sabéis bien que nunca se me ha dado especialmente bien escribir este tipo de mensajes, pero voy a intentarlo, que para algo esto se acaba.

Los últimos cuatro años han sido una auténtica montaña rusa. Pero, como me suele pasar con las montañas rusas, me lo he pasado increíble y he disfrutado muchísimo del viaje. Todo lo que he aprendido y, sobre todo, toda la gente maravillosa que he conocido durante este tiempo no tiene comparación ni precio.

En primer lugar, quiero dar un enorme gracias a mi DoS, la Dra. Rachel Schwartz-Narbonne, por todo el apoyo durante estos años y por mostrarme el camino cuando me veía completamente perdido. Sé lo cabezón que puedo llegar a ser, especialmente cuando las cosas no avanzan, y soy consciente de que no siempre ha sido fácil, pero gracias por todo, Rachel. Ojalá algún día pueda devolverte aunque sea una parte de todo lo que me has ayudado. También quiero agradecer al resto de mis supervisoras, la Dra. Laura Cole y la Dra. Sarah Forbes, por su apoyo y paciencia durante este camino. Sin vuestra guía, nada de esto habría sido posible.

En el ámbito académico, también quiero dar las gracias al equipo técnico de Sheffield Hallam University, especialmente a Mick, Jonathan y Jef (aunque ahora vayas con bata roja...). He perdido la cuenta de cuántas veces os he pedido ayuda y de cuántas veces os he dado la chapa por absolutamente todo. Gracias por vuestra paciencia infinita, por todo lo que me habéis enseñado durante estos años.

Yéndome un poco más lejos, a Glasgow para ser exactos, quiero agradecer a la Dra. Moyra McNaughtan y a la Dra. Joanne Roberts por introducirme en el maravilloso (aunque a veces desesperante) mundo de la investigación. Joanne, gracias de corazón por todo el apoyo, por mantener el contacto y por estar siempre ahí. Creo sinceramente que sin ti esto tampoco habría sido posible.

En Escocia también me gustaría agradecer a la Dra. Philippa Rickard, al Dr. Ryan Pereira y a la Dra. Juliane Bischoff por acogerme durante la fantástica (aunque también muy intensa) estancia en Heriot-Watt University. Gracias por vuestro tiempo, vuestra ayuda y por todo el conocimiento que compartisteis conmigo para conseguir esos increíbles datos polarográficos. Gracias también a Emma por literalmente salvarme los dedos, y a

Nair (pronto Dra. Nair!) por todos los buenos momentos y por el apoyo constante durante mi estancia en Edimburgo.

Del PhD me llevo muchísimo más que conocimientos: conferencias, viajes, historias y momentos que recordaré siempre. Y, por supuesto, no puedo olvidarme de mis compañeros del BMRC. ¡Qué buena gente! Menos mal que os he tenido, porque habéis hecho mi estancia en Sheffield y mi experiencia doctoral infinitamente mejor. Desde los que habéis estado desde el principio, tragándoos todo el proceso conmigo, hasta los nuevos (y no tan nuevos) que os habéis ido sumando por el camino: gracias por el apoyo, el cariño y los recuerdos que me llevo de cada uno de vosotros.

Si hay dos personas que me han visto en absolutamente todos mis estados posibles, esas sois Veronika y Liv. Liv, menos mal que te conocí en mi primer año. Lo feliz que me has hecho durante este tiempo es indescriptible. Sheila, Niall, Sarah y tú estuvisteis ahí cuando más falta hacía y conseguisteis que mi primer año (y alguno más) fuera mucho más llevadero, porque no fue nada fácil. Veronika, nunca pensé que encontraría a alguien que me apoyara tanto en todo y con quien compartiría tantos gustos. Me llevo de ti a una persona increíble con la que sé que siempre podré contar.

Andrea, fuiste mi mayor apoyo durante todo el doctorado y, sobre todo, durante mi primer año. No tengo palabras para agradecerte todo el apoyo y el cariño que me diste, y por ser una persona a la que admiro muchísimo. Ojalá nos veamos pronto en Suiza.

Marta (en español siempre serás Mirecka), gracias por estar siempre ahí, por darme fuerzas cuando más lo necesitaba y por esa actitud tan positiva que incluso en los momentos difíciles conseguía animarnos a todos.

Sheffield también ha sido un lugar de encuentro con muchísima gente maravillosa fuera de la universidad, que acabó convirtiéndose en mi apoyo y casi en mi familia. Son tantas las personas que han hecho de Sheffield un lugar que llevaré siempre en el corazón que sería imposible nombrarlas a todas, aunque hayan sido una parte fundamental de mi vida aquí. Especialmente, Maider, mi hermana vasca, que ha estado ahí siempre, que me ha visto crecer y que se ha comido todas mis turras sin quejarse (o al menos no mucho); Moya, una de las personas más alocadas e interesantes que he conocido aquí y que me ha dado tanto cariño que ha acabado marcándome muchísimo; Mori e Iago, con quienes formé una pequeña familia y con quienes aprendí que apoyarse de verdad hace que la vida en Inglaterra sea mucho más llevadera; Ane, por cuidar siempre de todos, por darlo todo sin pedir nada a cambio y por hacernos mejores personas; Javi y Emma, vaya txavales más increíbles. Aunque solo compartimos seis meses de Chefil, desde el minuto cero me disteis un apoyo y un cariño incondicional que hicieron que mi último año aquí fuera mucho más fácil; y, por supuesto, ¡Todos mis amigos griegos y mexicanos! Qué bien lo pasamos juntos, y qué falta vais a hacer siempre.

Desde España, gracias a todos mis amigos por estar siempre ahí, incluso en la distancia. En especial a Marcos y Jorge, gracias por hacerme creer en mí, por apoyarme en cada pasito y por no soltarme nunca. Paula, por todo el cariño, los momentazos, las charlas eternas para arreglar el mundo y las risas infinitas. Y a Nico, por siempre recibirme en Glasgow o allá donde estuvieras, por ser esa persona a la que ves una vez al año pero que te transmite tanto que parece que nunca os habéis separado y por ser tranquilo y tropical y por recordarme que la vida también va de bajar revoluciones.

Finalmente, el agradecimiento más grande va para mi familia, tanto a los que están como a los que ya no y, en especial, para Lola y Lucía. Vosotras sabéis mejor que nadie lo duro que ha sido este camino, no solo a nivel profesional, sino también a nivel mental. Lola, gracias por estar siempre ahí, por tu amor incondicional, por creer en mí incluso cuando yo no era capaz de hacerlo, y por no dejarme rendirme nunca. Lucía, gracias por caminar este camino conmigo, por tu paciencia, tu fortaleza y tu apoyo constante, sobre todo en los momentos en los que todo se hacía cuesta arriba. No podría haber completado este proyecto sin vosotras a mi lado, y estaré siempre agradecido por ello.

Statement on Data Availability and Loss

During the course of this doctoral research, a substantial portion of the raw data was stored on an external hard drive that subsequently suffered a critical failure. As a result, part of the original data became permanently inaccessible despite reasonable recovery attempts.

At the time of the data loss, a significant portion of the thesis had already been written, and the analyses and results presented in this document are based on the data that were available and processed prior to the failure. Consequently, the loss of data has only partially affected the final content of the thesis. However, the unavailability of the complete original dataset may limit the possibility of re-analysis or substantial modification of certain parts of the work.

Héctor de las Heras Prieto as author affirms that the results, interpretations, and conclusions presented in this thesis accurately reflect the research conducted and the data accessible at the time of writing.

Abstract

Foaming in activated sludge wastewater treatment plants represents a persistent operational challenge that can compromise treatment performance and increase operational costs. Activated sludge foaming can cause the release of inadequately treated wastewater to receiving waters systems, having detrimental consequences for ecosystems and living organisms, and posing risks to environmental and public health. This thesis aimed to investigate lipidomic profiles, biosurfactant production, and microbial community dynamics in activated sludge in order to improve understanding of the biochemical and microbial processes associated with foaming events.

Initially, robust experimental and analytical methodologies were developed to enable lipidomic investigation of foaming-associated bacteria, such as *Gordonia amarae*. Reproducible growth conditions for *Gordonia amarae* were established in media that supported foaming formation. In parallel, a sensitive and reliable liquid chromatography–mass spectrometry (LC–MS) method was developed for mycolic acid analysis, and cyclic ion mobility spectrometry (cIMS) parameters were optimised to achieve high-resolution separation of lipid isomers.

Application of cIMS revealed substantial isomeric complexity within mycolic acids from both *Gordonia amarae* and other mycobacteria species (*Mycobacterium tuberculosis*), with multiple conformations detected within single mass spectral peaks. Species-specific patterns of isomer separation and fragmentation were observed, highlighting the value of isomer-resolved lipid analysis for improved structural characterisation.

Biosurfactant production by *Gordonia amarae* was shown to be strongly induced under foaming-related conditions, particularly in the presence of hydrophobic carbon sources, while being negligible in nutrient-rich media. Lipidomic analyses revealed reproducible shifts in mycolic acid composition under these conditions, including increased unsaturation and changes in oxidation state, indicating adaptive lipid remodelling in foaming conditions.

Finally, investigation of wastewater mixed liquor suspended solids using 16S rRNA gene sequencing demonstrated that both foaming-related conditions and the presence of *Gordonia amarae* significantly influence microbial community structure and foaming potential. Distinct microbial interactions were observed, underscoring the importance of community-level processes in foaming behaviour.

Overall, this thesis demonstrates that foaming in activated sludge systems arises from the combined effects of lipid adaptations, biosurfactant production, and dynamic microbial interactions. The integrated analytical framework developed here provides a foundation for identifying lipid- and community-based biomarkers to improve prediction and management of foaming events in wastewater treatment plants.

Contents

Abbreviations

ΔIc	capacity current
AC	alternating current
AS	activated sludge
AU	absorbance units
bp	base pairs
CCS	collision cross section
CDFF	constant depth film fermenters
cIMS	cyclic ion mobility spectrometry
DC	direct constant voltage
DCM	dichloromethane
DMS	differential mobility spectrometry
DTIMS	drift tube ion mobility spectrometry
E	applied potential
ES	electrospray
ESI-MS	electrospray ionisation mass spectrometry
FAIMS	field asymmetric waveform ion mobility spectrometry
FWHM	full width half maxima
GC-MS	gas chromatography–mass spectrometry
HPLC	high performance liquid chromatography
IM	ion mobility
IMS	ion mobility spectrometry
IR	infrared
LC	liquid chromatography
LC-MS	liquid chromatography–mass spectrometry
MA	mycolic acids
MLSS	mixed liquor suspended solids
MS	mass spectrometry
OTUs	operational taxonomic units
PAO	polyphosphate-accumulating organisms
PCR	polymerase chain reaction
PCR-DGGE	polymerase chain reaction denaturing gradient gel electrophoresis
PHAs	polyhydroxyalkanoates
pzc	point of zero charge
Q-ToF	quadrupole time-of-flight
R	resolving power
RF	radio frequency
SACs	surface-active compounds
SAS	surface-active substances
SMDE	static mercury drop electrode
TIMS	trapped ion mobility spectrometry
ToF	time of flight
TSS	total suspended solids

TW	travelling waves
TWIMS	traveling wave ion mobility spectrometry
UPLC	ultraperformance liquid chromatography
V	volts
VSS	volatile suspended solids
WWTP	wastewater treatment plant

List of figures

List of tables

List of equations

Chapter 1: Thesis introduction

1.1. Waste water treatment plant overview

The release of inadequately treated wastewater into the environment represents one of the most significant and persistent sources of anthropogenic pollution, adversely affecting aquatic ecosystems worldwide and posing serious risks to public health. Accidental discharges of partially treated effluent can introduce hazardous substances, including reactive nitrogen species and phosphorus, into rivers and other aquatic systems. Such contaminant inputs contribute to environmental contamination and eutrophication (1), and may result in detrimental effects on both human health and ecological integrity (2), (3), (4). Wastewater treatment plants (WWTPs) play a critical role in mitigating these impacts by treating contaminated water originating from a diverse range of sources, including domestic, commercial, and laboratory activities.

WWTP are comprised of several processes (Fig. 1.1). During screening stage large and medium-sized floating solids are removed from the incoming wastewater to prevent damage to downstream equipment; this is typically achieved using bar racks. In the primary treatment stage, flow velocity is reduced to facilitate the removal of organic and inorganic suspended solids through sedimentation and flotation (5). The removed particles could be kept for further treatment, used as fertilizer or disposed in a landfill. Secondary treatment, commonly referred to as the activated sludge (AS) process, involves the biological treatment of wastewater, during which a diverse microbial community degrades the majority of organic matter under aerobic conditions (5). The resulting sludge containing high concentrations of microorganisms, is either partially recycled to the aeration tank to maintain biomass levels or transferred to a secondary clarifier for the removal of excess biomass (6). Finally, tertiary treatment employs additional physical and chemical processes to eliminate hazardous pathogenic microorganisms, through filtration and disinfection methods such as chlorination or UV irradiation. However, this treatment stage is not implemented in all WWTP.

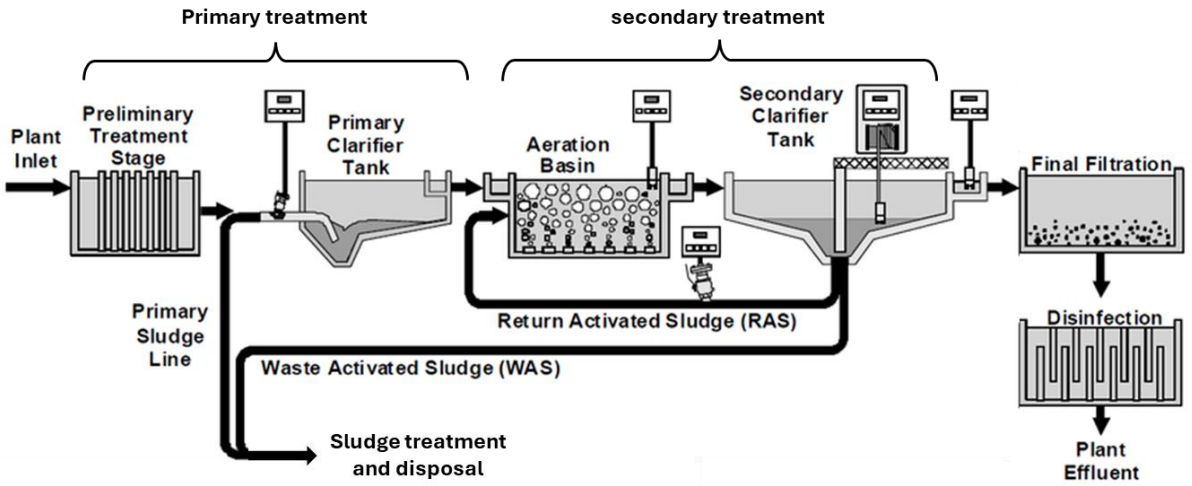

Figure 1.1: *Overview of a typical wastewater treatment plant (adapted in part from Majumder et al. (7)), showing the sequential stages of treatment: preliminary screening, primary sedimentation, biological treatment through activated sludge processes, secondary clarification, and disinfection prior to discharge.*

1.1.1. Importance of mixed bacteria communities

Mixed bacterial communities play a crucial role in WWTPs, as they provide a robust and efficient system for pollutant removal. Different bacterial groups exhibit distinct metabolic capabilities, enabling the biodegradation of a wide range of organic contaminants. In WWTPs, several key bacterial metabolic processes dominate treatment performance. Aerobic respiration is primarily responsible for the degradation of carbohydrates, proteins, lipids, and simple organic acids, converting these substrates into smaller molecules that are further oxidised mainly to carbon dioxide and water (8). Similar degradation pathways can also operate under anaerobic conditions through alternative metabolic routes (9). Bacterial nitrogen transformation processes are also fundamental to wastewater treatment. Ammonia is oxidised to nitrate, which is subsequently reduced to N_2 gas during denitrification (10). Ammonium oxidation for nitrogen removal can also be done anaerobically (11). These aerobic respiration and bacterial nitrogen transformation processes provide energy for the microorganisms that mediate them.

Phosphorus removal is typically achieved through an anaerobic–aerobic multistep process mediated by polyphosphate-accumulating organisms (PAOs). Under anaerobic conditions, PAOs hydrolyse intracellular polyphosphate reserves, releasing some phosphate (PO4) into the water, to generate energy for the uptake of volatile fatty acids (VFAs), such as acetate, which are stored intracellularly as polyhydroxyalkanoates (PHAs) (12). During the subsequent aerobic phase, PAOs oxidise these stored compounds to support growth and replenish polyphosphate reserves, resulting in net phosphorus uptake beyond normal metabolic requirements (13). Phosphorus-rich biomass is ultimately removed from the system through sludge settling.

Together, these microbial processes not only drive the biodegradation of organic matter but also underpin nutrient cycles, such as nitrogen and phosphorus, which are essential for maintaining ecological balance. Key microorganisms include ammonium- and nitrite-oxidising bacteria (with *Nitrobacter spp*. being dominant nitrifiers) and phosphate-accumulating bacteria, whose abundance correlates with treatment efficiency (14).

Moreover, in mixed bacterial communities, products or conditions generated by the biodegradative activity of one microorganism may be essential for the survival or metabolism of another (15). Mixed bacteria communities provide a wide range of enzymes and complement each other in a total multistep degradation of organic matter that would be impossible for a single microorganism. Furthermore, these communities have been reported to generate optimal conditions that promote beneficial bacteria while suppressing proliferation of undesirable species (16), enhancing stability and resilience within the community.

Other bacteria that play a crucial role in WWTPs are floc-former bacteria, these bacteria are able to form stable microbial aggregates that facilitate gravitational separation of treated water from sludge and enable effective AS recycling (17). These flocs are complex structures composed of microbial cells embedded within a matrix of extracellular polymeric substances, together with adsorbed organic and inorganic materials (18). Here filamentous bacteria act as a structural “scaffold” around which flocs develop (19), enhancing floc stability by increasing tensile strength and resistance to shear (20).

However, this balance is delicate, and disruptions can create favourable conditions for microbial overgrowth. Although filamentous floc-forming bacteria contribute to effective wastewater treatment under balanced conditions, their excessive proliferation can destabilise microbial community structure, suppress the growth of beneficial indigenous populations, and lead to operational problems such as sludge bulking and foaming. A prominent example is the Actinobacteria, particularly filamentous members of the Mycolata group such as *Gordonia amarae*. While *Gordonia amarae* demonstrates significant metabolic versatility (enabling the assimilation of both hydrophilic and hydrophobic substrates under aerobic, anoxic, and anaerobic conditions and contributing to system performance at moderate abundances (21)). Its overgrowth is strongly associated with foam formation and stabilisation (22), which could lead to operational disturbances in AS reactors. This behaviour has been attributed to the highly hydrophobic, mycolic acid–rich cell envelope of *Gordonia amarae* (23). Similarly, Candidatus "*Microthrix parvicella*" is also a filamentous bacterium that directly correlates with sludge foaming when overgrown (24). Additional genera including *Tetrasphaera*, *Trichococcus*, *Clostridium XI*, *Arcobacter*, and *Flavobacterium* have been found to be more abundant in foams than in normal activated sludge (24), (25).

Given the large density and diversity of microorganisms (mainly bacteria community (26)) that are found in WWTPs, coupled with the challenges associated with controlling disruptive bacterial species within mixed bacterial communities, WWTPs are continuously facing challenges to ensure proper operation and avoid both environmental contamination and exposure of humans to pathogens. Consequently, uncontrolled growth of foam-associated bacteria remains a critical concern, as it threatens effluent quality, and increases the risk of environmental contamination and potential detrimental effects to humans.

1.1.2. Microorganisms monitoring in WWTP

WWTPs employ several techniques to quantify and monitor microbial communities. Among these, gravimetric analysis is the most widely applied due to its speed and simplicity. This method estimates the total biomass in the system, typically expressed as total suspended solids (TSS) or volatile suspended solids (VSS). However, it does not distinguish between living and dead cells, nor does it provide taxonomic information, as

the measurement also includes bacterial residues released during lysis and non-biotic organic particulates introduced with the influent wastewater (27). Optical microscopy is another commonly used technique. It is more selective and is often applied to assess sludge health and estimate the abundance of particular microbial groups, such as filamentous bacteria (28). However, microscopy-based approaches have limitations. Their taxonomic resolution is low, since many bacterial species in activated sludge share similar morphologies, making them indistinguishable under bright-field or phase-contrast microscopy; consequently, they cannot reliably resolve microbial diversity at the genus or species level (29). Molecular methods, such as genomic and metagenomic analyses, such as Polymerase Chain Reaction Denaturing Gradient Gel Electrophoresis (PCR-DGGE), among others, are also occasionally employed in WWTPs to provide detailed taxonomic and functional insights, though their use is less frequent due to higher costs and technical requirements (30).

Lipids have been previously used as biomarkers to address environmental questions (31), (32). Moreover, lipidomic methods have been proposed as an emerging strategy for monitoring microbial communities in wastewater treatment systems, as they offer valuable approaches quantifying microorganisms and monitoring microbial community changes in WWTPs bioreactors without requiring molecular techniques (33). Lipids can provide information on both biomass composition and physiological status, such as growth stage and stress responses of key microorganisms (34), and provide quantitative descriptions of microbial assemblages without cultivation requirements, overcoming limitations of traditional culture-dependent approaches (35).

1.2. Foaming events in wastewater treatment plants

Foaming events in wastewater treatment plants are a well-recognised operational problem. They are not limited to activated sludge reactors but have also been frequently reported in anaerobic digesters (36). When foam stabilises there is a decrease in process efficiency leading to increasing maintenance and chemical costs to restore the reactor. The economic impact of a foaming event can be substantial. In Sweden, a wastewater treatment plant was forced to partially shut down for 10 weeks due to persistent foaming, resulting in an estimated direct loss of approximately 150,000 USD attributed to reduced energy production, additional labour requirements, and the use of dehydrating agents for digestion residues (37). Similarly, an anaerobic digester in Germany suffered severe damage as a consequence of foaming, with repair costs reaching approximately 600,000 USD (38). Foaming control measures can also entail increased operational costs. Researchers in Greece estimated foaming control measures to cost between 0.002 and 0.009 €/m^3 of wastewater, depending on the employed measure (39), (40). Beyond direct economic impacts, foaming also carries environmental costs, as it can result in the

discharge of insufficiently treated wastewater into water systems, posing risks to aquatic ecosystems, wildlife, and human health.

Although foaming events appearance and dissipation are not fully understood, several studies linked them primarily to the proliferation of filamentous, hydrophobic bacteria. Among these, *Gordonia amarae* (main bacteria analysed during this project) is one of the most reported organisms (41), (42). Its hydrophobic cell surface, lipid-rich cell wall, and production of biosurfactants enhance its ability to stabilise foam layers at the air–liquid interface (43).

Environmental factors also play a role. Temperature fluctuations, the presence of volatile fatty acids, and detergents have all been shown to stimulate filamentous bacteria to increase biosurfactant production.

1.2.1. Gordonia amarae

Gordonia genus are Gram-positive bacteria that comprises 40 species. Some of them are human pathogens (44), such as *Gordonia terrae*, which is considered to cause primary cutaneous infection (45). *Gordonia bronchialis* and *Gordonia araii* were isolated from the saliva of patients with pulmonary diseases (46). *Gordonia otitidis* was isolated from patients with otitis (47). However, most *Gordonia* bacteria are known to contribute in different ways to the biodegradation of pollutants in environment. Several species of *Gordonia* can modify or degrade halogenated and non-halogenated aromatic compounds, nitrile and xylene, among others (48).

Gordonia amarae (formerly *Nocardia amarae*) is a filamentous bacterium (bacteria that grow in long filament-like structures as they do not separate from each other after cell division (49)) that belongs to *Mycobacterium* genus. This organism is frequently associated with foaming events in activated sludge reactors at wastewater treatment plants (50), largely due to its ability to produce biosurfactants. These surface-active compounds promote foam accumulation and stabilisation, which can impair WWTP processes performance and reduce treatment efficiency. Such disruptions may lead to the release of inadequately treated wastewater, increasing the risk of environmental contamination.

Gordonia amarae was also found to effectively take up and utilise a range of hydrophilic and hydrophobic substrates under aerobic, anaerobic and anoxic conditions as part of its metabolic processes (21). This could explain the observed failures when *Gordonia amarae* associated foaming was attempted to be stopped by using anaerobic and anoxic selectors (21). Selectors are engineered process zones designed to manipulate microbial population dynamics, commonly to suppress the proliferation of filamentous bacteria in activated sludge systems (51). Anoxic selectors are characterized by the absence of dissolved oxygen while maintaining the presence of nitrate or nitrite, which serve as

terminal electron acceptors for microbial respiration and energy generation (52). In contrast, anaerobic selectors lack both dissolved oxygen and oxidized nitrogen species, thereby eliminating the availability of conventional inorganic electron acceptors (52).

1.2.2. Biosurfactants

Surfactants or surface-active compounds (SACs) are agents that modify the conditions present at interfacial surfaces, such as solid-liquid (metal-water), liquid-gas (water-air) and liquid-liquid (water-oil). Biosurfactants and bioemulsifiers are amphipathic molecules naturally synthesised by bacteria to facilitate interactions with compounds of differing polarities in their environment. Glycolipids (long chain fatty acids bonded to carbohydrates) are the most widely reported biosurfactants. Other classes, such as lipopeptides, heteropolysaccharides, and lipopolysaccharides, display greater structural complexity (53).

The ability of bacteria to produce biosurfactants is normally related to their capacity to grow in hydrophobic carbon sources (i.e. hydrocarbons) (54). *Gordonia* bacteria are known to be highly versatile in hydrocarbon-rich environments due to its production of surfactants and extracellular bioemulsifiers (55), (56), which reduce surface tension and help to solubilise hydrophobic substrates by producing an emulsion. Solubilisation of these substrates also makes *Gordonia* survival in foaming conditions possible (50).

Gordonia biosurfactants were analysed and reported to be constituted of glycolipids (57). Moreover, the genomic analysis of some strains verified the presence of all the genes necessary for glycolipids biosynthesis (57). Some strains of *Gordonia*, such as *Gordonia amarae*, produce trehalose lipids as their main biosurfactant (57), which are glycolipids containing ester bonds of sugar rings acylated with various fatty acids (58).

1.2.3. Mycobacteria and its mycolic acids

Mycobacteria cell wall is formed by an outer layer containing proteins, glucan and, in lower abundancies, lipids. And an inner layer with mycolic acids (MA), covalently and non-covalently bonded, in parallel arrangement (59). MA are 2-alkyl, 3-hydroxy fatty acids, which can have different chain lengths and chemical functions (59). Generally, they have long carbon chains and are essential for mycobacteria cell wall architecture, impermeability and survival. Although MA are unique, they are not exclusive to *Gordonia amarae*, being found in other related genera such as *Nocardia*, *Rhodococcus* and *Corynebacterium* (60). There are over 500 related chemical structures (59), although α, keto and methoxy are the three major classes of MAs in mycobacteria. A scheme of MA structures and mycobacteria cell wall are shown in Fig. 1.2.

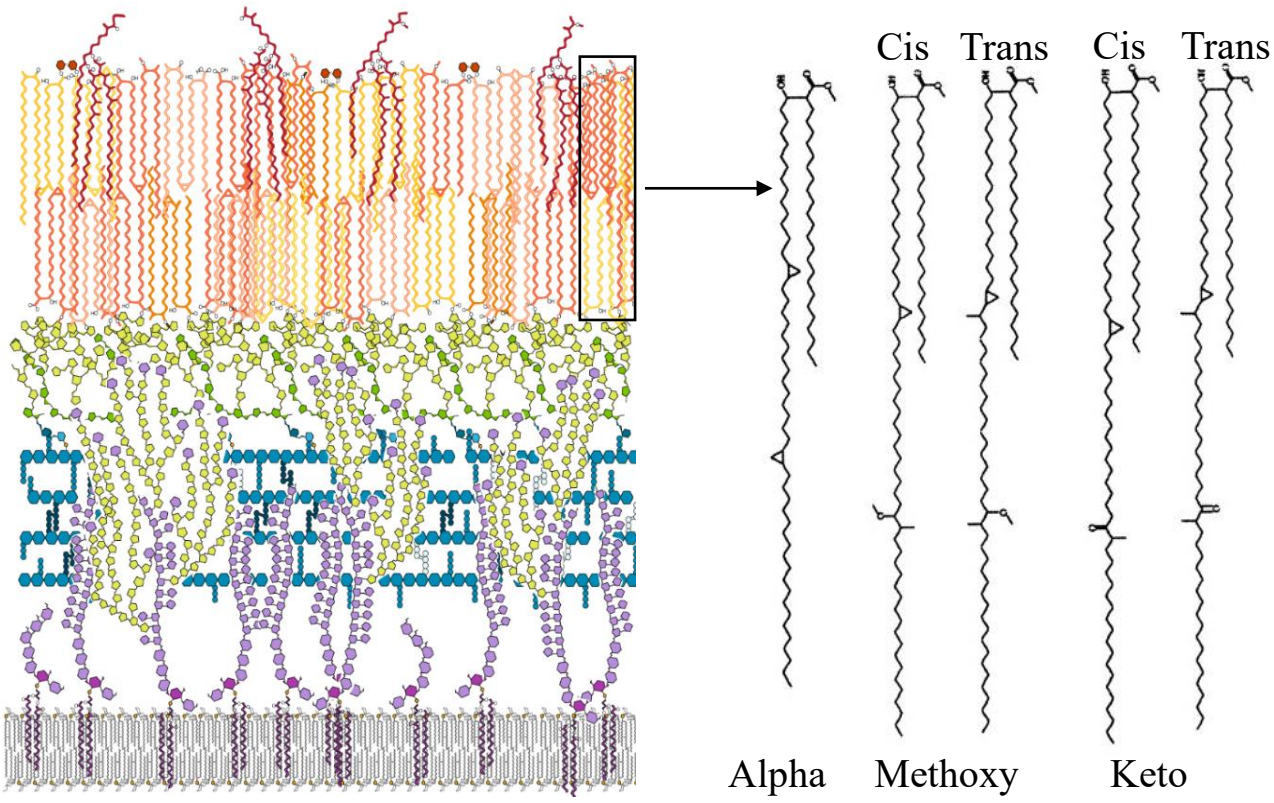

Figure 1.2: *Diagram of mycobacteria cell wall layers, with MA in yellow and orange, and selected MA structures (61).*

The genus *Mycobacterium* comprises a wide range of different species, some of which are human health pathogens, such as *Mycobacterium tuberculosis*, which is the cause of tuberculosis disease. Here, MA provide mechanical support, osmotic protection and contribute to the bacteria resistance to antibiotics (62) and survival inside macrophages (63). As they are also essential in the pathogenicity of the bacteria, the MA biosynthesis path has been targeted in other studies as an action site of anti-TB drugs and for the development of antimycobacterial drugs (64).

As other non-pathogenic mycobacteria (e.g., *Gordonia amarae*) have also been linked to environmental issues, understanding their lipid structure and dynamics could provide key information for effective prevention of environmental disturbances. MA in these bacteria are key components of the cellular envelope, with structural integrity being critical for bacterial survival (65). Structurally, MA in *Gordonia* genus have been reported to contain between 0 and 5 double bonds or unsaturations (66) and to exhibit variability in their carbon chain length. Specifically, studies on *Gordonia amarae* have identified mycolic acids comprising 31 to 54 (67) carbon atoms, with some reports indicating chain lengths extending up to 56 carbon atoms (66). Bacteria are known to change their lipid profile depending on the growing condition (68), (69). Consequently, the analysis and characterisation of mycobacteria MA can help to find biomarker structure changes or distinct biomarkers that could be used as key factors to indicate that foaming-related mycobacteria, such as *Gordonia amarae*, are posing an operational risk. This could be used in designing foaming prevention and mitigation processes.

1.3. High Performance Liquid Chromatography (HPLC)

High Performance Liquid Chromatography (HPLC) was developed in 1969 (70) and became popular across organic, inorganic and biochemical areas. Currently, HPLC is one of the most used techniques in analytical laboratories due to its ability to separate and analyse a wide range of analytes. HPLC systems are composed of: 1) solvents or mobile phase, used to make the analyte travel through the system, 2) Sample injection system, utilised to inject the sample into the system, 3) pumps, which force the mobile phase and sample into the column, 4) column, which separates analytes in the sample, and detectors, employed to detect analytes in the column eluent (71).

HPLC separation is based on interactions between the sample components, mobile phases and stationary phase in the column. Depending on the analyte of interest, different stationary phases can be used.

Normal phase: analytes separation is achieved on the bases of their affinity to a normal stationary phase. The type of packing materials that it uses are porous oxides such as silica (SiO_2) or alumina (Al_2O_3) which are hydrolysed to produce large number of OH groups making the surface polar (72). It uses a non-polar mobile phase, the proportion of which can be modified during a sample run by gradient elution to a more polar mobile phase, to control the time it takes to the analyte to elute. This phase is normally used for polar and moderately-polar analytes.

Reversed phase: employs dispersive forces for analyte separation (72). A reversed phase chromatography uses moderately-polar mobile phase and a nonpolar stationary phase, such as C8 or C18. The silanol groups of the stationary phase are reacted with an organochlorosilane to produce a non-polar stationary phase that normally have 8 or 18 hydrocarbons chain attached. The larger the adsorbent surface, the longer retention time of the analytes. Reversed phase is one of the most used phases for fatty acid analysis and it is the one that was used for mycolic acid separation.

Ion exchange: separation is based on the affinity of charged analyte ions to an oppositely charged stationary phase (72). For negatively charged ions (anion exchange chromatography) the stationary phase normally used is a quaternary amine attached to the column resins. For positively charged ions (cation exchange chromatography) the stationary phase used is SO_3^- attached to the resins. Retention times will be affected by the concentration of analyte with respect to the amount of other ions present (H^+ for cation exchange and OH^- for anion exchange), the pH and the ionic strength of mobile phase.

Size exclusion: separates molecules according to their sizes. The stationary phase has normally spherical beads with a specific pore size. Small molecules will be able to diffuse into the pores and be retained. Contrarily, large molecules will not enter the pores and

will be eluted earlier. Size exchange chromatography is very common for polymer molecular weight determination (72).

Liquid chromatography is normally attached to a mass spectrometer (LCMS) to perform further analysis on column eluent. This technique has become popular for lipidomic analysis (73) and, in a more specific way, for mycolic acid analysis too (74), (75).

1.4. Mass spectrometry

Mass spectrometry (MS) is an analytical technique that separates molecules, atoms and other ionized particles based on their mass/charge ratio (*m/z*). This technique is used for identification, detection and confirmation of molecules; as well as for quantitative analysis. MS instrumentation comprises: ion source, which ionises analyte molecules; single or multiple mass analyser, which sorts ions based on their *m/z* ratio applying electromagnetic fields, and fragments parent ion when tandem mass spectrometry is required; detector, which converts the current of ions into a measurable signal, providing data necessary for the calculation of the relative abundances of each ion present; and finally, a computer, which regulates the mass analyser and oversees the management of data obtained from the detector.

Fig. 1.3 displays a representation of the components in a mass spectrometer device.

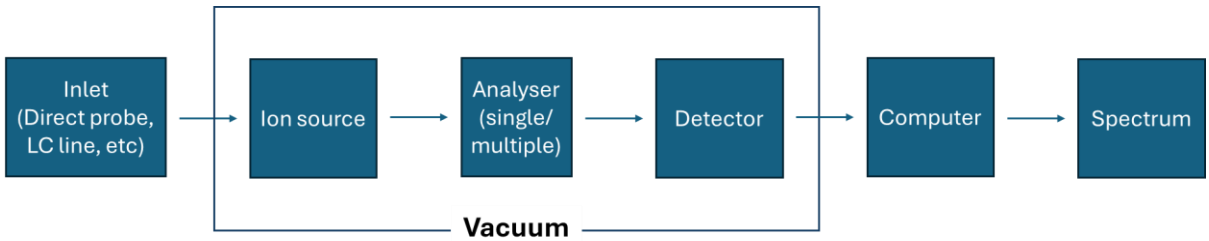

Figure 1.3: *Mass spectrometer composition, where vacuum components are kept under high vacuum.*

Ion sources and analysers employed in this PhD project are explained below.

1.4.1. Mass spectrometry instrumentation: Ion source

Electrospray ionisation mass spectrometry (ESI-MS) is a soft ionisation technique, which means that no or low fragmentation is produced in the ion source. The analyte (from LC column or via direct infusion, both techniques used in this PhD) is introduced into the ion source through a metal capillary, to which a high voltage (2-6 kV) is applied (76), this causes the dispersion of the sample solution, producing an aerosol of highly charged electrospray (ES) under atmospheric pressure (77). A flow of N_2 from around the capillary removes solvent and helps to get better nebulization (76). As a result of solvent removal, the size of the charged droplets get smaller until they reach the Rayleigh instability limit

(78), where they become unstable, and the electrostatic repulsions produce the "Coulomb explosion". The drying and explosion process happens repeatedly, creating individually charged nanodrops (79) that enter a heated capillary, where the complete desolvation of the ions is produced due to the temperature and action of a drying gas. Ions then pass through the MS detector at high vacuum. Fig. 1.4 shows a representation of the ESI mechanism.

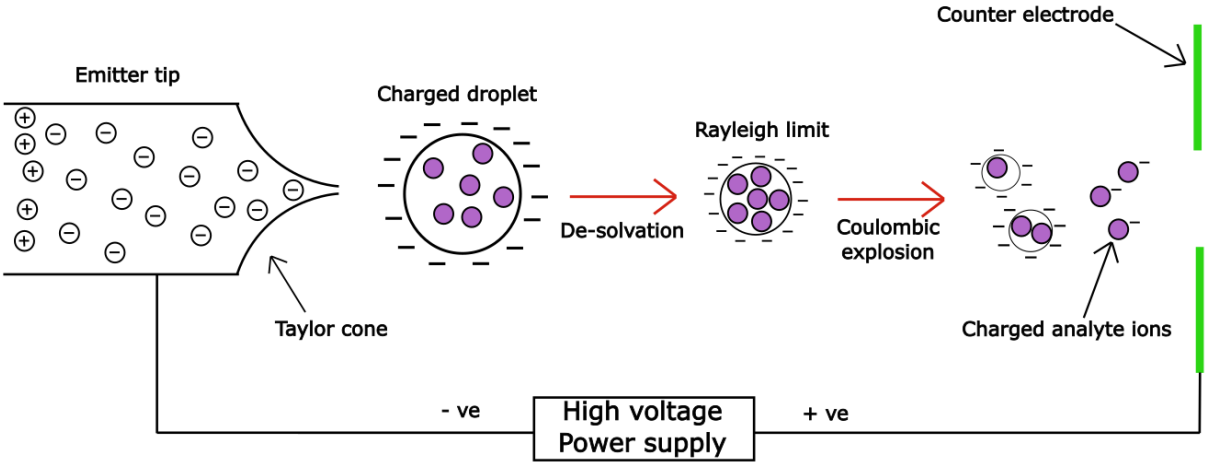

Figure 1.4: *ESI mechanism scheme.*

The ESI technique has been popular for the analysis of lipids in both, negative and positive modes, as it is a very sensitive, discriminating and straight method to evaluate changes in the cellular lipidome (80), (81), (82).

1.4.1. Mass spectrometry instrumentation: Mass analysers.

Ionised molecules are transported through the mass analyser, where ions are separated based on their *m/z* ratio. Different mass analysers separate ions in a different way. Only quadrupole time-of-flight (Q-ToF) mass analysers were used during the project. Therefore, only these will be introduced.

1.4.1.1. Quadrupole

In a quadrupole analyser four circular parallel rods (divided in 2 pairs of different polarity) are given a fixed direct constant voltage (DC) and alternating radio frequency (RF) field potentials (83). Ions are focused and directed through the centre of the rods. A preselected voltage will determine the motion of the ion travelling through the quadrupole, allowing only ions of a specific *m/z* to have a stable trajectory and reach the detector. All others will be deflected and strike the rods losing their energy. Fig. 1.5 displays the scheme of a quadrupole analyser.

The quadrupole DC and RF voltages can be ramped to allow ions with different *m/z* to pass through the rods, acquiring full mass spectrum (83), or fixed to only permit ions of specific *m/z* to reach the detector. This analyser is highly popular for the analysis of

known analytes, especially when multiple quadrupoles are used together (i.e. triple quadruple analysers) for tandem MS (MS/MS) studies. The first quadrupole selects a narrow range of *m/z*, and the following ones are used for fragmentation. Although quadrupole analysers are cheap and robust, they have low resolving power (84). Therefore, they are commonly coupled with other mass analysers, such as orbitrap or ToF, to improve the resolution.

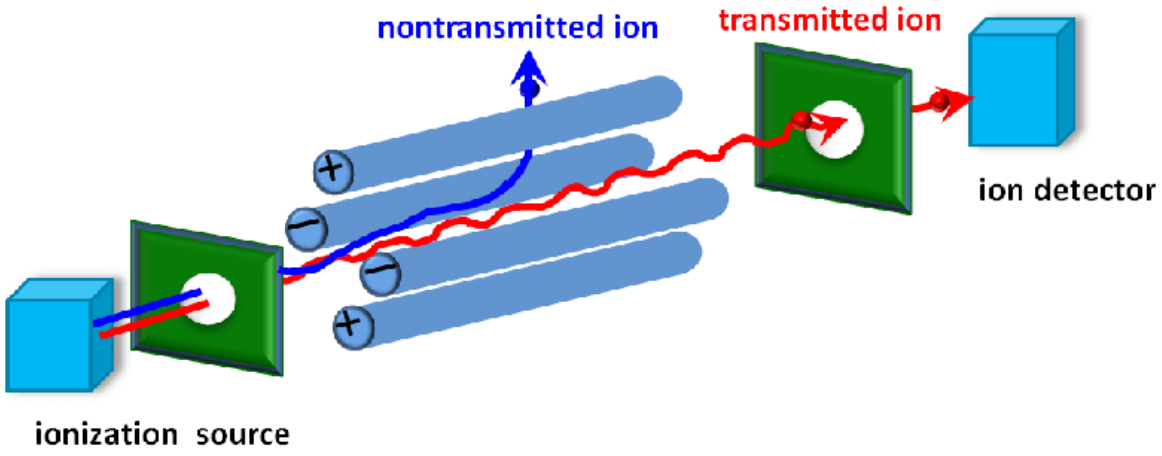

Figure 1.5: *Quadrupole mass analyser scheme (85).*

1.4.1.2. Time of Flight (ToF)

In a ToF analyser, ions are accelerated by a known electric field throughout a drift tube of a specified length (86), in which ions will separate based on their *m/z* ratio; lighter ions will reach the detector earlier than heavier ones. ToF analysers can be found in linear mode or reflectron mode. In linear ToF instruments ions travel directly to the detector. The main advantage of these instruments is that metastable ions, (ions that possess sufficient internal energy, acquired in the ion source, that can fragment during its flight, leading to diffuse mass spectra peaks (87)) conserve the velocity of precursor ions, allowing simultaneous detection and not reducing the intensity of a molecular ion signal (88). However, in reality, not all ions with same *m/z* will always be given the same initial kinetic energy to reach their ideal velocity, causing ions with same *m/z* to reach the detector at different times, and producing low mass resolutions.

Reflectron ToF analysers contain a series of high voltage operating ring electrodes (mirrors) that repel ions with the same polarity, curving or reversing their trajectory towards the detector. Ions with high kinetic energy, which travel faster than ions with lower kinetic energy, will be able to penetrate more deeply through the reflectron than ions with lower kinetic energy, making ions with high kinetic energy travel a longer path (89). This corrects velocity differences for ions with same *m/z*, and makes them reach the detector at the same time, improving resolution. However, not all ions have the stability to survive the electric field of a reflectron analyser.

A representation of linear and reflectron ToF analysers can be seen in Fig. 1.6.

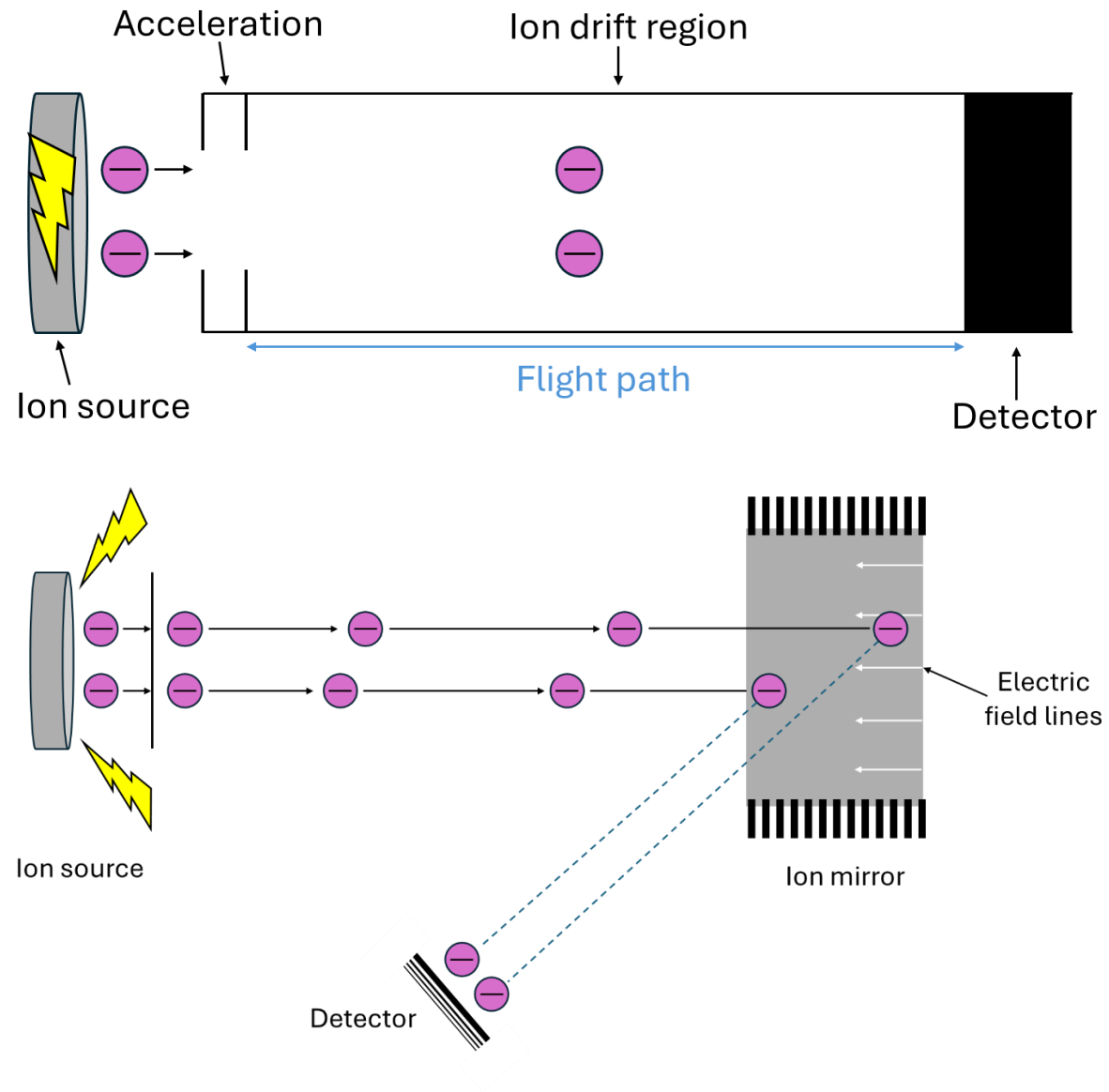

Figure 1.6: *Scheme of linear (top) and reflectron (bottom) ToF mass analysers.*

1.4.1.3. Hybrid mass spectrometers: Q-ToF

The Xevo® G2-XS QToF and Select Series Cyclic IMS instruments, which were used for the mass spectrometry analysis in this project contained both mass analysers coupled together, quadrupole and time of flight (Q-ToF). These instruments are high mass accuracy and high resolution mass spectrometers, > 10000 and > 100000 full width half maxima (FWHM) respectively. In both instruments, ions are continuously generated by ESI and directed as a beam through an orthogonal accelerator. When the accelerator is filled with an ion package, ions are pushed orthogonally to their original direction into the ToF (90). As the ions travel, the accelerator is refilled. The flight cycle concludes when the heaviest *m/z* ion reaches the detector, at which point the process repeated.

Whereas the Xevo® G2-XS QToF instrument is only includes a reflectron (‘V’ optics) in its ToF tube, the Select Series Cyclic IMS comprises a second reflectron (‘W’ optics) that allows the ions to follow a ‘W’ trajectory. ‘V’ mode relates to sensitivity whilst ‘W’ mode relates to high resolution.

Cyclic IMS also holds and ion mobility cell between both analysers that can be utilised for elucidation of isomers and other isobaric compounds.

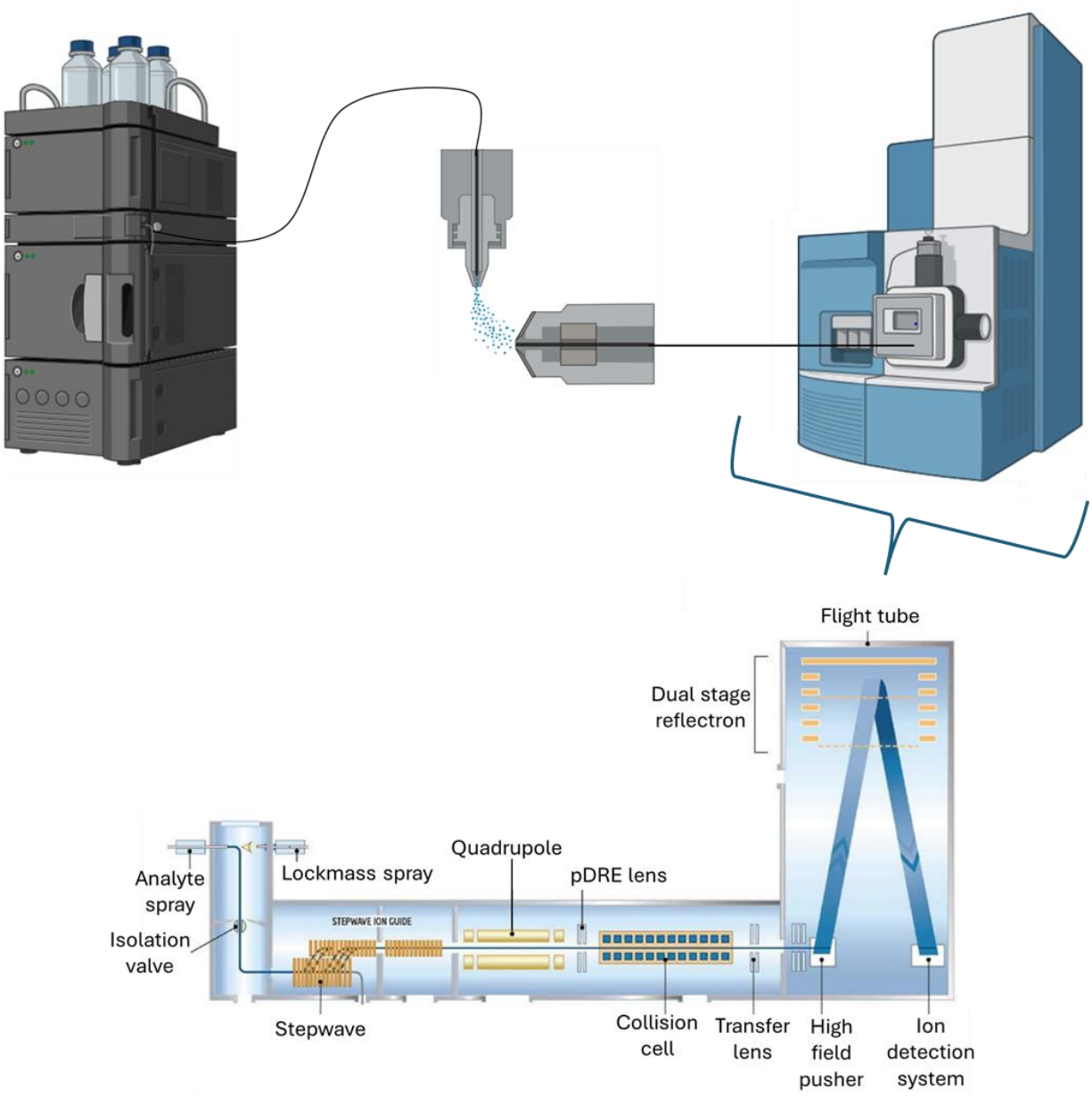

Figure 1.7: *Schematic representation of a LC–ESI–MS (QToF) system, showing the HPLC module (top left), electrospray ionisation source cones (top centre), QToF mass analyser (top right), and the internal architecture of the QToF instrument (bottom).*

1.4.2. Ion mobility

Ion mobility spectrometry (IMS) is a powerful technique that facilitates multidimensional characterization of analytes when it is combined with mass spectrometry (IMS-MS) (91). This allows the separation of isobaric compounds (compounds with the same exact mass that appear as a single peak in mass spectrum), and the addition of collision cross section (CCS) values to analytes to enhance their identification and characterization (91).

IMS separates ions in a buffer gas (inert gas) by application of an electric field, causing ions to travel at a velocity related to their specific mobility (92). Separation is achieved when more mobile ions (normally small ions) travel at a higher velocity than less mobile ions. This principle is portrayed in equation 1.1.

$$K = \frac{v_d}{E}$$

Equation 1.1: *IMS separation principle, K is analyte's mobility; v_d is the velocity at which ions travel through the buffer gas; and E is the applied electric field.*

Some analytical applications use calculated CCS values as representation of the measured mobility. Here, CCS describes how the ion collides with the buffer gas and gives information about the ion's structure and three-dimensional conformation as it travels through the drift area (93). There are a wide range of IMS instruments with different characteristics, such as different pressures, temperatures (in the ion mobility section), gas composition and applied field strength (91). These differences should be considered accordingly to the analysis required; CCS calculation, isomer separation, etc. Main ion mobility instruments are: drift tube ion mobility spectrometry (DTIMS), trapped ion mobility spectrometry (TIMS), traveling wave ion mobility spectrometry (TWIMS), field asymmetric waveform ion mobility spectrometry (FAIMS) and cyclic ion mobility spectrometry (cIMS).

1.4.2.1. Ion mobility instrumentation: Drift tube ion mobility spectrometry (DTIMS)

DTIMS is known as the classic IMS instrumentation. It has the capacity to measure mobility of ions, and therefore calculate CCS. DTIMS uses a no directional buffer gas flow in which ions travel along (91), under the influence of a homogenously applied weak electric field (94). Here, larger ions collide more with the gas, retaining them more strongly than smaller ions. Consequently, small ions with smaller CCS reach the detector earlier than those with larger CCS.

1.4.2.2. Ion mobility instrumentation: Traveling wave ion mobility spectrometry (TWIMS)

TWIMS is schematically very similar to DTIMS. However, TWIMS uses an oscillating electric field to cause voltage waves that push ions towards the mass analyser, through the drift gas (91). In the drift tube, ions experience the effect of an approaching wave and

start to travel through the gas. By changing waves speed and strength, ions can be separated based on their size. Smaller ions collide less frequently with gas molecules and move faster, while larger ions collide more and get delayed. Multiple travelling waves, in quick succession, can be sent to the device to separate complex mixtures (94).

1.4.2.3. Ion mobility instrumentation: Trapped Ion Mobility Spectrometry (TIMS)

TIMS is composed of electrodes that form 3 main regions in a "funnel": entrance funnel, ion mobility region and exit funnel. Entrance and exit funnel control ion focusing and deflection, ions in the mobility region are trapped by a non-uniform electric field, against a moving gas. Here, ion packages are separated based on their size to charge ratio before eluting from the "funnel". Ions with high charge to size ratio will elute earlier than small ones (94). Electric field ramp speed and gas velocity can be tuned depending on the experimental requirements. i.e. slow electric field ramping is more selective and can separate ions with similar mobilities more effectively than fast ramping.

1.4.2.4. Ion mobility instrumentation: field asymmetric waveform ion mobility spectrometry (FAIMS)

FAIMS is an atmospheric pressure IMS technique, which uses a small device placed between the ion source and the vacuum region of the mass spectrometer (91). FAIMS works as mobility filters by using a waveform to separate ions under a gas that flows alongside (95). The voltage switches between high and low electric field strengths, filtering based on how an ion's mobility changes with the field strength, rather than its absolute mobility (91). Because of the use of this asymmetric waveform, FAIMS cannot calculate CCS.

Other techniques such as differential mobility spectrometry (DMS) and differential ion mobility spectrometry (DIMS) operate electronically similar to FAIMS, only varying in the geometry of their electrodes (96).

1.4.2.5. Ion mobility instrumentation: cyclic Ion mobility spectrometry (cIMS).

A SELECT SERIES Cyclic IMS mass spectrometer (Waters Corporation, Wilmslow, UK) (Fig. 1.8) was the main ion mobility device used in this project. cIMS was initially conceptualized with the development of long path length TWIM devices in mind, to increase the resolving power (*R*) of ion mobility devices. Unlike traditional drift tubes, TWIM technologies do not require a simultaneous increase in drift voltage (~TW amplitude) when extending its path length (97). Moreover, TWIM devices use the same electrical potential at its start and end (98), which makes them optimal for closed-loop multipass separators (97).

The cIMS is designed as a quadrupole/cyclic ion mobility/time-of-flight instrument, which uses TWs for mobility separation in a closed loop. Ions entering the cIM section "surf" on a wavefront, while additional waves continuously pass through and overtake them. The mobility of the ions determines how frequently they are surpassed by the waves: ions with

lower mobility are surpassed more often and take longer to cross the section than higher mobility ions. This results in ion mobility (IM) separation (97).

The cIM device has an entry/exit array located at the base of the cIM loop, positioned between pre- and post-array ion storage areas. Ion packets from the trap are retained in the array until a voltage change allows them to move into the cyclic section, where ion mobility separation takes place. This configuration provides selectable mobility resolution and makes possible a wide range of ion mobility sequences (99), such as mobility selection, fragmentation, ion storage and IMS^n. Most of the functions are combined during IMS^n sequence, providing extended analysis when multiple ions are mobility separated from an apparently single ion. Here, individual mobility-separated isomers of interest are sent back to the pre-array storage, where they are held, while the remaining ions are directed to the ToF without being acquired. Stored ions can then be re-injected into the cyclic section, with or without fragmentation, allowing for additional separation or ejection steps. This process enables IM separation of fragment ions (if fragmentation was applied) and further fragmentation of selected fragment ions and so on.

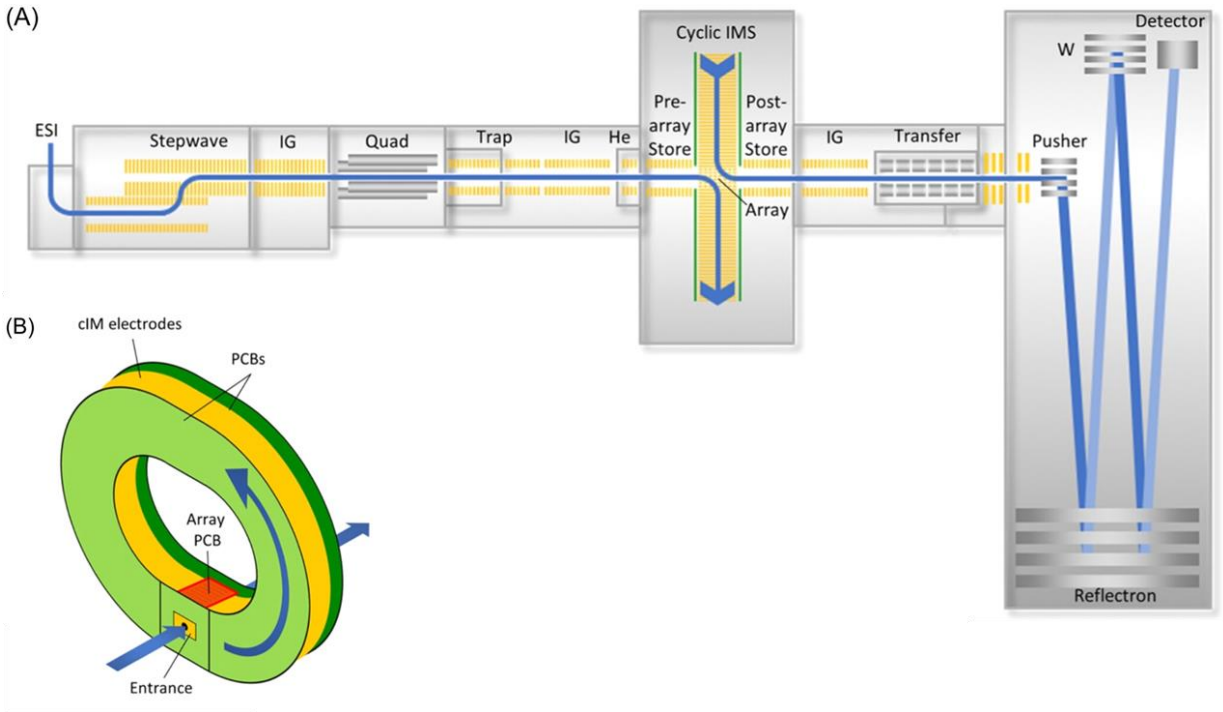

Figure 1.8: *Overview of the cyclic ion mobility spectrometry–mass spectrometry (cIMS–MS) system (A) and detailed schematic of the cIMS array (B), adapted from Giles et al. (97).*

The IM path length of the cyclic device is approximately 98 cm, producing a calculated resolving power of ~ 65 CCS/ΔCCS (or Ω/ΔΩ) (99). As the *R* of the cIMS device increases with the square root of the number of passes, the achieved *R* in a single or multipass IM experiment can be calculated using equation 1.2.

$$R \approx 65 \cdot \sqrt{N}$$

Equation 1.2: *cIM resolving power equation for a singly charged ion, where R is the resolving power and N is the number of passes that an ion has travelled around the cyclic section.*

1.5. Polarography

Another way to identify components of a sample (particularly biosurfactants) is by polarography. Polarography is an electrochemical technique that uses a hanging mercury drop electrode to which an alternating current is applied. This technique is long-stablished and has been applied for biosurfactant quantitation in aqueous solutions during the last decades (100), (101), (102). Biosurfactant adsorption at the mercury electrode produces reduction in interfacial surface tension, alterations in the electrode double layer capacity, and suppression of polarographic maxima (100). With alternating current (AC) polarography, after a known biosurfactant accumulation period, the decrease in the capacity current of the electrode is measured at the potential of the electrocapillary maximum (-0.6 V for mercury) (102). This effect is directly related to the amount of surfactant in a sample and can be used to calculate surfactant concentration when a calibration curve is conducted, by plotting the difference in capacity current (ΔIc) against concentration of a known surfactant (100). A representation of a polarograph can be observed in Fig. 1.9.

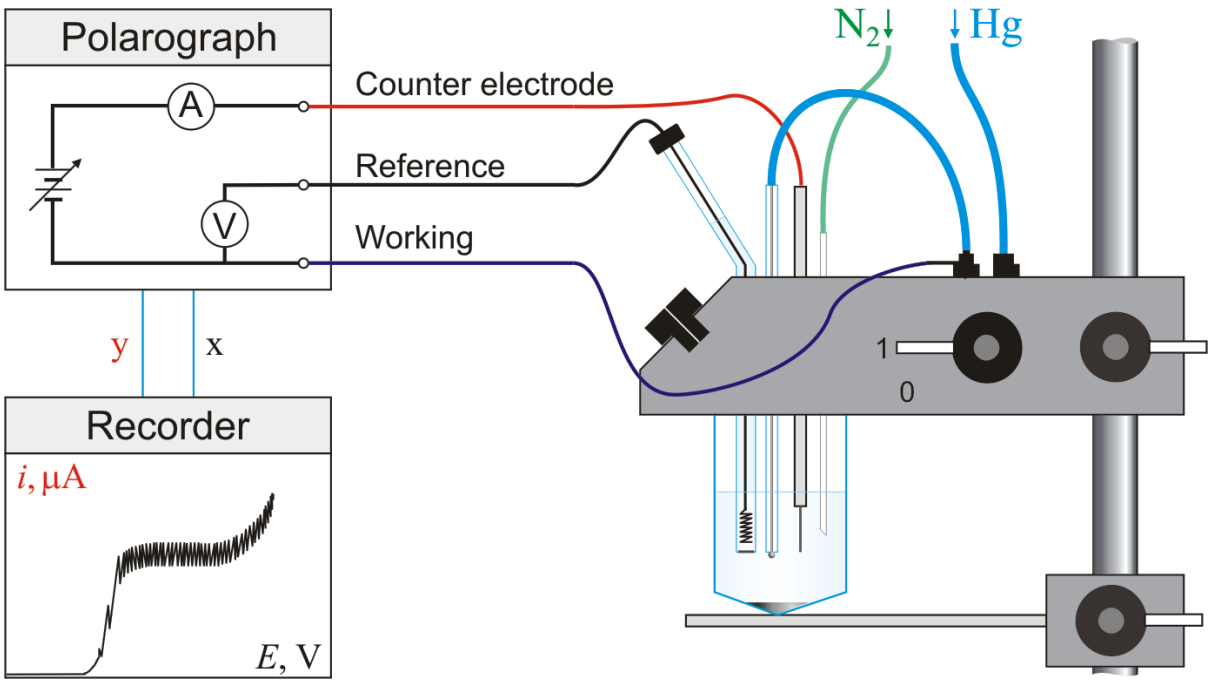

Figure 1.9: *schematic of a polarograph (103).*

Polarography measurements were reported to be affected by salinity concentration of solution and freeze/thaw degradation of samples (102). Therefore, proper sample

treatment, conditioning and salinity corrections are required prior to biosurfactants analysis.

1.6. 16s rRNA gene sequencing analysis

16S analysis is an amplicon sequencing technique used to identify and classify bacterial or archaeal communities based solely on the analysis of 16S rRNA gene of bacterial and archaea DNA. 16S rRNA is a gene that codes for the ribosome 16S subunit. This gene is around 1500 bases length and it is used as taxonomic marker to characterise microorganisms (104). This is because the 16S rRNA gene is highly conserved and found in all bacteria, whereas it also contains nine hypervariable regions (105). Variable regions can be used as a target to make possible the identification of individual bacterial species (105) or even strains if 16S rRNA gene alleles are analysed (106).

Primers designed to target conserved regions within the 16S gene are used to amplify a segment of the gene from all bacteria in a sample, via polymerase chain reaction (PCR). High efficiency sequencing then allows the complete DNA sequence of all PCR products to be determined (104). Variable regions normally contain sufficient taxonomic information to match each amplified fragment against a reference database of known 16S sequences, offering identification of the organism that carries that DNA (104). Bioinformatic analysis are used to classify sequences into operational taxonomic units (OTUs), often based on a 97% similarity threshold (107).

Compared to culture-dependent techniques, 16S rRNA sequencing offers superior resolution for identifying rare, uncultivable, or phenotypically ambiguous bacterial strains (108). Nonetheless, limitations remain, particularly in distinguishing closely related species and the requirement for advanced analytical resources (109). Despite these challenges, this method has become a major part of microbial ecology and environmental monitoring, among other fields (110), (111).

16S rRNA allows bacteria identification and quantitation (when known concentration of DNA from a bacterium unlikely to be found in a samples is added as an internal standard (112)) in environmental samples. Consequently, it serves as a precise and specific tool to study composition and changes in the microbiome of activated sludge.

Previous 16S rRNA studies of AS systems have consistently identified a number of dominant bacterial phyla, including Proteobacteria, Bacteroidetes, Actinobacteria, and Acidobacteria, among others (113), (114). At the genus level, key functional groups have been widely reported, such as *Nitrospira* and *Nitrosomonas*, which play central roles in nitrification. Genera including *Thauera*, *Dechloromonas*, and *Zoogloea* are commonly associated with denitrification and floc formation, while some members of

Dechloromonas and *Accumulibacter* are also recognized as important polyphosphate-accumulating organisms (PAOs) involved in biological phosphorus removal (115).

In addition, several filamentous and bulking-associated taxa linked to foaming events have also been identified in 16S rRNA studies of activated sludge systems, including *Candidatus* "*Microthrix*", *Haliscomenobacter*, and members of the orders *Burkholderiales*, *Rhodocyclales*, and *Sphingobacteriales* (116).

Collectively, these findings demonstrate that AS systems are not dominated by a small number of microorganisms but instead comprise complex and functionally diverse microbial consortia. Specially nitrifiers, denitrifiers, and polyphosphate-accumulating organisms, which together underpin treatment performance. Consequently, 16S rRNA gene sequencing has become a powerful tool for characterising microbial community composition and monitoring shifts in response to operational or environmental changes.

Aims

The aim of the thesis is to investigate the lipidomic profiles, biosurfactant production, and microbial communities in activated sludge, in order to evaluate biochemical changes associated with foaming events in wastewater treatment plants.

Objectives

The objectives of this project are linked to the following chapters:

1) Develop and apply lipidomic analysis of activated sludge foaming-related bacteria. The lipids produced, including isomers, by *Gordonia amarae* grown under normal and foaming-related conditions, will be analysed in this project by liquid chromatography and different mass spectrometry techniques (Chapters 2, 3 & 4).

2) Biosurfactant and foam production assessment of *Gordonia amarae* compared to activated sludge samples under both nutrient-rich and foaming-related growing conditions. Biosurfactant production by *Gordonia amarae* will be quantified using polarography, while foaming potential will be evaluated in *Gordonia amarae*-only cultures, activated sludge-only cultures, and activated sludge cultures following the introduction of *Gordonia amarae* (Chapters 4 and 5).

3) 16s rRNA analysis of wastewater activated sludge reactor samples under nutrient-rich and foaming-related growing conditions. Wastewater samples will be analysed with and without the introduction of *Gordonia amarae* to evaluate community structure in order to identify shifts in microbial composition and potential microbial biomarkers associated with the onset of foaming events (Chapter 5).

All this will allow me to define the relationships between lipid composition, biosurfactant production, and microbial community dynamics driving foaming events in wastewater treatment systems, and to identify biomarkers that may support the prediction and prevention of foaming events.

Chapter 2: Method development and implementation

2.1. Introduction

Mycobacteriales are an order of bacteria which are often characterized by the presence of high concentrations of mycolic acids (MAs) in their cell walls, which contribute to the formation of a thick, waxy barrier (117). MAs and related lipids are central to cell envelope integrity, metabolic adaptation, and ecological persistence. Mycobacteriales encompass the *Mycobacterium* genus which includes pathogenic species such as *Mycobacterium tuberculosis*, the causative agent of tuberculosis, a disease with high mortality if left untreated. It also includes environmentally relevant actinomycetes, such as *Gordonia amarae*, a well-documented contributor to foaming in activated sludge (AS) reactors of wastewater treatment plants (WWTPs), where its biosurfactant production compromises the WWTP process efficiency (50).

MAs are long-chain α-alkyl, β-hydroxy fatty acids that occur covalently bound to the cell wall or in unbound forms such as trehalose mono-/dimycolates, glycerol monomycolates, and glucose monomycolates (118), (59). They provide structural rigidity, regulate cell wall permeability, and modulate host–pathogen interactions (119), (118). MA are unique to mycobacteria and closely related genera, such as *Nocardia*, *Rhodococcus*, and *Corynebacterium* (120), (60). The main classes of MA in mycobacteria are alpha-, keto- and methoxy- MA. While metagenomic approaches have been employed to identify mycobacterial species within complex microbial communities (121), numerous studies have also highlighted the value of mycolic acid analysis, as these lipids can also serve as robust biomarkers for the detection of mycobacteria using mass spectrometry–based methods (122), (123).

Bacteria within the genus *Gordonia* are well known for playing environmental industrial roles, particularly in the biodegradation of pollutants in wastewater systems. Several species demonstrated the ability to metabolise halogenated and non-halogenated aromatic compounds, nitriles, and xylenes, among others (48). However, *Gordonia amarae* is a filamentous mycobacteria that is frequently detected in AS reactors in WWTPs, where it is able to contribute to foaming events by the production of biosurfactants that cause foam formation, accumulation, and stabilization (50). These foaming events are one of the main areas of concern in WWTPs as they reduce the process efficiency and increase operational costs due to the need for chemical treatment and maintenance. If a foaming AS reactor is left unaddressed, large fractions of biomass can be retained in the stable foam, leading to the release of inadequately treated wastewater (124), posing risks to both human and environmental health.

Gordonia amarae, a gram-positive bacterium*,* exhibits remarkable metabolic versatility, being capable of using both hydrophilic and hydrophobic substrates under aerobic, anaerobic, and anoxic growth conditions (21). Importantly, biosurfactants produced by *Gordonia amarae* facilitate the solubilization of hydrophobic substrates, which not only supports its survival under foaming conditions but also contributes to its persistence in

engineered environments (50). In contrast, *Mycobacterium tuberculosis* (or *Mycobacterium bovis*), the causative agent of tuberculosis, does not clearly relate to either Gram classification. Although the cell wall of *Mycobacterium tuberculosis* contains peptidoglycans characteristic of Gram-positive bacteria, its genome is phylogenetically closer to Gram-negative species (125). Its cell wall is distinctive for its richness in mycolic acids, in addition to peptidoglycans, phospholipids, and other complex lipids.

Although *Mycobacterium tuberculosis* and *Gordonia amarae* both produce MAs as major envelope lipids, their lipidomic profiles differ markedly. For example, *Mycobacterium tuberculosis* MAs typically fall in the 1090–1300 *m/z* (63), whereas those for *Gordonia amarae* are found between 550–880 *m/z* (67). Furthermore, while the mycolic acid composition of *Mycobacterium tuberculosis* has been extensively studied due to its biomedical relevance, comparatively little is known about the lipid profile of *Gordonia amarae*.

This knowledge gap is particularly important considering the chemical complexity of lipids (characterised by long hydrocarbon chains with variable oxygen content, small mass differences derived from unsaturations, wide dynamic ranges of abundancies and the frequent presence of isomeric or isobaric species, etc). Such features make their analysis challenging and underline the need to develop robust and reliable UPLC and MS methods to achieve the separation and detection of MAs with different chain lengths. In addition, advanced techniques such as cyclic ion mobility (cIMS) are crucial for resolving lipid isomers and improving the structural characterisation of these complex molecules.

Mycobacteriales are known to produce distinct lipid profiles depending on their growth conditions (126). *Gordonia amarae* has been reported to generate biosurfactants that promote foaming when cultured in media containing hydrophobic carbon sources (56). These observations raise the hypothesis that changes in growth media may directly affect the lipidomic profile of *Gordonia amarae*, potentially revealing biomarkers linked to its physiology and foaming behaviour.

To investigate this, growth conditions were systematically optimised with the aim of promoting biosurfactant production. The main carbon sources selected (*n*-hexadecane and a combination of *n*-hexadecane with acetate) were based on the work of Pagilla *et al.* (2002) (50), who demonstrated that *Gordonia amarae* produces biosurfactants to facilitate the solubilisation of *n*-hexadecane, and that the addition of a more readily metabolised carbon source such as acetate can further support bacterial growth. In parallel, alternative hydrophobic carbon sources, such as olive oil, were as well evaluated at varying concentrations. Olive oil was selected based on previous findings by Moussa *et al.* (2006) (127), which demonstrated biosurfactant production by *Gordonia amarae* when grown on this substrate, and due to its environmental relevance as a widely

used domestic cooking oil that can be introduced into WWTPs through household waste streams.

Bacterial growth was monitored by measuring changes in optical density at 600 nm (OD_{600}). The final medium was selected to provide a balance between supporting robust biomass accumulation and minimising optical interferences from hydrophobic carbon sources at 600 nm, thereby ensuring reliable conditions for subsequent lipidomic analyses.

Liquid chromatography–mass spectrometry (LC–MS) has been widely applied for the analysis, identification, and quantification of mycolic acids across diverse bacterial species. However, many established protocols rely on large volumes of chlorinated solvents such as chloroform or dichloromethane (DCM) (128), (129), (130). Chloroform, although effective, is highly toxic and is also not recommended by LC manufacturers because of its potential to corrode stainless steel components within chromatographic systems. In some studies, chloroform has been substituted with DCM as a less hazardous alternative (73). Nevertheless, DCM remains corrosive to instrumentation, limiting its suitability. These drawbacks highlight the need to optimise workflows that minimise the use of chlorinated solvents without compromising analytical performance.

In this context, the present study seeks to establish a robust LC-MS method for lipidomic analysis with enhanced resolution and sensitivity. The goal is to define conditions that enable comprehensive profiling of mycolic acids and other lipid species across a broad range of chain lengths, facilitating the analysis of extracts derived not only from individual bacterial cultures but also from mixed microbial communities. This approach ensures the applicability of the method to both controlled laboratory systems and more complex and environmentally relevant samples, such as AS samples.

While LC-MS and gas chromatography–mass spectrometry (GC-MS) are widely used for the separation and identification of lipids, these techniques are often unable to fully resolve isomers and isobaric species (compounds with identical exact masses). Lipids represent a chemically diverse class of biomolecules that frequently occur as multiple isomeric forms, including positional isomers (e.g., double-bond location), geometric isomers (cis/trans), and stereoisomers (R/S configurations) (131). To overcome these limitations, ion mobility spectrometry coupled to mass spectrometry (IMS-MS) has emerged as a powerful tool, providing an additional dimension of separation based on ion shape, size, and collision cross section, which directly influence ion mobility (132).

Cyclic ion mobility spectrometry (cIMS) is a relatively recent (commercially available since December 2019), state-of-the-art advancement that extends the capabilities of established IMS platforms such as travelling wave IMS (TWIMS), drift-tube IMS (DTIMS), trapped IMS (TIMS), and differential mobility spectrometry (DMS) (133). Unlike these techniques, which rely on a fixed ion mobility path and therefore provide limited resolving

power, cIMS employs a loop-shaped ion mobility cell. This design allows ions to traverse the mobility region multiple times, effectively increasing the mobility "path" and consequently, the resolving power with each pass (until wrap around or ion diffusion begins to occur) (133).

Beyond its selectable mobility resolution, cIMS also enables a combination of advanced functionalities such as ion storage and IMS^n (97). These unique features make cIMS a promising tool for multidimensional characterisation of mycolic acids and other complex lipid species.

2.2. Aim

The aim of this chapter is to develop and optimise an analytical workflow combining best bacterial cultivation strategy, LC–MS conditions, and cyclic ion mobility spectrometry parameters for the robust characterisation of mycolic acids from mycobacteria with different lipid carbon chain length, such as *Gordonia amarae* and *Mycobacterium tuberculosis*.

2.3. Objectives

The objectives of this study were to optimise the cultivation conditions of *Gordonia amarae* in minimal media supplemented with hydrophobic carbon sources to achieve reproducible growth with minimal interference, to develop and refine a robust LC–MS method capable of separating and detecting mycolic acids across a broad mass range to be able to analyse both single bacterial cultures and mixed microbial samples, and to apply cyclic ion mobility spectrometry to enhance the resolution and structural characterisation of mycolic acid isomers while minimising wrap-around and lipid fragments abundance loss.

2.4. Experimental

2.4.1. Materials

Reference mycolic acids from *Mycobacterium tuberculosis* (bovine strain) were bought from Avanti Polar Lipids. Sodium acetate and magnesium sulphate heptahydrate were obtained from Sigma-Aldrich®. M9 salts and n-hexadecane were obtained from MP Biomedicals. Ammonium formate, calcium chloride, acetonitrile (HPLC grade), isopropanol (HPLC grade) and methanol (UHPLC grade) were obtained from Fisher Scientific™. Chloroform (HPLC grade) was obtained from Macron Fine Chemicals™. 1-butanol (HPLC grade) and ammonium acetate were obtained from Honeywell. Nutrient

broth N° 2 (mainly composed of beef and yeast extract and peptone) was obtained from Oxoid Ltd. 18MΩ water was collected from Millipure S.A.S. water systems. Casamino acids were obtained from VWR. Olive oil (consisting of a mixture of refined and virgin olive oils and predominantly composed of oleic, linoleic, and stearic fatty acids) was obtained from Tesco UK.

Gordonia amarae (NCIB 11222 strain) was purchased from NCIMB LTD.

2.4.2. Methods

Parameters shown in this section are final conditions. Method optimisation is described in the results and discussion section.

2.4.3. Bacterial growth in different media

Gordonia amarae was cultured under varying nutrient conditions to evaluate planktonic growth. For nutrient-rich growth, 13 g of nutrient broth was dissolved in 1 L of Milli-Q water and sterilised by autoclaving at 120 °C for 15 min. A single colony from an agar plate was aseptically transferred to 20 mL of sterile nutrient broth and incubated at 30 °C for 24 h. The resulting pre-culture was used to inoculate 200 mL of fresh nutrient broth, which was subsequently incubated at 30 °C with agitation at 150 rpm. Bacterial growth was monitored by optical density at 600 nm (OD_{600}), measured twice daily over the course of one week, until cultures reached stationary phase.

For carbon-source-specific studies, 1 L of minimal media was prepared by adding 200 mL of minimal salts solution (56.4 g of M9 minimal salts in 1 L of water for 1 L stock) to 600 mL of MilliQ water. The mixture was supplemented with 2 mL of 1 M magnesium sulphate and 0.1 mL of 1 M calcium chloride. A 100 mL solution containing 10 % carbon source in MilliQ water was added to the media. The solution was sterilised via autoclave at 120 °C for 15 minutes. A separate 100 mL solution containing 0.1 g/mL of casamino acids in MilliQ water was filter-sterilised and added to the sterile media. 200 mL aliquots were inoculated with *Gordonia amarae* prior to incubation at 30 °C and 150 rpm. OD_{600} measurements were taken twice a day for a one-week period using a spectrophotometer until bacterial growth was completed. The carbon sources used for minimal media preparation were: (A) n-hexadecane (1 %), (B) n-hexadecane (1 %) + acetate (0.5 %) and (C) olive oil (1 %).

2.4.4. Bacterial mycolic acid extraction

Extractable MA isolation was achieved following Alshehry *et al.* (134) method, as follows. Bacterial culture samples were centrifuged for 10 min at 2000 rpm and the solid and biosurfactants supernatant (when produced in minimal media) layers were transferred to

a glass tube and freeze-dried. Dried solid was washed with 15 mL of 1-butanol/methanol (1:1) + 5 mM ammonium formate. The mixture was vortexed, sonicated for 1 h and centrifuged 10 min at 2000 rpm. The liquid layer was transferred to a round bottom flask and the wash, sonication, centrifuge and transfer steps repeated twice for the biomass residue. The solid residue was reserved for saponification. The combined liquid extracts were subsequently dried using a rotatory evaporator and lipids were transferred to a glass vial using chloroform and acetone rinses for analysis. These lipid extracts were dried and reconstituted in chloroform/methanol (1:2, v:v). When being reconstituted, samples to be used for cIMS by direct infusion had ammonium acetate added to make them up to a concentration of 5 mM.

The solid biomass residue was treated following a method modified from Vilchèze *et al*. (135). The solid was mixed with 2 mL of saponification reagents (methanol/water (1:1, v:v) + 25 % potassium hydroxide) and heated at 120 °C for 1h. Once cooled, 2 mL of chloroform and 1.5 mL of acidification reagent (hydrochloric acid/water (1:1, v:v)) were added. The chloroform layer was transferred to a glass vial, dried and reconstituted in chloroform/methanol (1:2, v:v). When being reconstituted, samples to be used for cIMS by direct infusion had ammonium acetate added to make them up to a concentration of 5 mM. All reconstituted samples were stored at -20 °C until analysis.

2.4.5. Instrumentation

The UPLC-HRMS data was acquired using a SELECT SERIES Cyclic IMS mass spectrometer (Waters Corporation, Wilmslow, UK) with electrospray ionization (ESI) and disabled ion mobility, fitted with a Waters Acquity H class quaternary solvent manager (pumps), Waters Acquity H class UPLC Autosampler and a column oven.

The cyclic ion mobility (cIMS) data was acquired using a SELECT SERIES Cyclic IMS mass spectrometer (Waters Corporation, Wilmslow, UK) with electrospray ionization (ESI) and enabled ion mobility, fitted with a syringe pump (Harvard Apparatus, Cambridge, UK) for direct infusion.

All data was processed using MassLynx software (v4.2) (Waters Corporation).

2.4.6. Final developed UPLC conditions

A waters ACQUITY BEH C18 1.7 µm, 2.1 mm X 150 mm column, with a Waters ACQUITY BEH C18 VabGuard™ 1.7 µm, 2.1 mm X 5 mm pre-column were used for lipid separation, in a column oven at 50 °C. The flow rate was 0.2 mL/min and the injection volume 5 µL.

Gradient elution: (A) acetonitrile/water (60:40) + 5mM ammonium acetate, (B) IPA/methanol/water (90:10:0.5) + 5mM ammonium acetate.

The main gradient elution steps used for lipid separation in this project are presented in Table 2.1.

Table 2.1: *Gradient elution method showing total UPLC run time vs percentage of mobile phase (B) and gradient curve.*

Total UPLC run time (minutes)	Percentage (%) mobile phase B	Gradient curve
0	5	-
2.5	5	1
58	90	2
60	5	1

A representation of mobile phase b composition during the analysis time is displayed in Fig. 2.1.

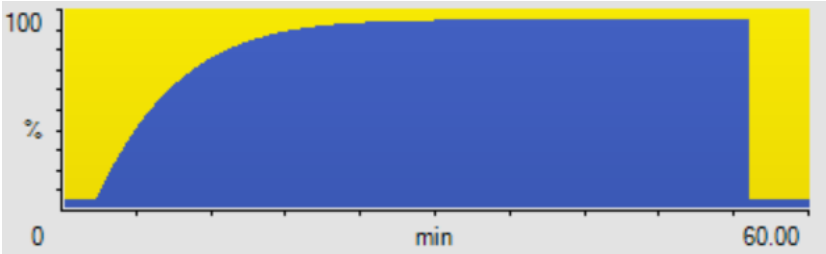

Figure 2.1: *Representation of gradient elution where blue section represents changes in mobile phase (B) composition during time.*

These were the final conditions used. The optimization is described in the Results and Discussion.

2.4.7. Final developed mass spectrometry conditions

Detection and analysis of lipids were acquired using a Waters Xevo G2-XS QToF mass spectrometer under the conditions shown in Table 2.2. The mass spectrometer was operated in negative mode with ESI ionization for analysis. To improve mass accuracy, the LockSpray tool was set to Leucine Enkephalin ($[M-H]^-$= 554.2624 m/z).

Table 2.2: *Final mass spectrometry conditions for UPLC-MS lipidomic analysis on the Waters Xevo G2-XS QToF mass spectrometer.*

MS parameters	
Ionisation mode	ESI
Polarity	Negative
Scan type	MSe
Scan range	100-2000 *m/z*
Capillary voltage	-3000 V
Sampling Cone voltage	75 V
Source Offset	80
Source temperature	120°C
Desolvation temperature	325°C
Cone gas flow	50L/h
Desolvation gas flow	580L/h
Resolution	> 22500 FWHM

These parameters were also used for detection and analysis of lipids using SELECT SERIES Cyclic IMS mass spectrometer on LC mode without enabled ion mobility. This instrument provided a resolution > 100000 FWHM.

2.4.8. Final developed cyclic ion mobility-mass spectrometry conditions

The analysis and separation of mycolic acid isomers were acquired using a Waters SELECT SERIES Cyclic IMS mass spectrometer, with enabled ion mobility, under the conditions displayed in Table 2.3. Mycolic acids were infused into the ESI at a flow rate of 10 µL/min.

Table 2.3: *Final mass spectrometry conditions for cIMS lipid isomers separation on the Waters SELECT SERIES Cyclic IMS mass spectrometer.*

MS parameters	
Ionisation mode	ESI
Polarity	Negative
Scan type	MS/MS
MS/MS transmission window	~1 *m/z*
Capillary voltage	-2000 V
Sampling Cone voltage	40 V
Source temperature	120 °C
Desolvation temperature	400 °C
Desolvation gas flow	580 L/h
N_2 cIM cell pressure	1.77 mbar
cIM separator path length	98 cm

The resolving power of cIMS for single charged ions is described by equation 2.1.

$$R \approx 65 \cdot \sqrt{N}$$

Equation 2.1: *cIM resolving power equation for a singly charged ion, where R is the resolving power and N is the number of passes that an ion has travelled around the cyclic section.*

R is the resolving power, 65 is the conservatively resolving power (calculated R of a single pass of the cIM instrument) and n is the number of passes that the ion has travelled around the cyclic device. R is measured in CCS/ΔCCS or Ω/ΔΩ.

2.5. Results and discussion

2.5.1. Bacterial conditions

The present study assessed the growth curves of mycobacteria *Gordonia amarae* when cultured in nutrient broth *vs* various minimal media with hydrophobic biomolecules as carbon sources that have been reported to induce biosurfactant production and therefore induce foaming (50), (56). Firstly, *Gordonia amarae* growth curve in nutrient media was monitored during a 5-day period to use it as control (beside blank carbon sources) for subsequent analysis. The growth profile (Fig. 2.2 a)) shows a lag phase for approximately 20 hours, with no increase in absorbance. A log phase occurred between 20 and 26 hours, in which a sharp absorbance increase (~2 AU) was observed. A final stationary phase was observed for the remainder of the experiment, during which the absorbance remained stable at around 2 AU.

Growth performance of *Gordonia amarae* was assessed in minimal media supplemented with different carbon sources, including n-hexadecane, olive oil, and a combination of n-hexadecane with acetate, at varying concentrations. Five-day growth curves of *Gordonia amarae* were obtained from cultures containing 1% olive oil, 1% n-hexadecane, 1% n-hexadecane + 0.5% acetate, 2% olive oil, 2% n-hexadecane and 10% olive oil (Fig. 2.2 b)). Distinct growth patterns were observed depending on both the type and concentration of the carbon source.

At higher hydrophobic carbon source concentrations (>2 %), growth curves exhibited strong fluctuations, characterised by sharp increases and decreases in OD_{600} values that were not consistent with real biomass or biosurfactant accumulation. This effect was particularly evident in cultures containing 10% olive oil, where the absence of a clear lag phase and rapid apparent growth were attributable to optical interference caused by excess hydrophobic carbon. Similar, though less pronounced, signal distortions were observed in cultures with 2% olive oil and 2% n-hexadecane, suggesting that OD_{600} values at elevated hydrophobic carbon source levels reflect interferences rather than true bacterial and biosurfactant proliferation. Consequently, 10% olive oil, 2% olive oil and 2% n-hexadecane media were not employed in further analysis.

In contrast, cultures grown in 1% olive oil, 1% n-hexadecane, or 1% n-hexadecane supplemented with 0.5% acetate displayed more reliable and reproducible growth profiles. Among these, *Gordonia amarae* cultures in 1% n-hexadecane reached the log phase the fastest and showed the highest overall OD_{600} measurement, indicating that it provided a suitable balance between hydrophobic carbon source content and growth and biosurfactant production measurement reliability. Contrary to the results observed by Pagilla *et al*. (2002) (50), who reported that co-supplementation with acetate accelerated growth and led to an earlier transition to the stationary phase compared to n-hexadecane alone, in the present study acetate addition appeared to sustain moderate growth but did not enhance performance beyond that of n-hexadecane as a sole carbon source. This discrepancy may be due to methodological differences in biomass quantitation. Pagilla *et al*. (2002) employed gravimetric determination of total suspended solids (TSS) after autoclaving, whereas in the present work bacterial growth was monitored by OD_{600} measurements. Both approaches are widely used but subject to limitations that may explain the differing observations. Gravimetric methods can be confounded by non-cellular mass, such as precipitates formed during autoclaving or residual carbon sources that contribute to dry weight (136). OD_{600} readings are susceptible to interference from light-scattering hydrophobic substrates and cell aggregation (137).

Results from Fig. 2.2 b). underscore the importance of optimising media composition when cultivating *Gordonia amarae* for further analysis, such as biosurfactant quantitation or lipidomic analysis.

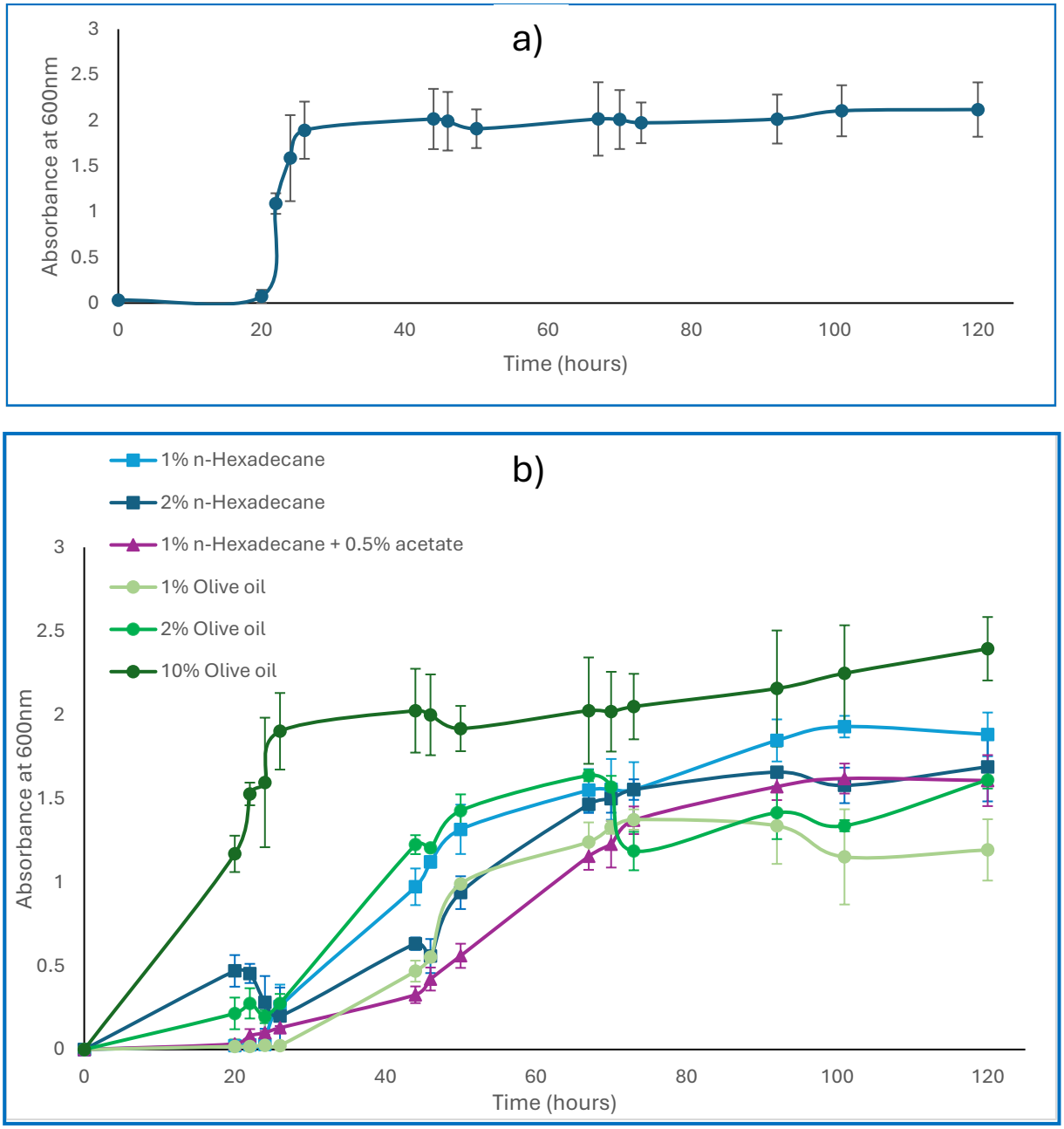

Figure 2.2: *A) Five-day growth curve of Gordonia amarae in nutrient broth. Data represent the mean of three biological replicates, with error bars indicating ± standard deviation. B) Gordonia amarae growth curves from 5-day cultures containing 1% n-hexadecane (light blue), 2% n-hexadecane (dark blue), 1% n-hexadecane + 0.5% acetate (purple), 1% olive oil (medium green), 2% olive oil (light green) and 10% olive oil (dark green). Data represent the mean of three biological replicates for each growth media, with error bars indicating ± standard deviation*.

2.5.2. Ultra-Performance Liquid Chromatography – High Resolution Mass Spectrometry (UPLC-HRMS) method development

Reference mycolic acids (250 mg/L) from *Mycobacterium tuberculosis* were analysed using the Xevo G2-XS QTof mass spectrometer. Conditions were varied until optimum results were obtained. These methods are described in Table 2.4. The developed method was then applied to analyse extracted mycolic acids from *Gordonia amarae* for final optimisation.

Table 2.4: *UPLC-HRMS method development process including methods applied from the literature and optimized methods T. Sakallioglu et al. (75), de Kok et al.(138) and de Kok et al. modified methods parameters, highlighting the changes from the original method.*

Parameters	**T. Sakallioglu *et al.* method**	**de Kok *et al.* method**	**de Kok *et al.* modification I**	**de Kok *et al.* modification II**
Mobile phase (A)	Acetonitrile/water (60:40) + 10 mM ammonium formate and formic acid (0.1%)	Acetonitrile/water (60:40) + 5 mM ammonium formate	Acetonitrile/water (60:40) + 5 mM **ammonium acetate**	Acetonitrile/water (60:40) + 5 mM **ammonium acetate**
Mobile phase (B)	2-propanol/acetonitrile (90:10) + 10 mM ammonium formate and formic acid (0.1%)	1-butanol/acetonitrile/water (90:10:0.5) + 5 mM ammonium formate	1-butanol/acetonitrile/water (90:10:0.5) + 5 mM **ammonium acetate**	**2-propanol/methanol**/water (90:10:0.5) + 5 mM **ammonium acetate**
Capillary voltage	-2000 V	-3000 V	-3000 V	-3000 V
Sampling Cone voltage	30 V	75 V	75 V	75 V
Source Offset	80	80	80	80
Source temperature	120 °C	120 °C	120 °C	120 °C
Desolvation temperature	550 °C	300 °C	300 °C	300 °C
Cone gas flow	50 L/h	50 L/h	50 L/h	50 L/h
Desolvation gas flow	600 L/h	580 L/h	580 L/h	580 L/h

Investigation of reference mycolic acids was firstly done following method proposed by T. Sakallioglu *et al*. (75) for separation of lipid classes related to mycobacteria, in which a mixture of 2-propanol/acetonitrile (90:10) + 10 mM ammonium formate and formic acid (0.1 %) was used as main eluting solvent. In this method, the main mass spectrometer parameters employed were a negative capillary voltage of 2000 V, a sampling cone voltage of 30 V and a desolvation temperature of 550 °C. However, due to the impossibility to find mycolic acids peaks in the LC chromatogram and the high background noise observed in the mass spectrum (Fig. 2.3 top left corner), it was discarded and a second method was tried. This may have occurred as Sakallioglu *et al*. (75) were analysing a different genus of mycobacteria, with a different chain length of mycolic acids.

de Kok *et al*. (2021) (138) developed a UHPLC-MS method for the separation of highly hydrophobic lipids in which a 1-butanol/acetonitrile/water (90:10:0.5, v:v:v) + 5 mM ammonium formate solution was utilized as principal eluting solvent. There were also some differences in the mass spectrometer parameters compared to the previously described method. The negative capillary and sampling cone voltages were increased to 3000 V and 75 V respectively, and the desolvation temperature was decreased to 300 °C. Nevertheless, the presence of ammonium formate produced a mass pattern in the mass spectrum that interfered with the mycolic acids mass peaks (Fig. 2.3 top right corner).

The de Kok *et al*. (2021) (138) MS parameters were kept and the LC method was modified. The ammonium formate was substituted in both mobile phases by ammonium acetate, resulting in de Kok *et al*. modification I. Although the resulting mass spectrum showed no interferences, a high background noise affected the relative abundance of the mycolic acids. The interference was also seen in the LC chromatogram. This was caused by the large proportion of 1-butanol utilised (Fig. 2.3 bottom left corner).

A final method was developed keeping mobile phase (A) and using the same mass spectrometry parameters. Mobile phase (B) was replaced with a 2-propanol/methanol/water (90:10:0.5, v:v:v) + 5 mM ammonium acetate solution. This method successfully produced a LC chromatogram with lower background noise and high abundance peaks for *Mycobacterium tuberculosis* reference mycolic acids (Fig. 2.3 bottom right corner).

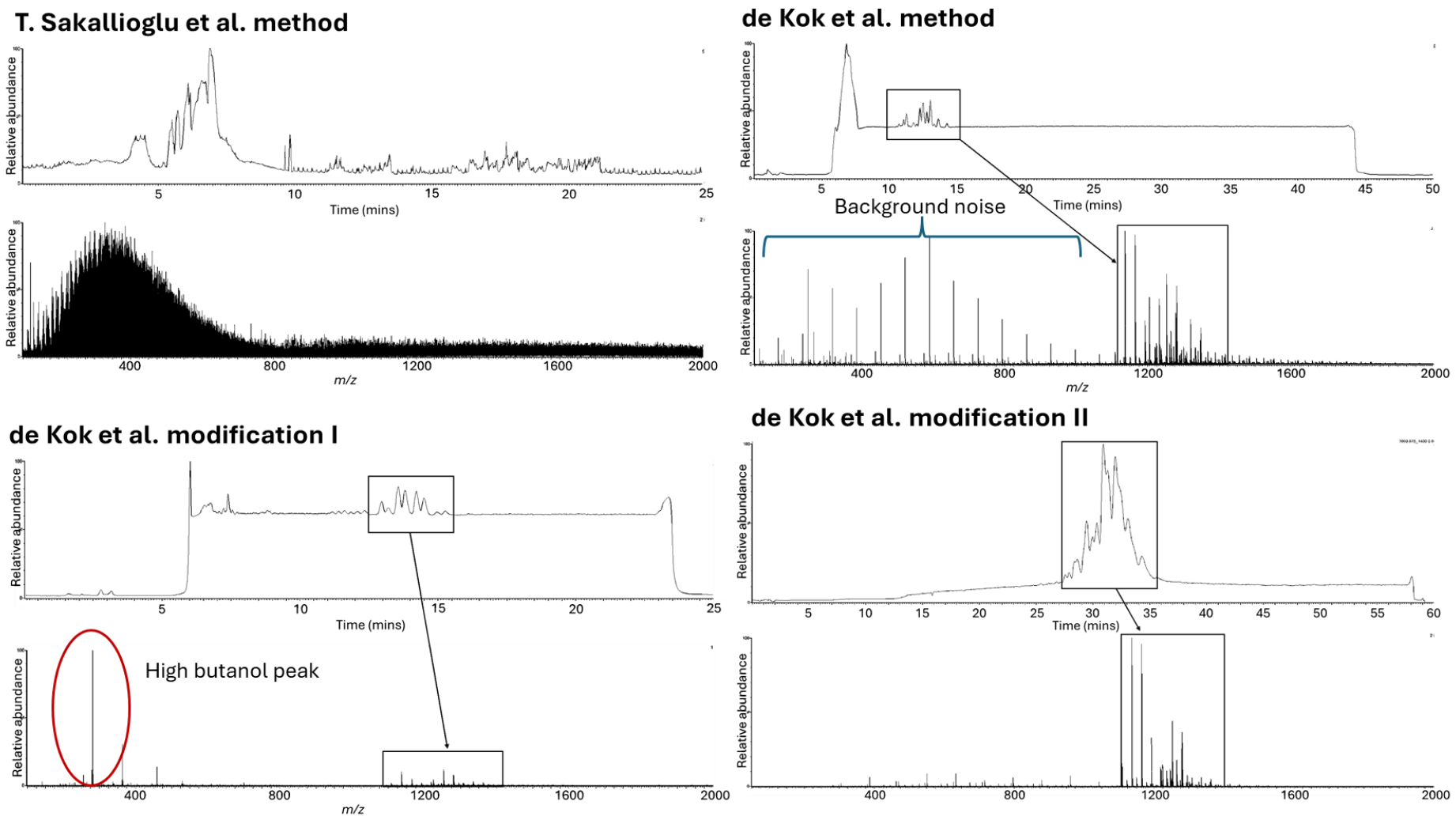

Figure 2.3: *LC-MS chromatograms and mass spectra produced during analysis of reference MA from Mycobacterium tuberculosis for method development. (Top left) initial results by using Sakallioglu et al. (75) method showing high background noise in mass spectrum. (Top right) result obtained using de Kok et al. (2021) method showing formate peaks interfering in the mass spectrum. (Bottom left) de Kok et al. modification I displaying a high interference of 1-butanol in the chromatogram and mass spectrum. (Bottom right) de Kok et al. modification II demonstrating low interference and high sensitivity.*

Reference MA from *Mycobacterium tuberculosis* (bovine strain) are 75 – 91 carbons long (139) and have a *m/z* range between 1,090 and 1,300. In contrast, *Gordonia amarae* MA consist of fatty acids chains with 47 – 76 carbon long (66) and have a lower *m/z* range (550 - 880) (67), although not all strains of a bacterial species would be expected to contain the same abundance of all their lipids. Due to their chain length differences, MA from *Gordonia amarae* were expected to elute earlier than those from *Mycobacterium tuberculosis*. Consequently, the developed method was required to be able to separate and analyse with low interference both higher- and lower-mass MAs. Further method development was carried out and two elution gradients were assessed.

The first elution gradient utilised a maximum amount of 95 % of the main eluting solvent (mobile phase B: 2-propanol/methanol/water (90:10:0.5, v:v:v) + 5 mM ammonium acetate) with a gradient curve of 2 and a run time of 60 minutes. The second elution gradient reduced the amount of the main eluting solvent to 90%, with an increased gradient curve of 4 and a run time of 50 minutes. Changes are described in Fig. 2.4.

Elution Gradient Method I		
Total UPLC run time (minutes)	Percentage (%) mobile phase B	Gradient curve
0	5	-
2.5	5	1
58	95	2
60	5	1

Elution Gradient Method II		
Total UPLC run time (minutes)	Percentage (%) mobile phase B	Gradient curve
0	5	-
2.5	5	1
48	90	4
50	5	1

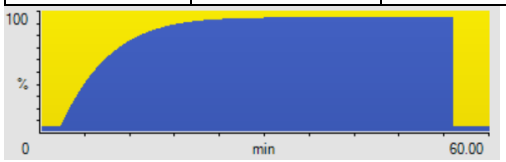

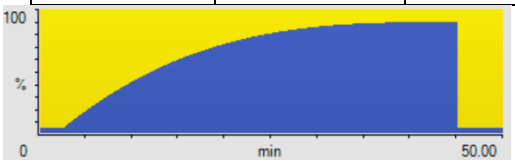

Figure 2.4: *(Top) table of gradient elution methods showing total UPLC run time vs percentage of mobile phase (B) and gradient curve. (Bottom) schematic of mobile phase B composition (blue) vs time of Elution Gradient Method I (left) and Elution Gradient Method II (right).*

Fig. 2.4 (bottom) shows a representation of mobile phase B composition during the analysis time. Here the change in addition rate of mobile phase B and the difference in its final composition percentage is displayed.

Extractable and saponified MA from *Gordonia amarae* were analysed using de Kok *et al.* modification II (Table 2.4), applying both elution gradients. Fig. 2.5 presents chromatograms and mass spectra with minimal background noise in both cases, showing a MA *m/z* range of 715–830, grouped into ion sets, with *m/z* 771.72 being the most abundant ion. A difference in elution times was observed: *Gordonia amarae's* MA eluted between 18 and 22 minutes using Elution Gradient Method I (Fig. 2.5 a)), whereas they eluted between 28 and 35 minutes using Elution Gradient Method II (Fig. 2.5 b)). Elution Gradient Method II resulted in a better-resolved chromatogram for these MA, enhancing peak separation and clarity.

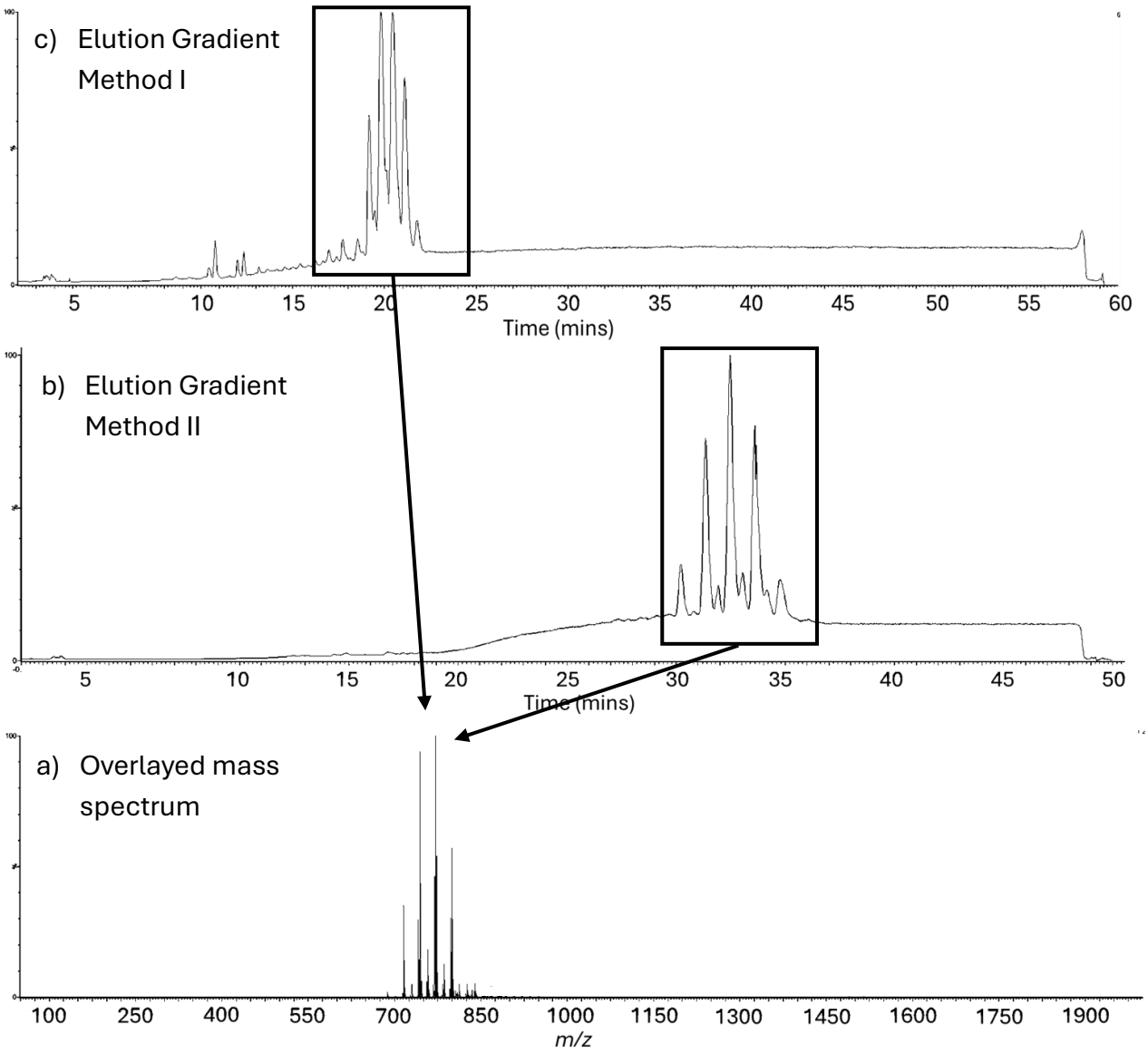

Figure 2.5: *LC-MS chromatograms for MA from Gordonia amarae obtained using a) Elution Gradient Method I, b) Elution Gradient Method II, and c) the overlayed mass spectrum for chromatogram a) between 18 and 23 minutes and b) between 28 and 36 minutes.*

Similarly, *Mycobacterium tuberculosis* reference mycolic acids were analysed applying both elution gradients. With the Elution Gradient Method I, MA eluted between 27 and 38 minutes (Fig. 2.6 a), whereas with the Elution Gradient Method II, MA elution began after 38 minutes (Fig. 2.6 b). Elution Gradient Method II produced a chromatogram with broad peaks extending to the end of the run time, suggesting that some MA may not have eluted. Mass spectra analysis further confirmed this, as the second elution gradient showed missing MA, indicating that certain MA were still retained in the LC column at the end of the run.

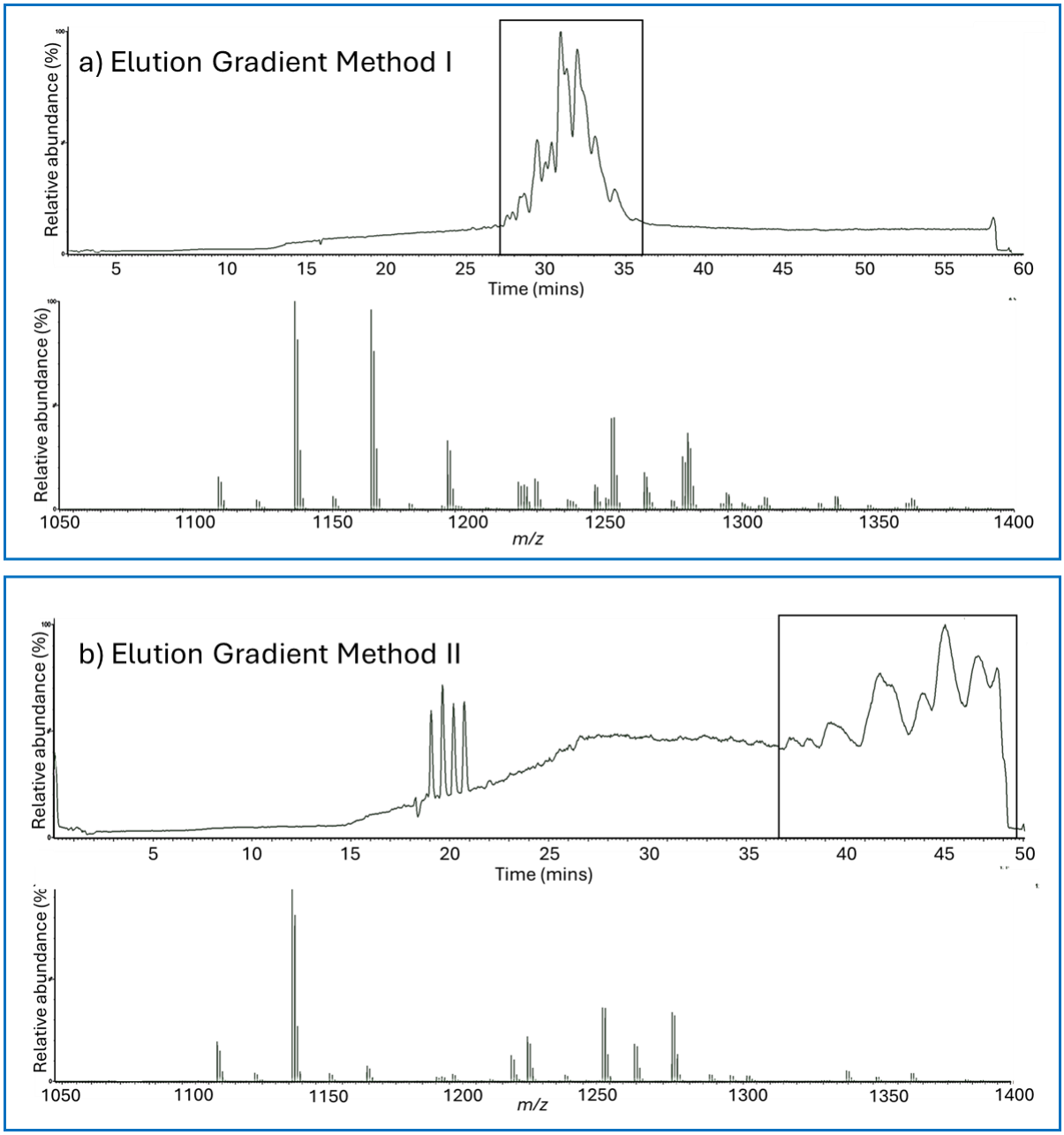

Figure 2.6: *Chromatograms and mass spectra for reference MA from Mycobacterium tuberculosis obtained using Elution Gradient Method I (a) and Elution Gradient Method II (b).*

Elution Gradient Method II achieved high-resolution separation of MA from *Gordonia amarae*, demonstrating its suitability for targeted analysis of this species. However, its elution strength was insufficient for complete recovery of the higher-mass MA characteristic of *Mycobacterium tuberculosis*. In contrast, Elution Gradient Method I enabled comprehensive elution and separation across the full MA mass range for both bacteria. Accordingly, Elution Gradient Method I was selected for the analysis of mixed bacterial extracts, where broad lipid coverage is required. Elution Gradient Method II was retained as a rapid, resource-efficient approach for analysing MA from single bacterial cultures of *Gordonia amarae*, reducing analysis time.

2.5.3. Cyclic Ion mobility (cIMS)

During cIMS method development, MA ions from *Gordonia amarae* were individually selected (at a narrow ion transmission window of approximately 1 *m/z*) for isomer separation analysis. Before and after a multiple-passes sequence, the instrument was set to MS/MS mode and transfer collision energy was applied to monitor the fragmentation pattern of the precursor MA.

The analysis started on most abundant lipid ion (*m/z* 771.72), which was fragmented prior to cIMS separation, showing two main fragments (*m/z* 253.22 and 281.25) with very similar relative abundancies. When *m/z* 771.72 was subjected to several passes, the abundance of the fragments was observed to decrease. This was mainly noticed for the fragment with *m/z* 253.22, which disappeared after 40 passes (Fig. 2.7). This effect was also detected for other MA.

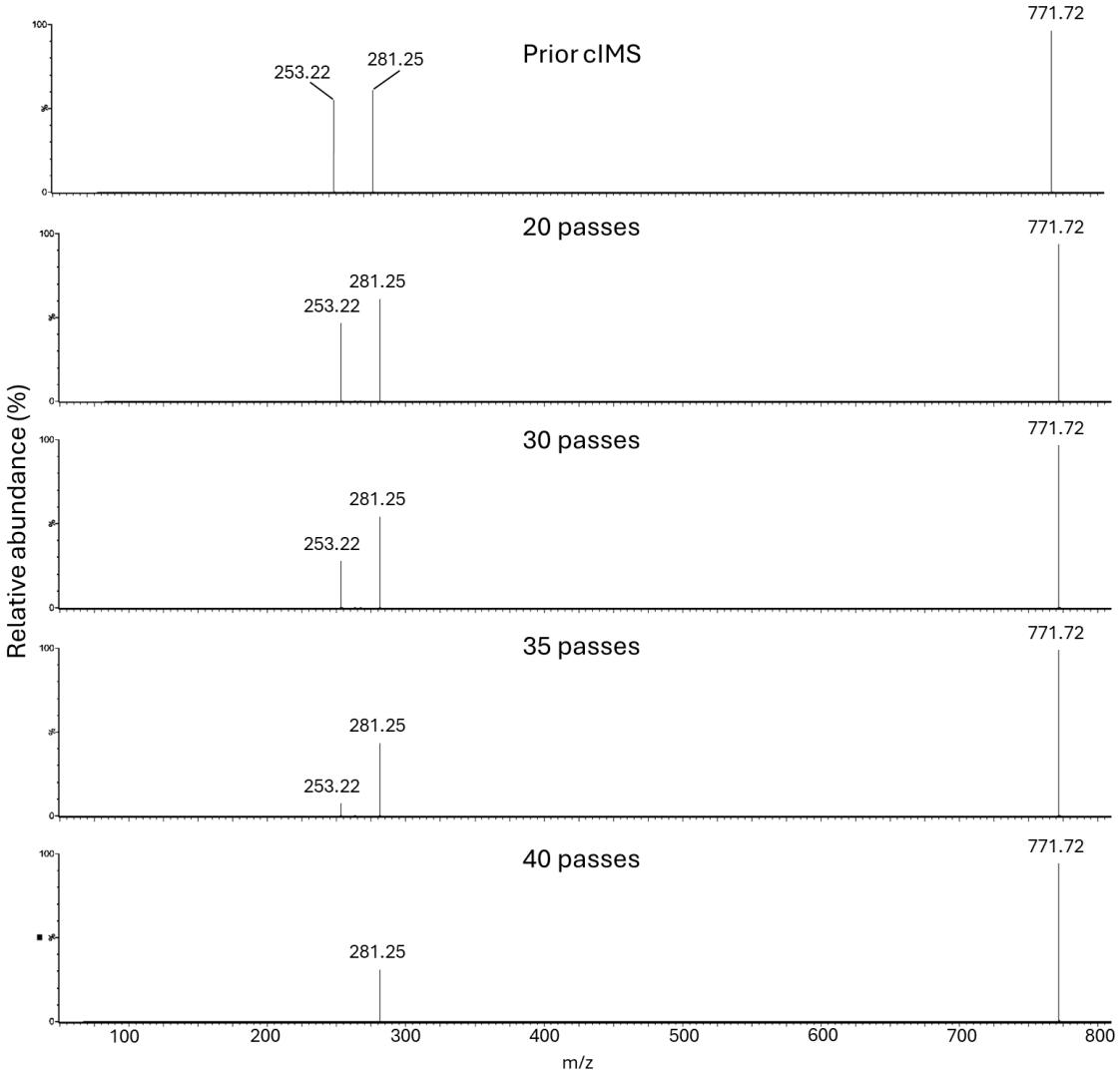

Figure 2.7: *Fragmentation pattern of m/z 771.72 mycolic acid from Gordonia amarae between 0 and 40 passes of the cyclic device at a collision energy of 44 V. Note the decrease in fragment abundance with increasing number of passes.*

Intensity loss was found to be caused by the use of high radiofrequency (RF) parameters during the IMS cycle. RF increased with increasing number of passes, resulting in less transmission of lower mass fragments (140). To solve this problem, default MS/MS ramp mode on RF ramp settings was changed to manual and MS/MS ramp final was focused on *m/z* 200 (300 less than default), successfully improving low mass transmission.

Another effect observed during cIMS method development was “wrap-around”. Wrap-around is a phenomenon that occurs when higher mobility separated isomer ions overtake slower mobility ions, compromising the separation and resulting in loss of information. Wrap-around phenomenon can also occur when a single ion (with no separated isomers) undergoes an excessive number of passes, causing ion elongation, where the front of the ion catches up the with its tail.

This phenomenon was perceived when the most abundant lipid ion from *Gordonia amarae* (*m/z* 771.72) was subjected to more than 70 passes (Fig. 2.8). Beyond 70 passes, the highest mobility conformation began overtaking the lower mobility one. Fig. 2.8 shows how *m/z* 771.72 peaks start broadening and deteriorating after 75 passes compared to 70 passes of the cyclic device.

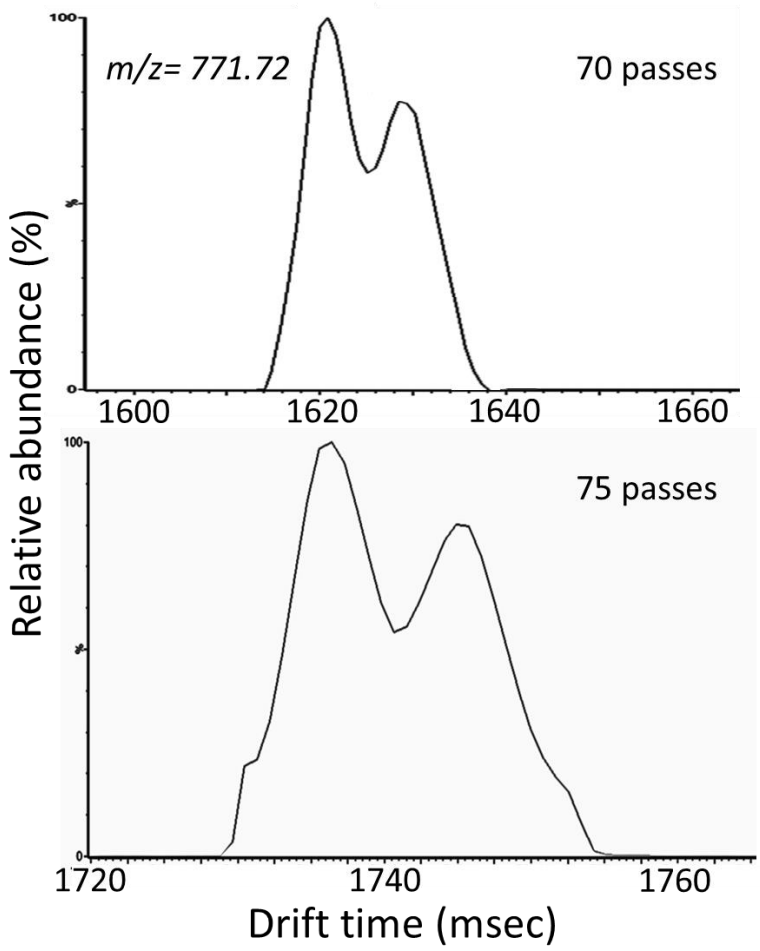

Figure 2.8: *ATDs comparison of MA m/z = 771.72 from Gordonia amarae after 70 passes (top) and 75 passes (bottom) of the cyclic device.*

Similarly, cIMS analysis of the MA with *m/z* 773.74 (+2 *m/z* of the most abundant ion) initially resolved three conformations after 20 passes. Beyond 20 passes, the highest mobility conformation began overtaking the lower mobility one. Fig. 2.9 shows how *m/z* 773.74 isomer peaks start broadening and deteriorating after 25 passes compared to 20 passes of the cyclic device.

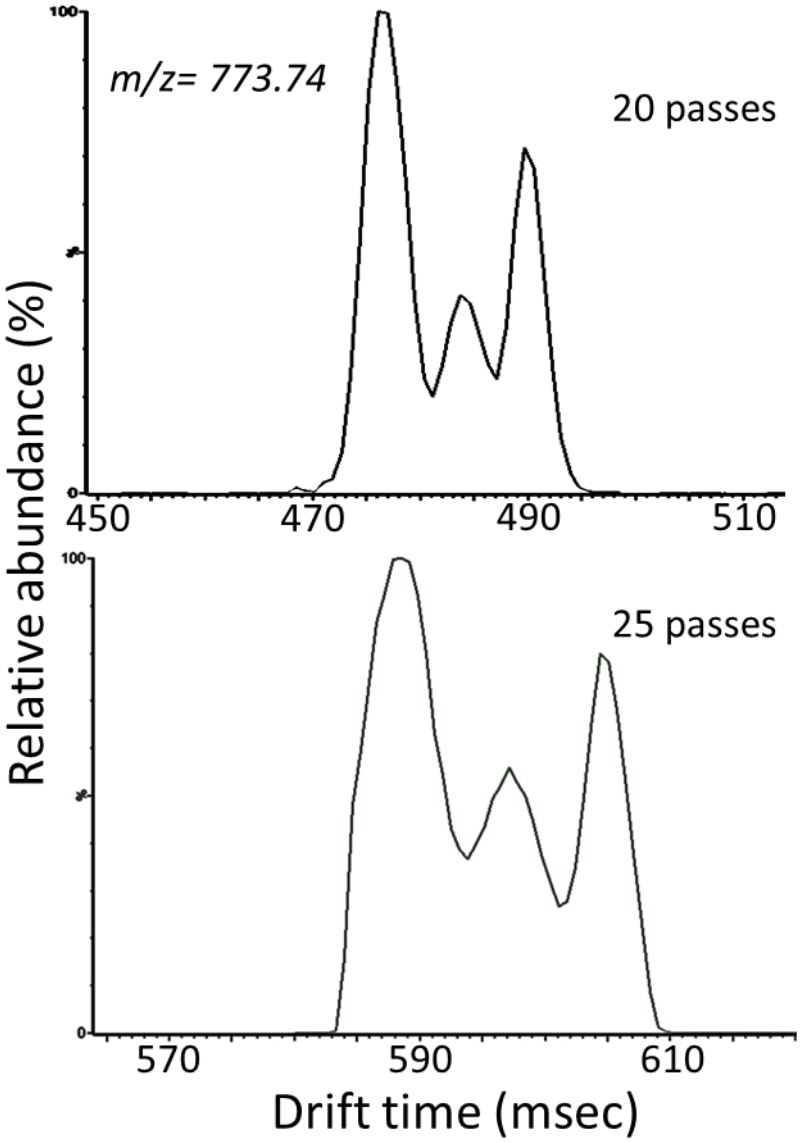

Figure 2.9: *ATDs comparison of MA m/z = 773.74 from Gordonia amarae after 70 passes (top) and 75 passes (bottom) of the cyclic device.*

To avoid separation loss due to wrap-around, it was established that cIMS analysis of lipid ions with one or no separated conformations should be limited to a maximum of 70 passes before any further analysis, such as fragmentation. For lipid ions exhibiting three conformations after 20 passes, the analysis should be stopped at this point, allowing each conformation to be individually isolated in the isomer device for subsequent cIMS analysis (further 50 passes, to a maximum of 70 passes) and fragmentation.

Reference MAs from *Mycobacterium tuberculosis* were also analysed using cIMS. Due to their larger size compared to the MAs from *Gordonia amarae*, a longer analysis time was required. A maximum of 75 passes was established, beyond which wrap-around effects became noticeable.

2.6. Conclusions

2.6.1. Bacterial conditions

Gordonia amarae was successfully grown in minimal media supplemented with varying concentrations of carbon sources during a five-day period. Growth curves were generated for cultures containing 1% olive oil, 1% n-hexadecane, 1% n-hexadecane + 0.5% acetate, 2% olive oil, 2% n-hexadecane, and 10% olive oil. Among these conditions, cultures supplemented with 1% n-hexadecane, 1% olive oil, and a combination of 1% n-hexadecane with 0.5% acetate demonstrated optimal growth with minimal interference, allowing for clear and reproducible growth curves.

2.6.2. LC-MS methods

Commercially available reference mycolic acids (MAs) from *Mycobacterium tuberculosis* were utilised to develop a liquid chromatography – mass spectrometry method (LC-MS). Initially, Sakallioglu *et al.* (75) and de Kok *et al.* (138) LC parameters were adapted until a final method was developed. The optimised eluting solvents contained: acetonitrile/water (60:40) + 5mM ammonium acetate (mobile phase A), IPA/methanol/water (90:10:0.5) + 5mM ammonium acetate (mobile phase B). Gradient parameters chosen for MA extracted from mixed bacterial cultures or high-mass MA: 5% mobile phase B was held for 2.5 minutes, then it was increased up to 95% over 55.5 minutes at a gradient curve of 2, and finally returned to initial conditions with 5% mobile phase B in 2 minutes at a gradient curve of 1. Gradient parameters chosen for MA extracted from single bacterial cultures of *Gordonia amarae*: 5% mobile phase B was held for 2.5 minutes, then it was increased up to 90% over 45.5 minutes at a gradient curve of 4, and finally returned to initial conditions with 5% mobile phase B in 2 minutes at a gradient curve of 1. MS parameters were based on the method described by de Kok et al (138).

The final LC-MS developed method successfully displayed a LC chromatogram and mass spectrum with low background noise and high abundance MAs. Reference MAs from *Mycobacterium tuberculosis* and MAs from *Gordonia amarae* were observed to have a *m/z* range of 1090–1300, and 715–830 respectively.

2.6.3. Cyclic IMS (cIMS)

High mobility resolution and low interference fragmentation MA isomer analysis for MA from *Gordonia amarae* and *Mycobacterium tuberculosis* was accomplished by using cIMS. To achieve this, wrap-around phenomenon was avoided by limiting the number of passes of the cyclic device for MA ions. For *Mycobacterium tuberculosis* MA ions, a maximum of 75 passes was stablished. *Gordonia amarae* MA ions with one or no separated conformations were limited to a maximum of 70 passes. For *Gordonia amarae* MA ions displaying three conformations after 20 passes, separation was stopped at this point, and each conformation was individually isolated in the cyclic device before undergoing further cIMS analysis (additional 50 passes, to a total of 70 passes).

Proper fragmentation and improvement of reduced transmission of low-mass fragments after high number of passes was obtained by implementing a manual MS/MS RF ramp mode, with initial and final *m/z* settings of 50 and 200, respectively.

Chapter 3: Separation of mycolic acid isomers by cyclic ion mobility-mass spectrometry

Chapter adapted from a publication in *Rapid Communications in Mass Spectrometry* (Doi: https://doi.org/10.1002/rcm.9917).

Authors: Hector de las Heras Prieto[1], Laura M Cole[1], Sarah Forbes[1], Martin Palmer[2], Rachel Schwartz-Narbonne[1].

[1]Biomolecular Research Centre, Sheffield Hallam University, Sheffield, UK. [2]Waters Corporation, Wilmslow, UK

3.1. Introduction

The genus *Mycobacterium* encloses more than 190 species that contain high concentrations of mycolic acids in their cell walls (117). Certain mycobacterial species are human pathogens; for example, *Mycobacterium bovis* is the causative agent of tuberculosis, which has a high mortality if left untreated (117). Other non-pathogenic mycobacteria, such as *Gordonia*, are associated with environmental issues. For example, *Gordonia amarae* is a known contributor to foaming events in activated sludge (AS) reactors of wastewater treatment plants, producing biosurfactants that alter the process efficiency (50) and consequently, leading to environmental contamination by the release of non-properly treated wastewater into the environment .

Mycolic acids (MA) are long chain fatty acids found in the two outer mycobacteria membrane leaflets, including trehalose mono/di-mycolate and glucose monomycolate (60). These are composed of an alkyl side chain and a hydroxyl group (2-alkyl, 3-hydroxy) (59) and can be covalently or non-covalently bound to the mycobacterial cell wall (59), providing essential functions in the biosynthesis and permeability of the wall. Although MA are structurally unique, they are not exclusive to mycobacteria, being found in other related genera such as *Nocardia*, *Rhodococcus* and *Corynebacterium* (60). The main classes of MA in mycobacteria are alpha-, keto- and methoxy- MA.

MA in *Mycobacterium bovis* provide mechanical support, osmotic protection and contribute towards both antimicrobial resistance (62) and immune recalcitrance through supporting bacterial survival inside macrophages (63). Since they are also essential in the pathogenicity of the bacteria, the MA biosynthesis path has been targeted as an action site of anti-TB drugs and for the wider development of antimycobacterial drugs (64). MA in *Gordonia* are mostly constituted of an even-number of carbon chain length with a total number of carbon atoms ranging from 40 to 66. They typically have between 0 and 5 double bonds or unsaturations (66), however, this is strain dependent. Lipidomic analysis is therefore a powerful technique to identify bacterial species (126) and to identify targets for lipid-based treatments (64). Previous studies show considerable interest in elucidating MA isomers employing ion mobility (141), however, to date, cIM has not been applied to this question. cIM therefore has the potential to provide an improved method for identification, isolation and fragmentation of MA isomers.

3.1.1. Cyclic Ion Mobility (cIM)

Ion mobility spectrometry (IMS) is a powerful technique; when coupled with a mass spectrometer it allows the possibility of a multidimensional characterization of the analytes (91), providing further separation of isobaric species. There are a wide range of IMS systems with different modes of operation such as: drift tube ion mobility spectrometry (DTIMS), trapped ion mobility spectrometry (TIMS), traveling wave ion

mobility spectrometry (TWIMS), field asymmetric waveform ion mobility spectrometry (FAIMS), etc. (91). TWIMS was introduced in 2006 by Waters Corporation (142) and has been further developed to the modern cyclic ion mobility systems.

cIM provides selectable mobility resolution and permits experiments combining numerous functions such as mobility selection, ion storage and IMS^n (97). The cIM is designed as a quadrupole/cyclic ion mobility/time-of-flight instrument which uses travelling waves (TWs) for mobility separation in a closed loop region (97). Ions that enter the cIM section "surf" on a wavefront, while waves that are passing through the section repeatedly overtake them. The mobility of the ions determines how frequently they are surpassed by the waves, with lower mobility ions being overtaken more frequently and taking longer to traverse the section than higher mobility ions, leading to IM separation (97).

The cIM device consists of an entry/exit array situated at the bottom of the cIM loop in the middle of a pre- and post- array ion store areas which make possible a wide range of ion mobility sequences (99). Ion packets coming from the trap are held in the array until a change in voltage allows them to enter the cyclic section where IM separation occurs (97). After separation ions can be ejected directly to the post-array store and then to the ToF analyser. Data acquisition can be triggered or not depending on the experimental aim. Other ejection functions can be applied such as IMS^n, where multiple isomers can be resolved for a single ion; individual mobility separated isomers of interest are ejected back to the pre-array store and held while the rest get ejected to ToF without acquiring. Stored ions can then be re-injected to the cyclic section with or without activation and further separation/ejection steps can be selected, allowing the possibility of IM separation of fragment ions (if activation was selected) and further fragmentation of selected fragment ions and so on. Most of these functions were used for data acquisition in this project.

3.2. Aim

The main aim of this study was to develop and apply a high-resolution mass spectrometry–based lipidomic approach using cyclic ion mobility mass spectrometry (cIM-MS) to achieve enhanced separation and characterisation of mycolic acid isomers from selected mycobacterial species.

3.3. Objectives

The objectives of this study were to apply cyclic ion mobility mass spectrometry for the analysis of mycolic acids from *Gordonia amarae* and *Mycobacterium bovis*, to optimise ion selection and multi-pass mobility separation for the resolution of previously

unresolved isobaric mycolic acid isomers, and to perform mobility-resolved fragmentation for structural characterisation.

3.4. Experimental

3.4.1. Bacteria strains

Gordonia amarae (NCIB 11222 strain) was purchased from NCIMB LTD.

3.4.2. Materials

Reference mycolic acids from *Mycobacterium bovis* were bought from Avanti Polar Lipids. Ammonium acetate was obtained from Honeywell. Potassium hydroxide, ammonium formate, acetone, hydrochloric acid and methanol (UHPLC grade) were obtained from Fisher Scientific™. Chloroform (HPLC grade) was obtained from Macron Fine Chemicals™. Nutrient broth was obtained from Oxoid Ltd. 18MΩ water was collected from Millipore S.A.S. water systems.

3.4.3. Bacterial growth

Mycobacteria *Gordonia amarae* was grown in nutrient agar and broth. 20 mL liquid cultures were grown at 30 °C for 1 week.

3.4.4. Bacterial lipid extraction

Extractable MA isolation was achieved following Alshehry *et al.* (134). In brief, biomass was harvested and centrifuged (10 min, 2000 rpm). The biomass was transferred to a glass tube and freeze-dried. 15 mL of 1-butanol/methanol (1:1, v:v) + 5 mM ammonium formate was added, and the mixture was vortexed, sonicated (1 h) and centrifuged (10 min, 2000 rpm). The liquid layer was transferred to a round bottom flask; the previous steps were repeated twice for the biomass residue. The solid residue was reserved for saponification. The liquid was dried using a rotatory evaporator and transferred to a glass vial using chloroform and acetone rinses. These lipid extracts were dried and reconstituted in chloroform/methanol (1:2, v:v) + 5 mM ammonium acetate.

The solid residue was saponified to extract MA covalently bonded to the cell wall following a method modified from Vilchèze *et al.* (135). Biomass residue was mixed with 2 mL of saponification reagents (methanol/water, 1:1, v:v + 25 % potassium hydroxide) and heated (120 °C for 1 h). Once cooled, 2 mL of chloroform and 1.5 mL of acidification reagent (hydrochloric acid/water, 1:1, v:v) were added. The chloroform layer was

extracted, dried (40 °C under a flow of nitrogen) and reconstituted in chloroform/methanol (1:2) + 5 mM ammonium acetate.

Prior to analysis, the extractable and saponified MA extracts were combined to a total *Gordonia* mycolic acid extract. Samples were stored at -20 °C until analysis.

Samples of reference mycolic acids from *Mycobacterium bovis* were prepared to a concentration of 250 µg/mL in chloroform/methanol (1:2, v:v) + 5 mM ammonium acetate and stored at -20 °C until analysis.

3.4.5. Instrumentation

All data were acquired using a SELECT SERIES Cyclic IMS mass spectrometer (Waters Corporation, Wilmslow, UK) with electrospray ionization (ESI) and by direct infusion of the sample using a syringe pump (Harvard Apparatus, Cambridge, UK) at a flow rate of 10 µL/min. MS full scan acquisitions in time-of-flight and ion mobility modes for MA from both bacteria were carried out in negative mode with the following instrument settings: capillary voltage, 2 kV; cone voltage, 40 V; source temperature, 120 °C; desolvation temperature, 400 °C; desolvation gas flow rate, 580 L/hour and N_2 cIM cell pressure, 1.77 mbar. The cIM separator (98 cm path length) had a resolving power (R) of ≈ 65 x (n. of passes)$^{0.5}$ ($\Omega/\Delta\Omega$) (97).

Data were acquired and processed using MassLynx software (v4.2) (Waters Corporation).

3.4.6. Cyclic IM isomer separation and fragmentation

Target lipid *m/z* values were chosen based on a MS full-scan acquisition. The instrument was then switched to ion mobility enabled MS/MS mode where the quadrupole was centred on the target precursor *m/z* value with a narrow transmission window of ions (~1 *m/z* units), manual MS/MS RF ramp mode was selected, and initial and final *m/z* ramp was set to 50 and 200, respectively. The following travelling wave parameters were applied: cyclic velocity and array velocities were adjusted to 375 m/s, static height was set to 22 V.

Separation of isomers was achieved by manually increasing the number of passes of the selected ions in the cyclic ion mobility (cIM) device. Unwanted background ions were ejected from the device to improve signal to noise and allow higher resolving powers to be achieved with reduced interference. When multiple isomers were observed for a given precursor, each ion mobility (IM) separated isomer was further targeted using a multi-step process using IM isolation as described previously (97). To achieve this, individual MA ions were selected by the quadrupole and passed into the cIM, individual isomer conformations were isolated within the cIM whilst the other (unwanted) conformations

were ejected and discarded from the cyclic device. Following this selection, additional passes were used for further separation, and the selection and ejection steps were repeated (where necessary) to fully isolate each conformation for fragmentation. If no isomer separation was observed after elevated separation times for *Gordonia amarae* and *Mycobacterium bovis* (70 and 75 passes, circa 1.5 – 3.5s respectively), no further separation or IM isolation was attempted. As the ion mobility resolving power of the instrument increases with the square root of the number of passes (97), it would therefore require a significant increase in the number of passes required and hence resolution to observe any unresolved features. So, at this point, these analytes were considered to have only one (resolvable) conformation under the conditions employed. Finally, mass and mobility-isolated ions were fragmented by applying a post-mobility transfer collision energy between 38 and 46 V depending on the lipid carbon chain length for *Gordonia amarae* MA, and between 65 and 75 V for *Mycobacterium bovis* MA.

3.5. Results and discussion

3.5.1. *Gordonia amarae* MA cIM isomer separation

Mycolic acids from *Gordonia amarae* strains are C_{31} – C_{54} (*m/z* 550 – 880) (67). However, not all strains of a bacterial species would be expected to contain the same abundance of all their lipids. This is seen in Fig. 3.1, in which the bacteria tested had the main distribution of MAs between *m/z* 715 and 830. The MAs are typically observed clustered into sets (sets a) to d)). The presence of ions separated by 2 *m/z* within a set corresponds to a variation in the number of double bonds within the aliphatic chains. The separation of 28 *m/z* between sets corresponds to an increase of two carbons within the aliphatic chains of the MAs. The most abundant MA species was observed at *m/z* = 771.72, found in set c).

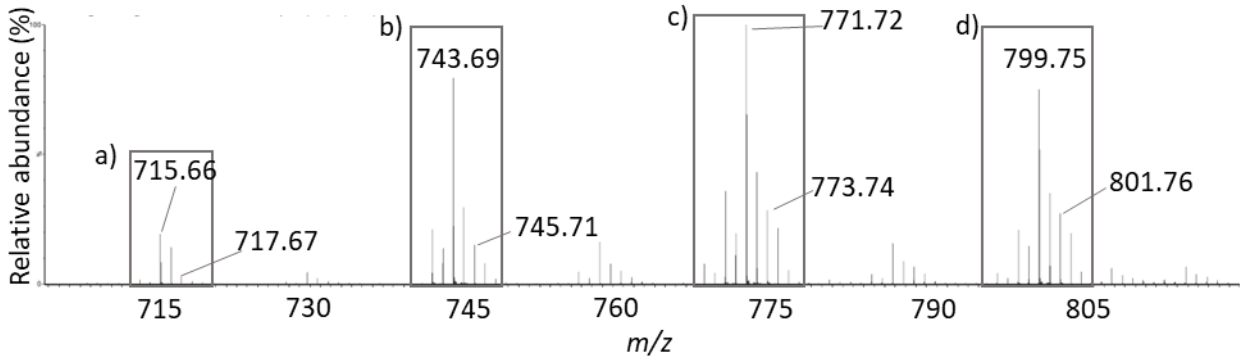

Figure 3.1: *Full scan mass spectrum of Gordonia amarae from m/z 700 – 820; showing four main sets of mycolic acids (a) to d)).*

A survey mobility analysis was carried out on all ions in MA set c) individually (*m/z* 769 – 774) to investigate the presence of possible isobaric compounds and their isomer patterns.

Two isobaric isomers were resolved from the *m/z* = 771.72 mycolic acid ion (Fig. 3.2). Separation was initially visible after 30 passes when a slight shoulder appeared. This second conformation was partially separated after 70 passes of the cyclic device, which corresponds to a resolving power of ~544 $\Omega/\Delta\Omega$. Each cIM separated peak was then post-mobility fragmented in isolation (Fig. 3.2). First isomer produced a main fragment at *m/z* = 281.25. Second isomer main fragment was observed at *m/z* = 253.22.

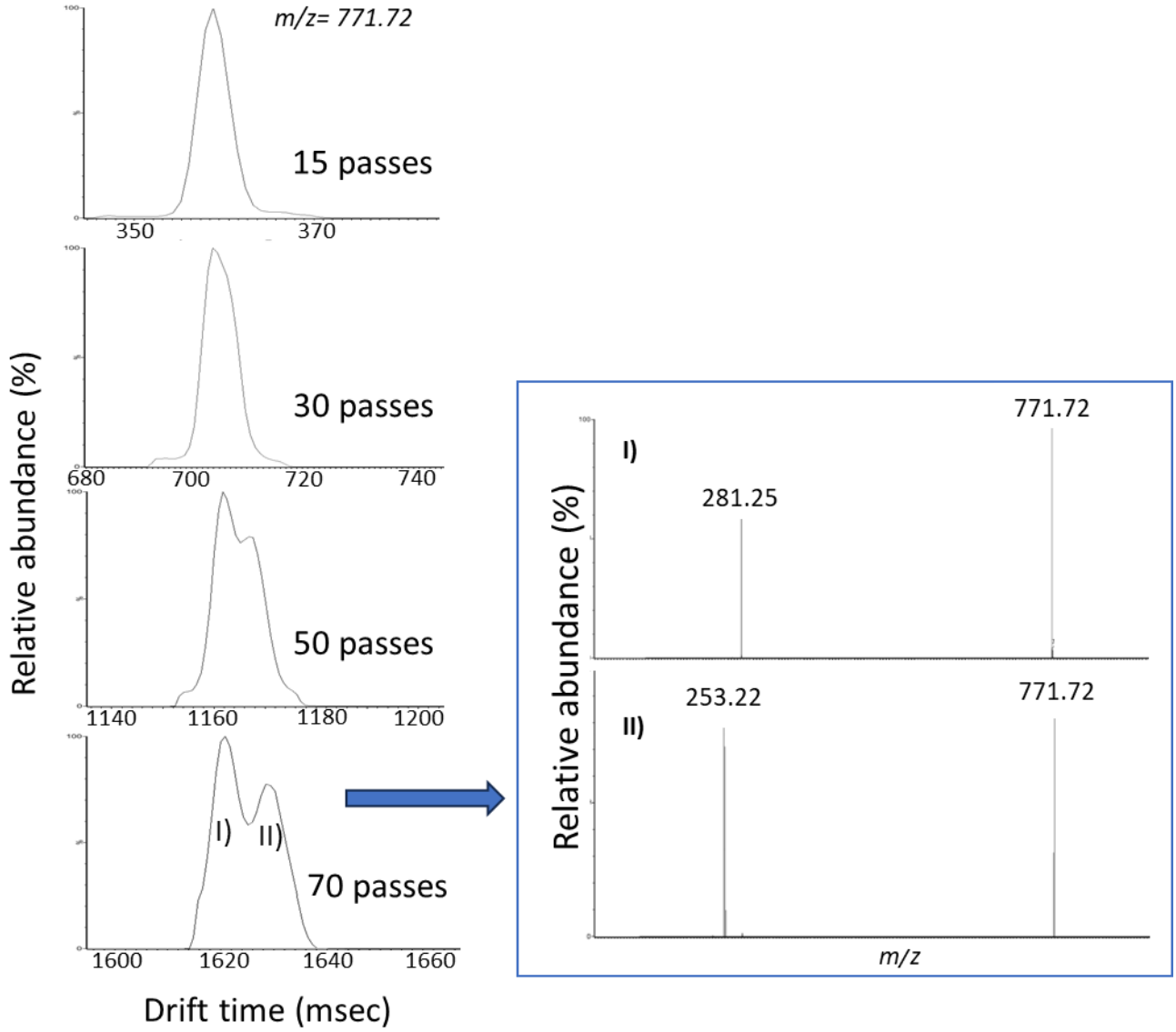

Figure 3.10: *Cyclic IM separation process from 15 to 70 passes for m/z 771.72 mycolic acid from Gordonia amarae. Two isomers are observed from a single peak after 70 passes of the cyclic device. Fragmentation of the two separated peaks occurred with a transfer collision energy of 44 V (right box).*

Similar analysis was conducted for +2 *m/z* of the most abundant ion in set c), *m/z* = 773.74, to investigate if there was any difference compared to the most abundant ion.

Three isomers were resolved after 20 passes of the cyclic device, from the initially single peak in the arrival time distribution (ATD) for the MA ion at *m/z* = 773.74 as observed in Fig. 3.3. After 6 passes of the cIM device, a second conformation was resolved from the main peak. A third isomer was visible after 14 passes, and 3 isomers were resolved (albeit not baseline resolved) after 20 passes, corresponding to a resolving power of ~291 $\Omega/\Delta\Omega$.

As resolution is mobility dependant, each compound and isomer requires a different separation time and hence a different number of passes. More passes were needed to separate isobaric compounds from *m/z* = 771.72 MA (70 passes) than for *m/z* = 773.74 (20 passes), in a first instance.

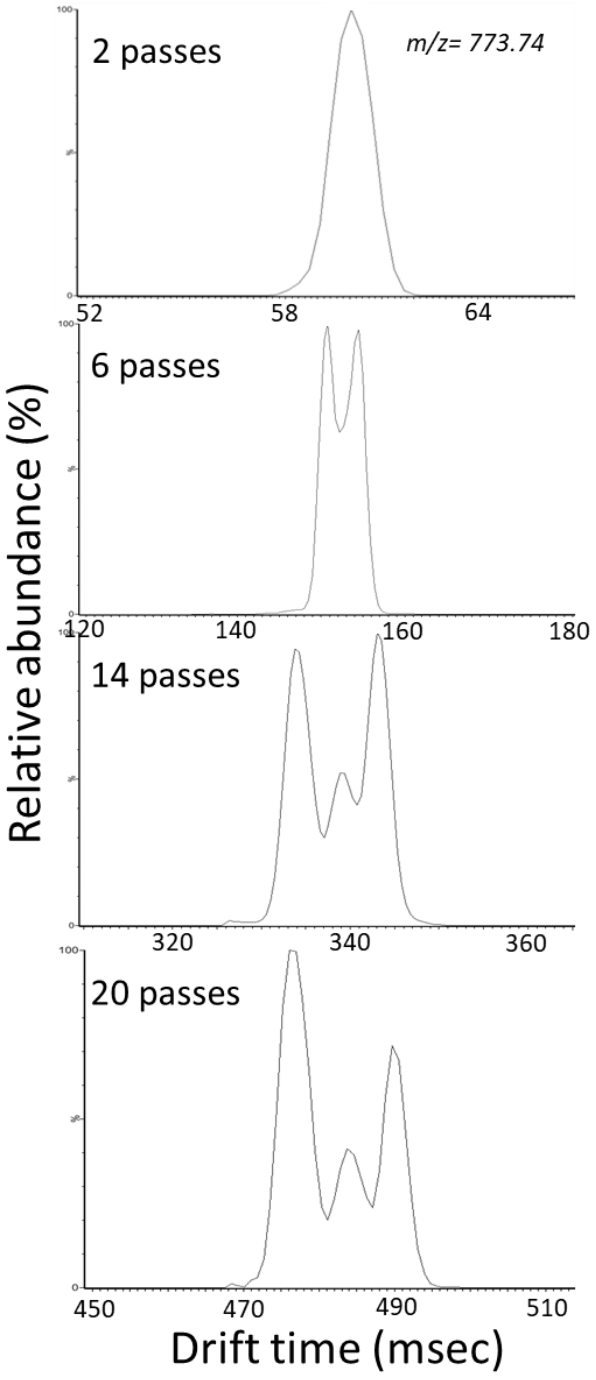

Figure 3.3: cIM separation process from 2 to 20 passes for MA m/z 773.74 from Gordonia amarae. Three isomers are resolved from an initial single peak.

Beyond 20 passes, the most mobile MA isomer caught up with the least mobile ion and therefore separation was lost as the cyclic mobility device was full (wrap-around). To avoid this, each individual isomer resolved from the *m/z* = 773.74 lipid ion was isolated in the mobility device and the other conformations were discarded. Each isolated isomer was subjected to additional 50 passes of the cyclic device (70 passes in total) and then fragmented using post-mobility transfer collision energy. As exhibited in Fig. 3.4, other conformations (labelled a) to f)) were resolved from the first 3 observed peaks. Post-mobility fragmentation showed four main fragments (*m/z* = 253.22, 255.23, 281.25 and 283.26), with each individual fragment corresponding to a separate conformation. Possible structures for the fragments are proposed (Fig. 3.4). Fragment *m/z* = 253.22 could correspond to a chemical formula of $C_{16}H_{29}O_2$ (2 unsaturations) with a mass accuracy of -6.32 ppm when the observed mass is compared to its theoretical mass. Fragment *m/z* = 281.25 could correspond to a chemical formula of $C_{18}H_{33}O_2$ (2 unsaturations) giving a mass accuracy of -6.40 ppm when the observed mass is compared to its theoretical mass; this would also correspond to the fragments observed for *m/z* = 771.72. Fragments *m/z* = 255.23 and 283.26 structures could be similar to the ones from *m/z* = 253.22 and *m/z* = 281.25, with 1 unsaturation, corresponding to $C_{16}H_{31}O_2$ and $C_{18}H_{35}O_2$ respectively. As the fragments' possible chemical formulas are within a ± 10.00 ppm limit, they can be considered a potential match.

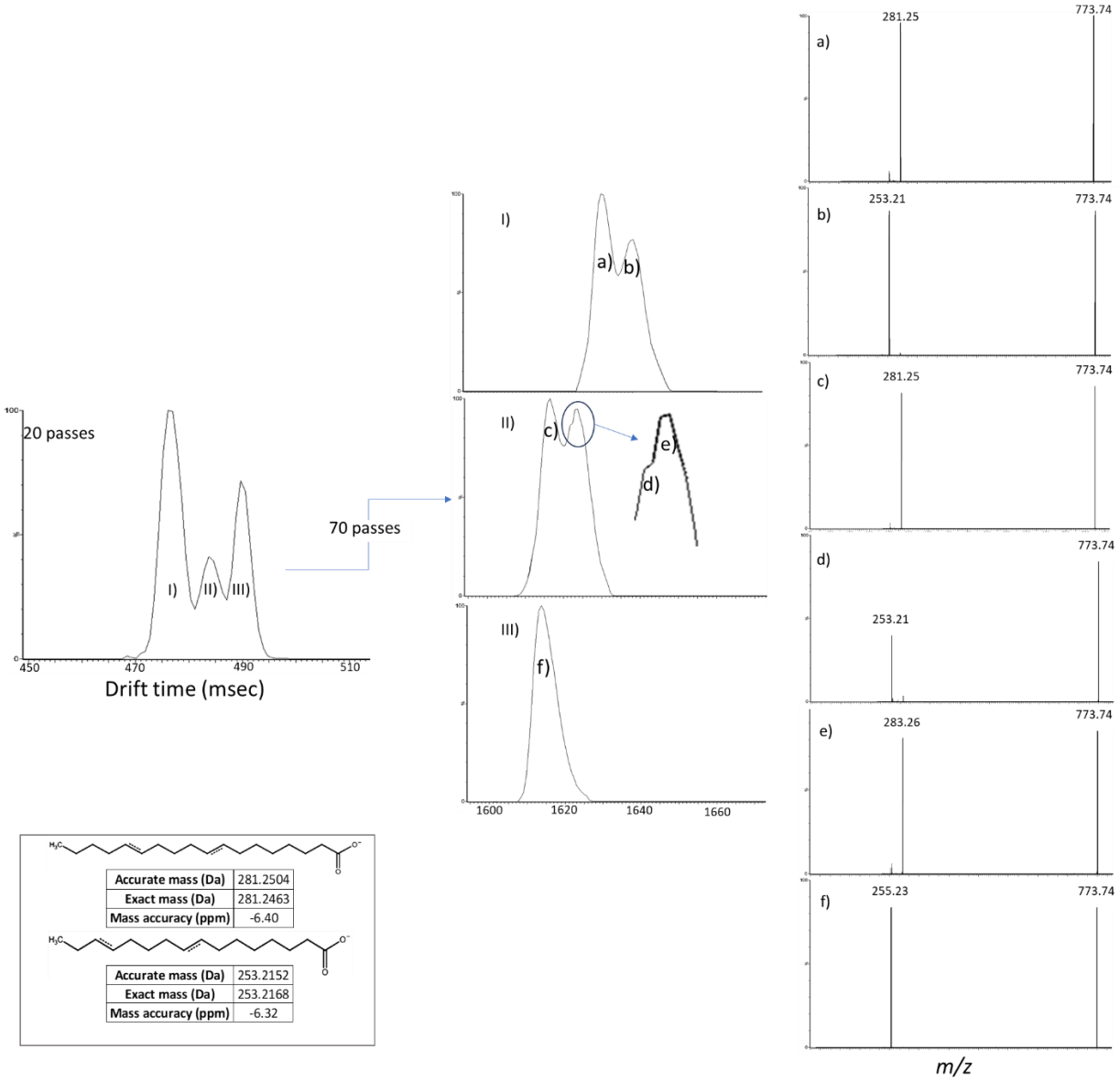

Figure 3.4: *Extracted arrival time distributions (ATDs) for m/z 773.74 after 20 passes of the cyclic device (top left), further separation of resolved peaks I), II) and III) (middle), fragmentation of the separated peaks with a transfer collision energy of 44 V (right), and possible main fragment structures (bottom left). Note the position of unsaturations cannot be determined via this method.*

Further analysis was done on *m/z* = 773.74 lipid ion due to the possibility that one of the mobility separated conformations was a result of $^{13}C_2$ isotope from the most abundant ion in the set (*m/z* = 771.72) and not an isomer of *m/z* = 773.74. When the ATD of both MA ions were compared after 20 passes of the cyclic device (Fig. 3.5), a direct overlay of *m/z* = 771.72 over the resolved peak I) from *m/z* = 773.74 was observed. After peak I) was isolated and subjected to 50 additional passes of the cyclic device (70 passes in total), similar separation and ATD to *m/z* = 771.72 was shown. ATD comparison together with identical fragmentation patterns (Fig. 3.2 and Fig. 3.4) confirm that the origin of this conformation was a *m/z* = 771.72 $^{13}C_2$ isotope.

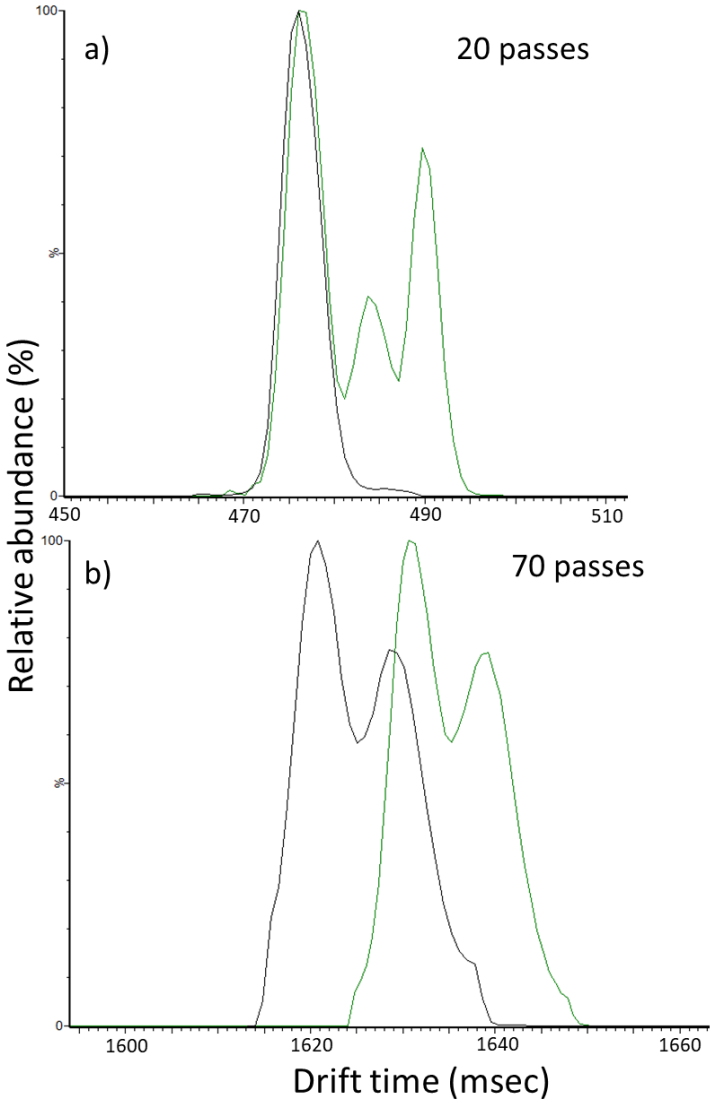

Figure 3.5: *ATDs comparison of MA m/z =771.72 (black) and m/z =773.74 (green) from Gordonia amarae after 20 passes of the cyclic device (a)), and ATDs comparison of MA m/z =771.72 (black) and isolated ion mobility separated peak I) from m/z =773.74 (green), after 70 passes of the cyclic device (b)).*

The remaining MA ions in set c) (see Fig. 3.1 for full scan) from *Gordonia amarae* were also analysed by cIM. No further resolvable conformations were found for *m/z* = 769.75 and 770.76, (-2 *m/z* and -1 *m/z* of the most abundant ion of the set respectively). *m/z* = 772.78 (+1 *m/z* of the most abundant ion of the set) displayed a very similar separation and fragmentation process to *m/z* =771.72, with two conformations separated after 70 passes of the cyclic device and *m/z* = 281.25 as the main fragment of the first conformation and *m/z* = 253.21 as the main fragment of the second conformation. *m/z* = 774.80 had an identical separation and fragmentation process to *m/z* = 773.74; three isomers were resolved after 20 passes and then three extra conformations were separated after 50 additional passes, with *m/z* = 253.22, 255.23, 281.25 and 283.26 fragments present. *m/z* = 772.78 and *m/z* = 774.80 are ^{13}C isotopes from *m/z* = 771.72 and *m/z* = 773.74, hence, identical separation is expected and observed.

Based on the obtained results, the most abundant ion and the ion +2 *m/z* within all the MA sets from *Gordonia amarae* from *m/z* = 715 to 830 were selected for cIM isomer separation and fragmentation analysis. The results are summarized in Table 3.1. An ion was reported as having 1 (resolvable) conformation if no isomers were observed after 70 passes.

Table 3.1: *Mycolic acid isomers observed in Gordonia amarae. The most abundant ion of each set of MA was marked with *. Predicted chemical formulas for MA ions with at least one ^{13}C were marked with **. Number of double bonds for predicted chemical formulas include unsaturations and C=O from acid and keto groups. Where multiple fragments were present, the most abundant fragment was underlined. If isolation and further separation was required to show other conformations, these were denoted as conformation X.2 and X.3.*

Lipid ion observed mass	Predicted formula	Mass accuracy (ppm)	n° of double bonds	MA group	n° of conformations	n° of passes	Transfer CE (V)	Fragments *m/z*					
								Conf. 1		Conf. 2			Conf. 3
								1.1	1.2	2.1	2.2	2.3	
715.6593*	$C_{47}H_{87}O_4$	-1.59	4	a)	1	70	38	253+281					
717.6736	$C_{47}H_{89}O_4$	-3.46	3		3	70	42	253+281		253			255
743.6932*	$C_{49}H_{91}O_4$	1.97	4	b)	2	70	40	281	253				
745.7065	$C_{49}H_{93}O_4$	-1.19	3		6	70	42	281	253	281	253	283	255
769.7081	$C_{51}H_{93}O_4$	0.93	5	c)	1	70	42	253+281					
770.7095	$^{**}C_{51}H_{93}O_4$				1	70	42	253+281					
771.7237*	$C_{51}H_{95}O_4$	0.86	4		2	70	44	281	253				
772.7264	$^{**}C_{51}H_{95}O_4$				2	70	45	281	253				
773.7379	$C_{51}H_{97}O_4$	-1.02	3		6	70	44	281	253	281	253	283	255
774.7418	$^{**}C_{51}H_{97}O_4$				6	70	44	281	253	281	253	283	255
799.7542*	$C_{53}H_{99}O_4$	-0.17	4	d)	2	70	42	281	253				
801.7630	$C_{53}H_{101}O_4$	-8.71	3		6	70	46	281	253	281	253	283	255

The most abundant ion of each set of MA have 1-2 conformations, while the MA +2 *m/z* have 3-6 conformations. The number of passes required for isomer separation is greater for the most abundant MA in each set than for the +2 *m/z* MA (Table 3.1) which suggests that isomers from the most abundant ions are structurally more similar to each other than those from +2 *m/z*. *m/z* = 281.25 and 253.22 were the main fragments present in all lipid ions. Fragments *m/z* = 255.23 and 283.26 fragments were also present in some lipid isomer confrontations from +2 *m/z* MA, although not always simultaneously. These distinctive isomer patterns could provide potential biomarker targets to identify the presence of *Gordonia amarae* in wastewater treatment plants.

3.5.2. *Mycobacterium bovis* MA cyclic IM isomer separation

The same process was applied to *Mycobacterium bovis* as a comparison to MA lipids in *Gordonia amarae*. *Mycobacterium bovis* MA are C_{75} – C_{91} and therefore are found between *m/z* = 1090 and 1300. They are composed of three MA classes: alpha, keto and methoxy (63). Two sets from each class of mycolic acids were selected for analysis from an MS full-scan spectrum (Fig. 3.6). As with the previous analysis of *Gordonia amarae*, the most abundant ion of each set and those with 2 *m/z* greater than the most abundant ion were chosen for cIM analysis.

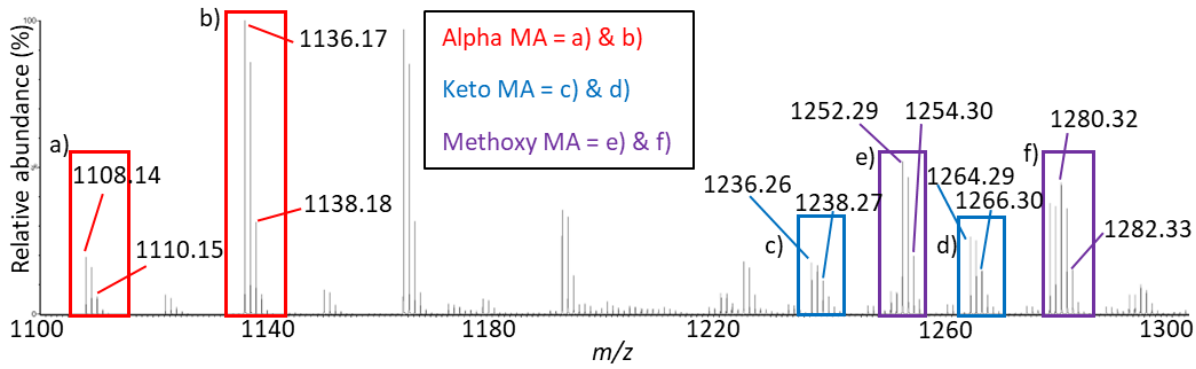

Figure 3.6: *Full mass spectrum of reference mycolic acids from Mycobacterium bovis, showing the three different classes of MA.*

Analysis was performed following the same methods applied to MA lipids in *Gordonia amarae* (Fig. 3.7). As MA from *Mycobacterium bovis* are larger than MA from *Gordonia amarae*, a longer analysis was required. All selected MA from to *Mycobacterium bovis* were analysed with 75 passes of the cyclic device, corresponding to a resolving power of ~563 $\Omega/\Delta\Omega$.

cIM analysis from alpha (sets a) and b)) and methoxy (sets e) and f)) MA did not resolve any conformations during the separation process, as seen in Fig. 3.7 for *m/z* = 1136.17 (alpha) and 1252.29 (methoxy), suggesting no isobaric compounds could be resolved under the applied conditions. Two conformations were separated from keto-MA (sets c) and d)). For example, in *m/z* = 1236.26 (Fig. 3.7; Table 3.2), a shoulder was visible after 50 passes of the cyclic device and two isomers were partially resolved after 75 passes, although they were not baseline resolved.

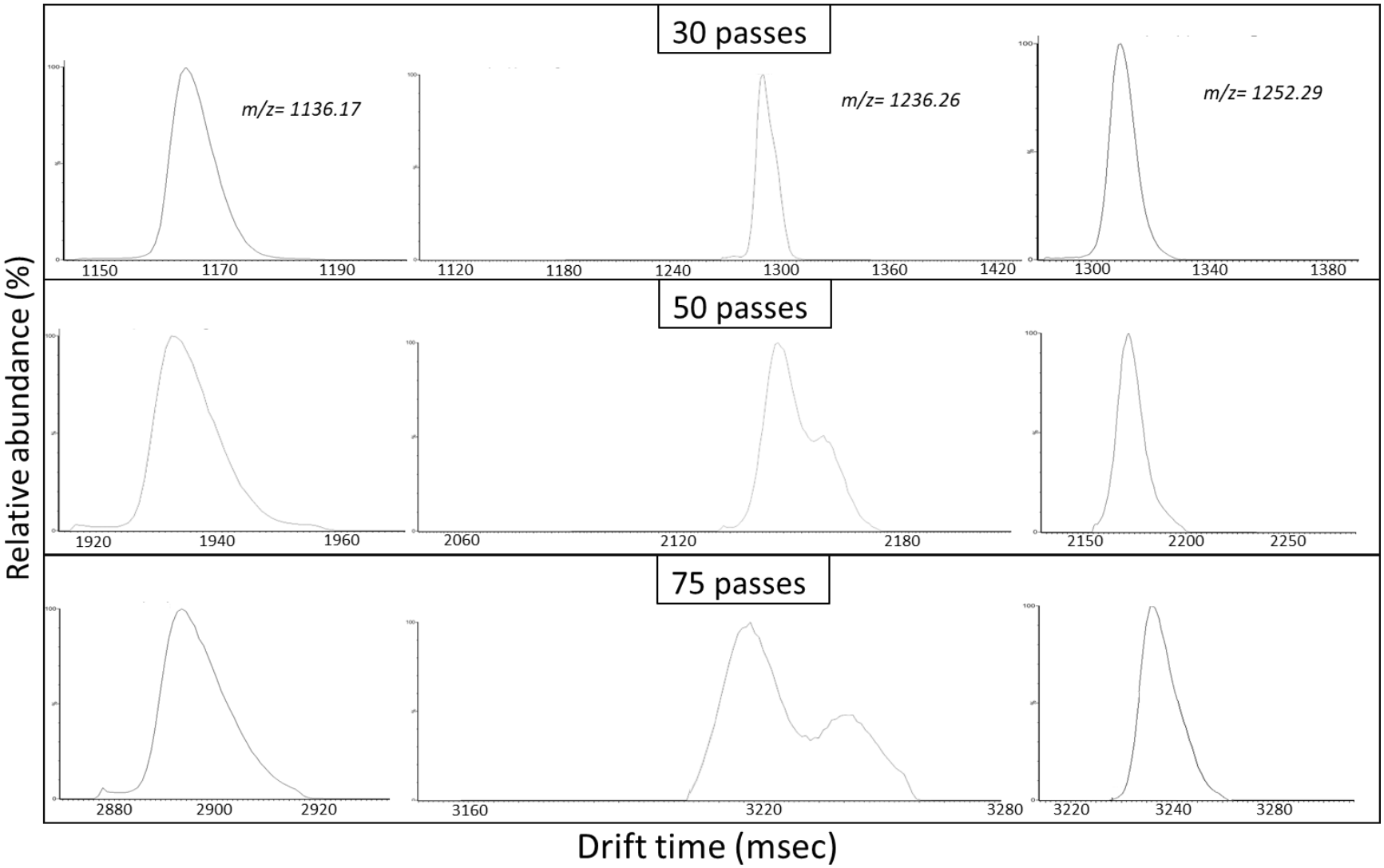

Figure 3.7: *Cyclic IM separation process from 30 to 75 passes for m/z 1136.17 (left), 1236.26 (middle) and 1252.29 (right) alpha, keto and methoxy mycolic acids, respectively, from Mycobacterium bovis.*

Three different MA (*m/z* = 1136.17, 1236.26, and 1252.29) were fragmented, including each individually resolved isomer for *m/z* = 1236.26. Similar analysis was performed for the other selected MA (Fig. 3.6), and results were collected in Table 3.2. The fragment *m/z* = 395.38 is present in all MA. An additional *m/z* = 367.35 fragment was also observed in the MA analytes that have a parent mass less than *m/z* = 1254; it is the most abundant fragment in the two measured MA with a parent mass less than *m/z* = 1136.

Fragment *m/z* = 395.38 could correspond to a chemical formula of $C_{26}H_{51}O_2$ with a mass accuracy of -1.03 ppm when the observed mass is compared to its theoretical mass. Fragment *m/z* = 367.35 could correspond to a chemical formula of $C_{24}H_{47}O_2$ giving a mass accuracy of -3.28 ppm when the observed mass is compared to its theoretical mass. As both fragments' possible chemical formulas are within a ± 10.00 ppm limit, they can be considered a potential match.

The chemical formulae shown in Table 3.2 for observed mycolic acids are derived from their mass accuracies, which are within ± 5 ppm limit for parent ions, and can therefore be considered a potential match. Future research could include the addition of thin layer chromatography (TLC) to explore mycolic acid decoration diversity.

Table 3.2: *MA isomers resolved from Mycobacterium bovis after 75 passes of the cyclic device. The most abundant ion of each set of MA was marked with *. Number of double bonds for predicted chemical formulas include unsaturations and C=O from acid and keto groups. Where multiple fragments were present, the most abundant fragment was underlined.*

Lipid ion observed mass	Predicted formula	Mass accuracy (ppm)	n° of double bonds	Lipid class	n° of conformations	n° of passes	Transfer CE (V)	Fragments *m/z*	
								Conf. 1	Conf. 2
1108.1356*	$C_{76}H_{147}O_3$	0.52	3	alpha	1	75	65	367+395	
1110.1504	$C_{76}H_{149}O_3$	-0.25	2	alpha	1	75	65	367+396	
1136.1705*	$C_{78}H_{151}O_3$	3.68	3	alpha	1	75	65	367+395	
1138.1862	$C_{78}H_{153}O_3$	3.71	2	alpha	1	75	65	367+395	
1236.2562*	$C_{84}H_{163}O_4$	0.86	3	keto	2	75	70	367+395	367+395
1238.2683	$C_{84}H_{165}O_4$	-2.01	2	keto	2	75	70	367+395	395
1252.2897*	$C_{85}H_{167}O_4$	2.6	2	methoxy	1	75	70	367+395	
1254.3032	$C_{85}H_{169}O_4$	0.89	1	methoxy	1	75	70	367+395	
1264.2874*	$C_{86}H_{167}O_4$	0.76	3	keto	2	75	70	395	395
1266.3054	$C_{86}H_{169}O_4$	2.61	2	keto	1	75	70	395	
1280.3174*	$C_{87}H_{171}O_4$	-0.26	2	methoxy	1	75	75	395	
1282.3325	$C_{87}H_{173}O_4$	-0.69	1	methoxy	1	75	75	395	

Ion mobility analysis of a wider range of parent masses from *Mycobacterium bovis* and closely related species could reveal whether this pattern holds more widely, thus providing insight into biosynthetic pathways of these lipids and potentially into lipid-targeting medical treatments. Future work could also extend cIM analysis to other mycobacteria, such as *Mycobacterium smegmatis*, *Mycobacterium tuberculosis* H37Rv and other non-tuberculous *Mycobacterium*.

3.6. Conclusion

Mycolic acid (MA) isomers from the foaming-related bacteria *Gordonia amarae* and pathogenic bacteria *Mycobacterium bovis* were successfully resolved from lipid ions that appeared as single peaks in a full scan mass spectrum. This was achieved by individually targeting the most abundant ions within each set of MA, as well as the ion 2 *m/z* higher, with the quadrupole and performing multiple passes of the cyclic ion mobility device. Not only did this allow separation of previously unresolved isomers, it additionally allowed fragmentation of each conformation separately. The patterns of isomerization and fragmentation varied between the two bacterial species, potentially suggesting biosynthetic differences. This technique offers the possibility to obtain a higher level of separation to get an improved lipidomic characterisation, which could help future projects in the analysis and understanding of lipids isomers from vital bacteria. Results obtained in this study from *Gordonia amarae* and *Mycobacterium bovis* could aid in designing foaming prevention processes and in understanding how isomers could be used for the development of new anti-tuberculosis drugs, respectively.

Chapter 4: Foaming quantitation and lipidomic characterisation of foaming related bacteria *Gordonia amarae*

4.1. Introduction

Foaming events are a significant operational challenge in the activated sludge reactors of wastewater treatment plants (WWTPs) and are frequently reported worldwide (23), (143). Foam consists of gas bubbles enclosed by thin liquid films (lamellae) and arises from the dispersion of a gas within a liquid (144).

The main conditions required for foam formation are the presence of a surface-active compound capable of reducing surface tension, and a source of gas bubbles (such as the air supplied in aeration tanks) to be entrapped within the liquid films (145). Consequently, foaming is present as a stable, bubbly layer (varying from a few centimetres to over a meter) that commonly accumulates on the surface of water in aeration tanks (25).

Yet foaming in WWTPs' underlying mechanisms remain only partially understood. Foaming is generally attributed to the excessive growth of filamentous, hydrophobic bacteria that produce biosurfactants that accumulate at the air–liquid interface. Among these microorganisms, *Gordonia* has emerged as one of the most frequently reported foaming agents (146), (147). *Gordonia* contain a lipid-rich cell wall, a strongly hydrophobic cell surface (reduces drainage from foam lamellae through their hydrophobic cell surfaces), and it is able to produce surface-active substances (SAS) or biosurfactants (148). All these characteristics promote foam stabilisation.

Foam development, however, cannot be explained by microbial characteristics alone. Environmental conditions strongly influence the extent of foaming. Elevated temperatures, the presence of fatty acids or hydrophobic substrates, and detergents have all been implicated as important drivers. Frigon *et al*. hypothesised that higher temperatures accelerate the hydrolysis of these compounds, thereby increasing abundancies of foam-forming microbial population (149). These conditions stimulate filamentous bacteria to form longer chains and increase biosurfactant production. Such morphological and physiological adaptations promote the formation of bioflocs in a network structure, which affects the sedimentation of solids and solid-liquid separation (150). The combination of microbial adaptations and environmental triggers underpins the complexity of foaming events, highlighting the need for a better understanding of these events in order to mitigate their impacts.

The presence of foam in WWTPs can lead to serious operational issues, including reduced treatment efficiency, unintentional discharge of untreated or partially treated effluent, and increased maintenance and restoring costs (49). Foam-associated filamentous bacteria have been observed to migrate into anaerobic digesters from surplus activated sludge streams, where they can persist in oxygen-depleted environments (151). This has led to increasing reports of foaming in anaerobic digesters as well (152).

Foaming events in WWTPs and microbial community dynamics are closely interlinked, functioning in a bidirectional manner. On one hand, environmental, biological or operational conditions can alter activated sludge properties, causing shifts in microbial community composition, that could trigger foaming. On the other hand, foaming stabilisation itself can also produce microbial composition changes, often favouring the growth of filamentous, hydrophobic bacteria such as mycobacteria (151).

4.1.1. *Gordonia amarae* and its mycolic acids

Gordonia amarae is a filamentous bacterium that belongs to *Mycobacterium* genus, known for its ability to assimilate a broad range of hydrophilic and hydrophobic substrates under aerobic, anaerobic, and anoxic conditions (21). Biosurfactants produced by *Gordonia amarae* play a crucial role in enabling the bacterium to survive during activated sludge foaming events by facilitating the solubilization of hydrophobic substrates present in the foam layer. To metabolise these water-insoluble compounds as carbon sources, *Gordonia amarae* secretes surface-active agents that emulsify the substrates, increasing their bioavailability for uptake and degradation (50).

Gordonia amarae cell walls contain high levels of mycolic acids (50) which are associated to bacteria hydrophobicity and foaming potential. These lipids, characterised by a 2-alkyl, 3-hydroxy structure (59), can be covalently or non-covalently bound within the cell envelope, influencing its interactions with surrounding media.

Previous studies have reported shifts in the mycolic acid composition of mycobacteria depending on environmental conditions, including the synthesis of unique lipid species under specific growth scenarios (126), remarking the possibility of using mycolic acids as biomarkers. In this context, the feasibility that *Gordonia amarae* may similarly modulate its mycolic acid profile in response to foaming-inducing environments presents a plausible hypothesis for identifying lipid-based indicators (biomarkers) that could support foaming prediction and mitigation processes in wastewater treatment plants.

Although *Gordonia amarae* has been associated with foaming events in AS reactors (25) and biosurfactant production (153), lipidomic changes of *Gordonia amarae* related to growth conditions and their link to biosurfactant production and foam remain underexplored. Liquid chromatography–mass spectrometry (LC-MS) is a widely established analytical technique for the investigation of microbial lipidomes in complex matrices (154), including detailed analysis of mycolic acids (128), (155). In this study, ultraperformance liquid chromatography-mass spectrometry (UPLC-MS) was employed to investigate lipidomic variations in pure cultures of *Gordonia amarae* grown under different conditions, with a focus on linking mycolic acid profiles to biosurfactant production and foaming potential. Moreover, analysing pure cultures prior to mixed-community investigations provides a critical baseline, helping to distinguish whether

observed mycolic acid variability in activated sludge arises from phenotypic shifts within *Gordonia amarae*, or because of shifts in dominant species among varying MA-producing bacteria.

4.1.2. Biosurfactants produced by mycobacteria

Biosurfactants are amphipathic, surface-active compounds produced by various microorganisms, including mycobacteria, particularly when grown in presence of non-water-soluble carbon sources. These molecules function as emulsifying agents, enabling the utilization of otherwise inaccessible hydrophobic substrates (50). Structurally, biosurfactants typically consist of a hydrophilic fraction (e.g., charged groups or amino acids) and a hydrophobic fatty acid chain (156). This dual affinity allows them to reduce the interfacial tension between immiscible phases, facilitating the formation of emulsions (57).

In the context of activated sludge reactors, biosurfactants accumulate at the air–water interface of aeration-induced bubbles, where they lower water's surface tension and enhance bubble stability. This action plays a critical role in the initiation and persistence of stable foam in aeration tanks.

Recent studies have characterised the biosurfactants produced by *Gordonia* species as glycolipids (57). Moreover, genomic studies have verified that multiple *Gordonia* strains carry all the necessary genes required for glycolipids biosynthesis (57). Some strains of *Gordonia*, such as *Gordonia amarae*, are capable of producing trehalose lipids as main biosurfactant (57), a class of glycolipids consisting of acylated trehalose molecules linked via ester bonds to diverse fatty acids (58). These biosurfactants contribute not only to substrate emulsification but also to foam stabilization.

4.1.3. Biosurfactant quantitation

Biosurfactants produced by *Gordonia* species have been previously quantified by performing several assays, such as oil spreading, drop-collapse, Emulsion index, and Bacterial adhesion to hydrocarbons assays (57). While these techniques offer valuable insights into surface activity, emulsification potential, and changes in cell surface hydrophobicity, they are typically qualitative or semi-quantitative, and their outcomes can be influenced by environmental factors or assay conditions.

Polarography was employed in the present study as a quantitative electrochemical method for assessing surface-active substances (SAS). Polarography enables the direct measurement of surface activity based on the suppression of the capacity current at a dropping mercury electrode, providing a sensitive and reproducible estimation of biosurfactant concentration. As such, polarography offers a useful complementary tool

for biosurfactant analysis, especially when comparing biosurfactants production levels across different growth conditions.

4.1.4. Polarography

The principle of polarographic SAS quantification is based on the adsorption of surface-active molecules onto the mercury electrode, measured as a change in capacitive current (ΔIc) at a fixed potential of −0.6 V. (157), (101). This potential corresponds approximately to the electrocapillary maximum and the point of zero charge (pzc) (158), (159). The method has been widely used to quantify SAS in environmental samples, particularly in seawater (100), (102). Despite its proven sensitivity and robustness, polarography has not been widely adopted for the analysis of biosurfactants produced by culture-grown bacteria. Given the often saline nature of microbial media, the high potential biosurfactant yields in bacterial cultures, and the relatively simple sample preparation required, polarography presents a valuable yet underutilized tool for biosurfactant quantification. By applying polarography in this context, this work also aims to demonstrate its relevance and reliability for the accurate quantification of biosurfactants produced by mycobacteria, such as *Gordonia amarae*.

4.2. Aims

The aims of this study were to investigate the lipidomic adaptations and quantify biosurfactant production of *Gordonia amarae* under foaming and non-foaming conditions.

4.3. Objectives

This study is designed to achieve two primary objectives. First, to quantify biosurfactant production by *Gordonia amarae* throughout its growth curve in minimal media supplemented with different hydrophobic carbon sources, compared to nutrient-rich media, using polarography. Second, to assess lipidomic shifts under these conditions with Ultra-Performance Liquid Chromatography coupled with Quadrupole Time-of-Flight Mass Spectrometry (UPLC-QToF MS), in order to determine whether growth conditions drive variability in mycolic acid composition.

4.4. Materials and methods

4.4.1. Materials

Sodium acetate, Triton T-X-100, citric acid and magnesium sulphate heptahydrate were obtained from Sigma-Aldrich®. M9 salts and n-hexadecane were obtained from MP Biomedicals. Ammonium formate, calcium chloride, sodium bicarbonate, acetonitrile (HPLC grade), isopropanol (HPLC grade) and methanol (UHPLC grade) were obtained from Fisher Scientific™. Chloroform (HPLC grade) was obtained from Macron Fine Chemicals™. 1-butanol (HPLC grade) and ammonium acetate were obtained from Honeywell. Nutrient broth was obtained from Oxoid Ltd. 18MΩ water was collected from Millipore S.A.S. water systems, USA. Casamino acids were obtained from VWR. Olive oil (consisting of a mixture of refined and virgin olive oils and predominantly composed of oleic, linoleic, and stearic fatty acids) was obtained from Tesco UK.

Gordonia amarae (NCIB 11222 strain) was purchased from NCIMB LTD.

4.4.2. Bacterial growth in different media

Mycobacteria *Gordonia amarae* were grown in varying media to evaluate planktonic growth. For the growth in nutrient-rich media, 13 g of nutrient broth was dissolved in 1L of MilliQ water. The solution was sterilized via autoclave at 120 °C for 15 minutes. A single colony of *Gordonia amarae* was aseptically transferred from an agar plate and used to inoculate 20 mL of nutrient broth. The culture was incubated at 30 °C for 24 h. Aliquots were transferred to 200 mL of fresh nutrient broth prior to incubation at 30 °C and 150 rpm. OD_{600} measurements were taken twice a day for a one-week period using a spectrophotometer until bacterial growth was completed.

1 L of minimal media was prepared by diluting 200 mL of minimal salts stock solution (stock: 56.4 g of M9 minimal salts in 1 L of water) in 600 mL of MilliQ water. The mixture was supplemented with 2 mL of 1 M magnesium sulphate and 0.1 mL of 1 M calcium chloride. A 100 mL solution containing 10% carbon source in MilliQ water was added to the media. The solution was sterilized via autoclave at 120 °C for 15 minutes. A separate 100 mL solution containing 0.1 g/mL of casamino acids in MilliQ water was filter-sterilized and added to the sterile media. 200 mL aliquots were inoculated with *Gordonia amarae* prior to shaking incubation at 30 °C and 150 rpm. OD_{600} measurements were taken twice a day for a one-week period using a spectrophotometer until bacterial growth was completed. A 5 mL culture aliquot was taken once a day for biosurfactant analysis.

The carbon sources used for minimal media preparation were: (A) n-hexadecane (1%), (B) n-hexadecane (1%) + acetate (0.5%) and (C) olive oil (1%). The minimal media selected for bacterial growth was chosen on the basis of its ability to induce biosurfactant production (50).

4.4.3. Foaming induction

Foaming induction was achieved by adding a mixture of 1.52 g of citric acid and 2.88 g of sodium bicarbonate to 200 mL of liquid bacterial culture at the end of its growth curve. This produced carbon dioxide bubbles, which, in the presence of biosurfactants, were stabilised due to the reduced surface tension at the air–water interface. This method simulates the aeration conditions in AS reactors of WWTPs, where air bubbles rise from the bottom. The reaction was left for 20 seconds before recording the observed foam produced.

4.4.4. Surfactant activity (SA)

4.4.4.1. Analytical protocol

The analysis of surface-active substances (SAS) was carried out using phase-sensitive alternating current (AC) voltammetry, following the general approach outlined by Ćosović *et al.* (101). A three-electrode system was employed, consisting of a hanging Hg drop electrode as working electrode, an Ag/AgCl reference electrode in 3 mol/L KCl, and a platinum coil as auxiliary electrode. Measurements were performed using a 663 VA Voltammeter coupled with an Autolab potentiostat (Metrohm, Switzerland) operating in Static Mercury Drop Electrode (SMDE) mode.

Surfactant activity (SA) quantification is based on SAS adsorption onto the surface of the Hg electrode, which induces a measurable change in ΔIc at an applied potential (E) of −0.6 V (157), (101), This potential approximates the electrocapillary maximum and the point of zero charge (pzc) of Hg (158), (159). Table 4.1 outlines the instrument settings used throughout the analysis.

Table 4.1: *instruments settings for SA activity analysis.*

Stirrer speed (RPM)	2000
Start potential (V)	-0.59
End potential (V)	-1
Step (V)	-0.01
Modulation time (s)	0.2
Frequency (Hz)	75
Phase angle (deg)	90

Prior to measurement, all glassware was precombusted at 450 °C for a minimum of four hours, and acid cleaned with 10 % HCl and rinsed with Milli-Q water between samples. A four-point calibration (linear range) was performed using a nonionic, water-soluble surfactant (Triton X-100) in a 0.55 mol/L NaCl solution to standards concentration range of 0.2 - 3 mg/L.

4.4.4.2. Culture biosurfactant analysis

The salinity of T0 samples was verified and adjusted using defined volumes of 0.55 mol/L NaCl, as detailed in Table 4.2. For subsequent samples, further dilution with 0.55 mol/L NaCl was performed whenever adsorption saturation of the Hg electrode surface occurred within 5 seconds. SA results were expressed as T-X-100 eq. (mg/L), in accordance with calibration standards.

Table 4.2: *Polarographic sample preparation for Gordonia amarae cultures across the 0–144 h experimental period, presenting dilution factors for each growth condition, with final volumes indicated in brackets (mL).*

Culture time (h)	1% n-hexadecane	1% n-hexadecane + 0.5% acetate	1% olive oil	Nutrient broth
0	1:20 (10 mL)	1:80 (20 mL)	1:80 (20 mL)	1:80 (20 mL)
24	1:20 (10 mL)	1:80 (20 mL)	1:80 (20 mL)	1:80 (20 mL)
48	1:200 (10 mL)	1:200 (10 mL)	1:80 (20 mL)	1:80 (20 mL)
72	1:200 (10 mL)	1:200 (10 mL)	1:80 (20 mL)	1:80 (20 mL)
96	1:200 (10 mL)	1:200 (10 mL)	1:200 (10 mL)	1:80 (20 mL)
120	1:400 (20 mL)	1:400 (20 mL)	1:800 (20 mL)	1:80 (20 mL)
144	1:400 (20 mL)	1:400 (20 mL)	1:800 (20 mL)	1:80 (20 mL)

4.4.5. Lipidomic analysis

4.4.5.1. Bacterial mycolic acid extraction

Polarity-extractable MA isolation was achieved following Alshehry *et al.* (134) method. 15 mL bacterial cultures were aliquoted and freeze-dried. Dried solid was washed with 15 mL of 1-butanol/methanol (1:1) + 5 mM ammonium formate. The mixture was vortexed, sonicated for 1 h and centrifuged 10 min at 2000 rpm. The liquid layer was transferred to a round bottom flask and the wash, sonication, centrifuge and transfer steps repeated twice for the biomass residue. The solid residue was reserved for saponification. The combined liquid extracts were subsequently dried using a rotatory evaporator and lipids were transferred to a glass vial using chloroform and acetone rinses for analysis. These lipid extracts were dried and reconstituted in chloroform/methanol (1:2).

The solid biomass residue was saponified following a method modified from Vilchèze *et al.* (135). The solid was mixed with 2 mL of saponification reagents (methanol/water (1:1) + 25 % potassium hydroxide) and heated at 120 °C for 1 h. Once cooled, 2 mL of chloroform and 1.5 mL of acidification reagent (hydrochloric acid/water (1:1)) were added. The chloroform layer was transferred to a glass vial, dried and reconstituted in chloroform/methanol (1:2).

All reconstituted samples (polarity-extractable and saponified extracts) were stored at -20 °C until analysis.

For preliminary MA analysis, the polarity-extractable and saponified MA extracts were combined into a total *Gordonia amarae* mycolic acid extract. Polarity-extractable and

saponified MA extracts were also measured separately for comparison between *Gordonia amarae* growth in different media.

4.4.5.2. UPLC conditions

A Waters ACQUITY BEH C18 1.7 µm, 2.1 mm X 150 mm column, with a Waters ACQUITY BEH C18 VabGuard™ 1.7 µm, 2.1 mm X 5 mm pre-column were used for lipid separation. The column oven was 50 °C. The flow rate was 0.2 mL/min and the injection volume 5 µL.

Gradient elution: (A) acetonitrile/water (60:40) + 5mM ammonium acetate, (B) IPA/methanol/water (90:10:0.5) + 5mM ammonium acetate.

Table 4.3 describes the gradient elution points used for lipid separation.

Table 4.3: *Gradient elution points utilised for lipid separation during the experiment. Showing total run time (minutes) vs mobile phase (%) and gradient curve.*

Total UPLC run time (minutes)	Percentage (%) mobile phase B	Gradient curve
0	5	-
2.5	5	1
48	90	4
50	5	1

4.4.5.3. Mass spectrometry conditions

Detection and analysis of lipids were acquired using a Waters SELECT SERIES Cyclic IMS mass spectrometer on LC mode without enabled ion mobility, under the conditions shown in Table 4.4. The mass spectrometer was operated in negative mode with ESI ionisation for analysis. To improve mass accuracy, LockSpray tool was set to Leucine Enkephalin (*m/z* $[M-H]^-$= 554.2624).

Table 4.4: *Waters SELECT SERIES Cyclic IMS mass spectrometer parameters utilised for lipid detection (ion mobility disabled).*

MS parameters	
Ionisation mode	ESI
Polarity	Negative
Scan type	MSe
Scan range	100-2000 *m/z*
Capillary voltage	-3000 V
Sampling Cone voltage	75 V
Source Offset	80
Source temperature	120°C
Desolvation temperature	300°C
Cone gas flow	50L/h
Desolvation gas flow	580L/h
Resolution	> 100000 FWHM

4.4.5.4. Statistical analysis

Data normality was assessed using the Shapiro–Wilk test at a significance level of $\alpha = 0.05$ prior to subsequent statistical analyses. The test was performed using the Stats Kingdom online platform (160).

Statistical analyses of lipid abundance data were performed using Microsoft Excel 365. Differences between growth medias were assessed using two-sample t-tests (assuming equal variances) and ANOVA single factor. Statistical significance was determined at a threshold of $p < 0.01$.

4.5. Results and discussion

4.5.1. *Gordonia amarae* growth monitoring

The growth of *Gordonia amarae* was monitored over a one-week period in nutrient broth and three minimal-media-containing hydrophobic carbon sources: 1% n-hexadecane, 1% olive oil, and 1% n-hexadecane + 0.5% acetate. Bacterial growth was assessed via optical density measurements at 600 nm (OD_{600}) (Fig. 4.1).

In nutrient broth, *Gordonia amarae* exhibited the shortest lag phase (~24 h) followed by a moderate log phase lasting until 54 h, with OD_{600} increasing to approximately 1.5 AU. This was followed by a stable stationary phase for the remainder of the experiment. The rapid growth and short lag phase in this nutrient-rich media indicate that readily metabolizable carbon sources were immediately available, reducing the need for metabolic adaptation by the bacteria.

In contrast, all cultures containing hydrophobic carbon sources exhibited extended lag phases, reflecting the need for metabolic adaptation, such as production of biosurfactants, to access hydrophobic substrates (56). Among them, 1% n-hexadecane showed the most rapid and extensive growth. After a lag phase of ~30 h, the culture entered a vigorous log phase between 30 and 96 h, achieving a maximum OD_{600} of 5.9 ± 1.08 AU by the conclusion of the experiment (Fig 4.1). Similarly, cultures in 1% n-hexadecane + 0.5% acetate media displayed a comparable lag phase, followed by a prolonged log phase until ~120 h, reaching a lower OD_{600} (~3.7 AU), which gradually declined to ~3.5 AU by the end of the experiment (Fig. 4.1). The 1% olive oil media presented the longest lag phase (~54 h) and exhibited steady growth until ~150 h, reaching OD_{600} values around 5.0 AU, with no substantial change thereafter (Fig. 4.1).

The OD_{600} measurements in these cultures reflect both biomass accumulation and biosurfactant production, as SAS, such as biosurfactants, can interfere with light transmission in absorbance measurements. To get better understanding about *Gordonia amarae's* biosurfactant production in each media, a direct quantification of SAS was performed by polarography.

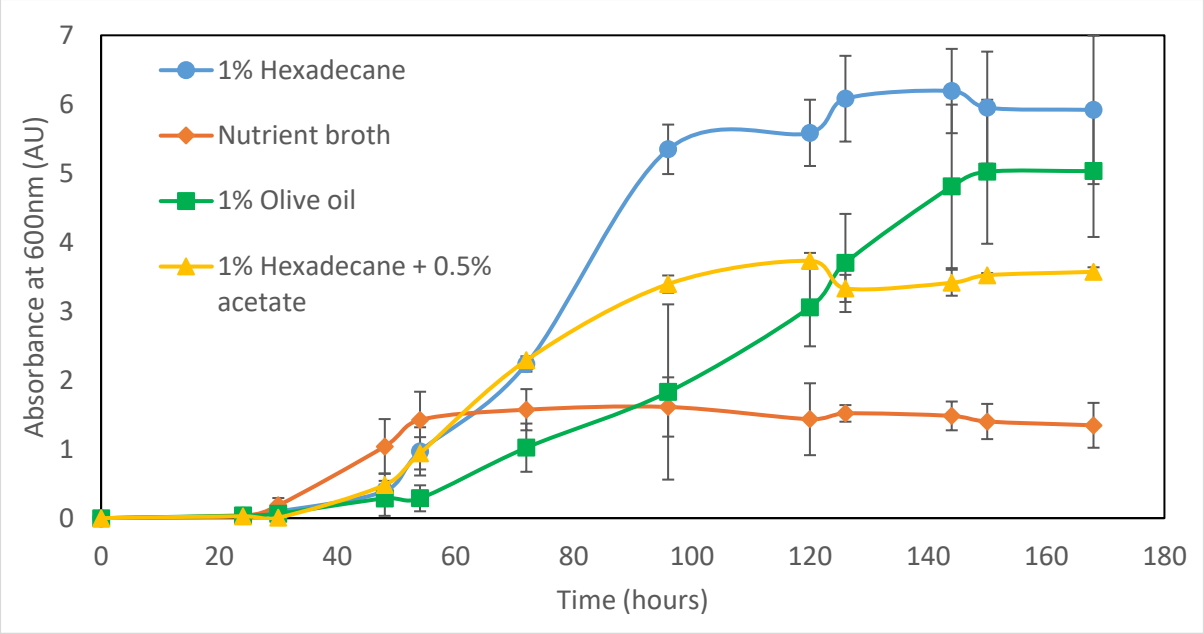

Figure 4.1: *One-week growth curve of Gordonia amarae in nutrient broth (orange), 1% n-hexadecane (blue), 1% n-hexadecane + 0.5% acetate (yellow) and 1% olive oil (green). Errors bars represent standard deviation of triplicates cultures for each media.*

4.5.2. Polarograph

Based on Rickard *et al.* (102), a four-point, blank corrected, calibration curve was performed using Triton-X-100 at a concentration range of 0.2 - 3 mg/L. Each standard was analysed in triplicate giving standard deviations < 0.025 µA. Intercept and slope (0.066 and 0.93 respectively) (Fig. 4.2) were used to calculate biosurfactant concentration from *Gordonia amarae* cultures.

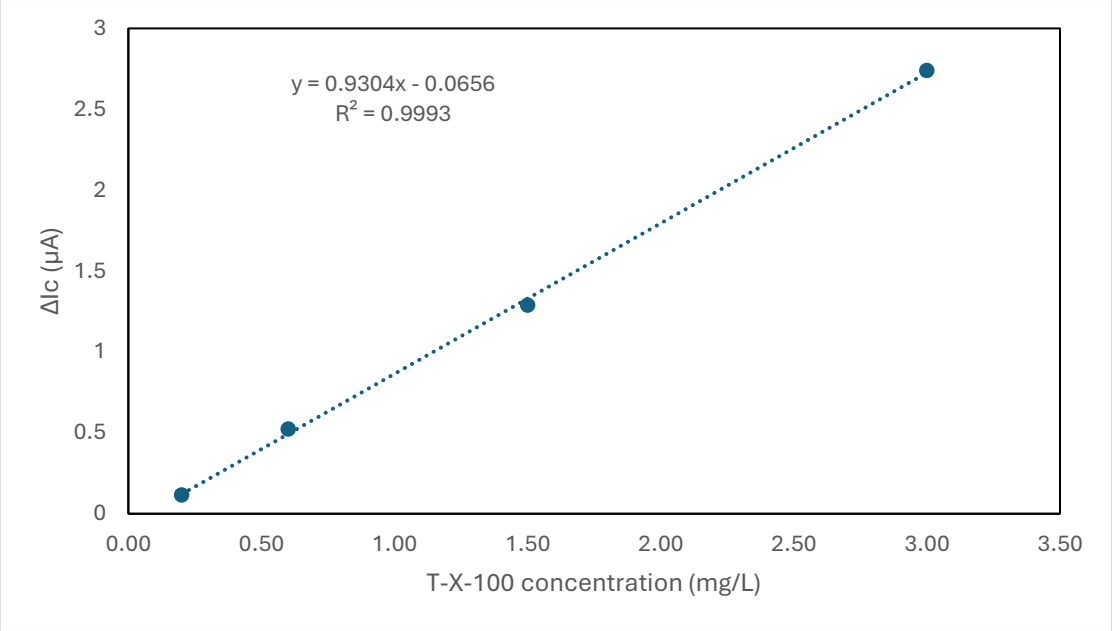

Figure 4.2: *Blank-corrected calibration curve for T-X-100 (0.2-3 mg/L) and capacity current variation at -0.6 V (ΔIc: μA).*

Biosurfactant production by *Gordonia amarae* was daily evaluated in the four carbon sources over a 144 h incubation period, with SAS quantified as Triton X-100 equivalents (mg/L) (Fig. 4.3). Distinct biosurfactant production trends were observed depending on the carbon source provided, with hydrophobic carbon sources significantly enhancing biosurfactant production compared to nutrient broth.

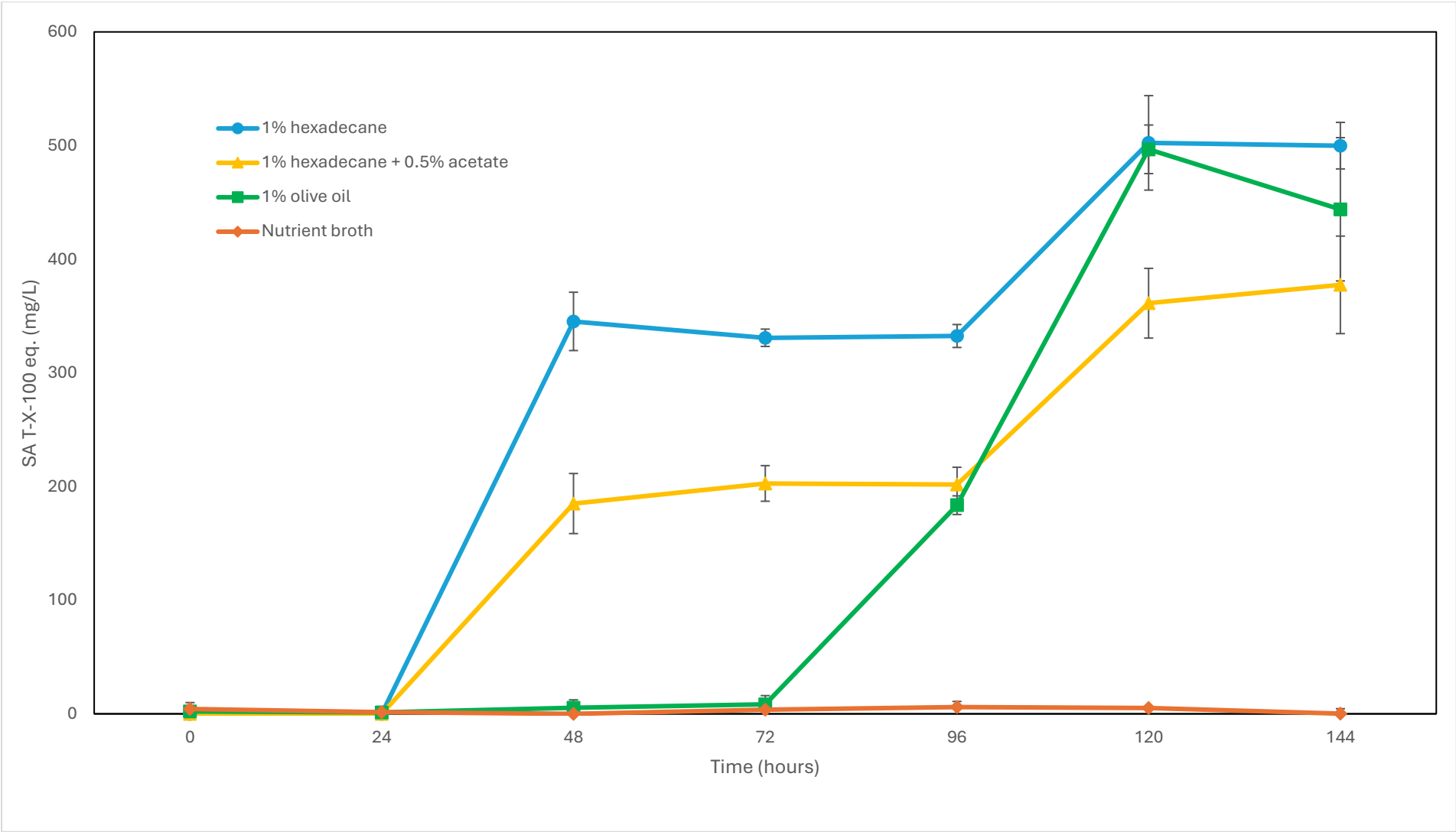

Figure 4.3: *Concentration of biosurfactants expressed as SA (mg/L T-X-100 eq.), for Gordonia amarae one-week cultures in different media. Error bars correspond to the standard deviation of the biosurfactant calculation from triplicate cultures.*

SAS concentrations remained negligible in nutrient broth (<6 mg/L), consistent with the absence of hydrophobic carbon sources and the lack of metabolic induction required for biosurfactant synthesis. In contrast, significant biosurfactant production was observed in all cultures containing hydrophobic carbon sources, with trends closely reflecting the growth dynamics. Cultures in 1 % n-hexadecane achieved the highest SAS concentrations (502.37 ± 41.56 mg/L at 120 h), correlating with the steep log phase growth. Similarly, 1% olive oil media supported substantial biosurfactant production, peaking at 496.71 ± 21.37 mg/L after 120 h, albeit following a delayed growth pattern corresponding to the extended lag phase observed in the growth curves. Biosurfactant production in the 1% n-hexadecane + 0.5% acetate media reached a maximum of 377.44 ± 42.91 mg/L after 144 h, which was lower than that observed in the single hydrocarbon media.

The alignment between OD_{600} measurements and biosurfactant production strongly supports the role of biosurfactant synthesis in facilitating the access and utilization of hydrophobic substrates by *Gordonia amarae*. The prolonged lag phases in all cultures containing hydrophobic carbon sources also suggest the requirement of adaptation to initiate biosurfactant synthesis before efficient hydrocarbon uptake can occur (161).

Interestingly, although the addition of 0.5% acetate to 1% n-hexadecane was expected to increase biosurfactant production due to the availability of a more readily metabolizable co-substrate, it instead resulted in comparatively lower SAS production and lower growth performance. This result contrasts with previous findings (50) and may reflect strain-specific metabolic preferences, as different *Gordonia* strains have been shown to exhibit varied responses to mixed-substrate media (56).

The delayed biosurfactant production observed in the olive oil medium is likely related to the complexity of olive oil composition, which contains a mixture of triacylglycerols rich in fatty acids such as oleic acid (C18:1), linoleic acid (C18:2), and stearic acid (C18:0) (162). The metabolic processing of these larger, structurally diverse molecules may require additional adaptation time, explaining the prolonged lag phase (163) and gradual increase in SAS production.

These results support the hypothesis that biosurfactant synthesis by *Gordonia amarae* is closely regulated by substrate availability and accessibility, with maximal production occurring in cultures containing hydrophobic carbon sources that require emulsification for uptake. The lack of SAS production in nutrient broth further confirms that biosurfactant synthesis is specifically induced by the metabolic demand for hydrophobic substrate assimilation rather than being constitutively produced.

4.5.3. Foaming induction

Foaming induction was carried out by adding a mixture of citric acid and sodium bicarbonate to *Gordonia amarae* cultures which reacted to produce carbon dioxide bubbles. In the presence of biosurfactants, which reduce the surface tension at the air–water interface and thereby lower the energy barrier for bubble formation, carbon dioxide bubbles are stabilised and accumulate as foam, imitating the aeration process in an activated sludge reactor. (Fig. 4.4). Successful foam formation was observed in all cultures containing hydrophobic carbon sources, whereas no foaming was detected in the nutrient broth culture. This lack of foam in nutrient broth is consistent with the biosurfactant quantification results, which indicated minimal production of surface-active substances under this condition.

Among the cultures containing hydrophobic carbon sources, 1% olive oil culture produced the highest visible foam volume 20 seconds after induction (Fig. 4.4). However, this foam was short-lived, dissipating completely within 3 hours. In contrast, 1% n-hexadecane and 1% n-hexadecane + 0.5% acetate cultures formed more persistent foams, lasting over 7 hours. 1 % n-hexadecane culture produced the most stable foam, which persisted for over 24 hours.

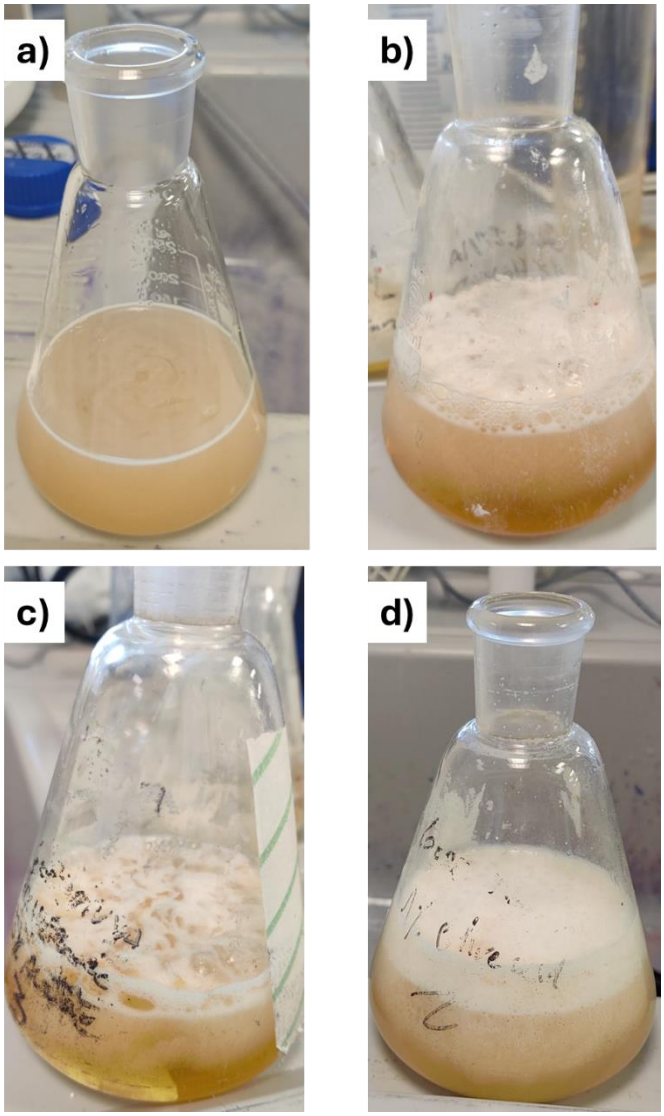

Figure 4.4: *Photographs of cultures 20 seconds after foaming was induced through carbon dioxide production and subsequent bubbling in a) nutrient broth, b) 1 % n-hexadecane, c) 1 % n-hexadecane + 0.5 % acetate, and d) 1% olive oil IV). Persistent foam was observed in b), c), and d).*

4.5.4. MA Lipidomics

A mixture of polarity-extractable and saponified MA from *Gordonia amarae* cultured in nutrient broth was analysed by UPLC-QToF-MS to establish MA in baseline conditions. Chromatographic separation revealed eight distinct peaks eluting between 28 and 35 minutes: four major peaks (a, c, e, g) and four minor peaks (b, d, f, h) located between the major ones (Fig. 4.5). In most cases (all except (g)), mass spectra corresponding to each chromatographic peak showed 2-3 lipid ion groups per peak, typically separated by intervals of a *m/z* of 26 Da, corresponding to the mass of C_2H_2, suggesting chain length and unsaturation differences. Chromatogram peak (g) contained six groups of lipids separated by a *m/z* of 13 Da, suggesting the possible co-elution of multiple unresolved species, potentially indicating an embedded and unseparated minor chromatographic peak presence.

Chromatographic separation of major and minor peaks (Fig. 4.5) separated both, MA hypothesized to have the same carbon backbone but differing degrees of unsaturation, as well as MA with distinct carbon backbones. For example, ions with *m/z* of 769.71, 771.72, and 773.74 Da eluted at approximately c) 29.5, e) 30.5, and g) 31.5 minutes, respectively (Fig. 4.5). These ions are predicted to correspond to the molecular formula $C_{51}H_{93}O_4$, differing by one double bond each (5, 4, and 3 double bonds, respectively). The proposed chemical formulas were assigned based on close agreement between the observed and theoretical exact masses, with mass accuracies of 0.93, 0.86, and –1.02 ppm, respectively. The progressive shift in retention time aligns with decreasing number of unsaturations. Although double bonds between C atoms do not directly increase the chemical polarity of lipids, they induce conformational changes that can alter the shape and packing of the lipid molecule (164). These conformational changes can expose polar functional groups, such as hydroxyl, keto or methoxy, increasing the overall polarity of the molecule. Consequently, lipids with a greater number of double bonds exhibit weaker interactions with the hydrophobic stationary phase of the reverse-phase column, resulting in earlier elution. This relationship between unsaturation and elution time is consistent with the observed chromatographic patterns.

Exact mass-based structural characterisation suggested that the major and minor peaks contained distinct lipid species. For example, lipid ions from mass spectrum a) with a *m/z* of 715.66 and 741.67 were predicted to correspond to $C_{47}H_{87}O_4$ (4 double bonds, -1.59 ppm mass accuracy) and $C_{49}H_{89}O_4$ (5 double bonds, -2.00 ppm mass accuracy) respectively. Lipid ions from peak (b) with a *m/z* of 729.75 and 755.77 were predicted to correspond to $C_{50}H_{97}O_2$ (2 double bonds, -2.82 ppm mass accuracy) and $C_{52}H_{99}O_2$ (3 double bonds, 1.45 ppm mass accuracy) respectively. These observations suggest the co-occurrence of structurally distinct MA species with varying degrees of unsaturation and possibly different backbone structures, contributing to the complexity of the MA lipid profile of *Gordonia amarae*.

Since mass spectra are represented as relative abundances, low-intensity lipid ions present in major chromatographic peaks may be eclipsed by co-eluting ions of significantly higher abundance. Nonetheless, these lower-abundance ions can still be detected in full-scan mass spectra.

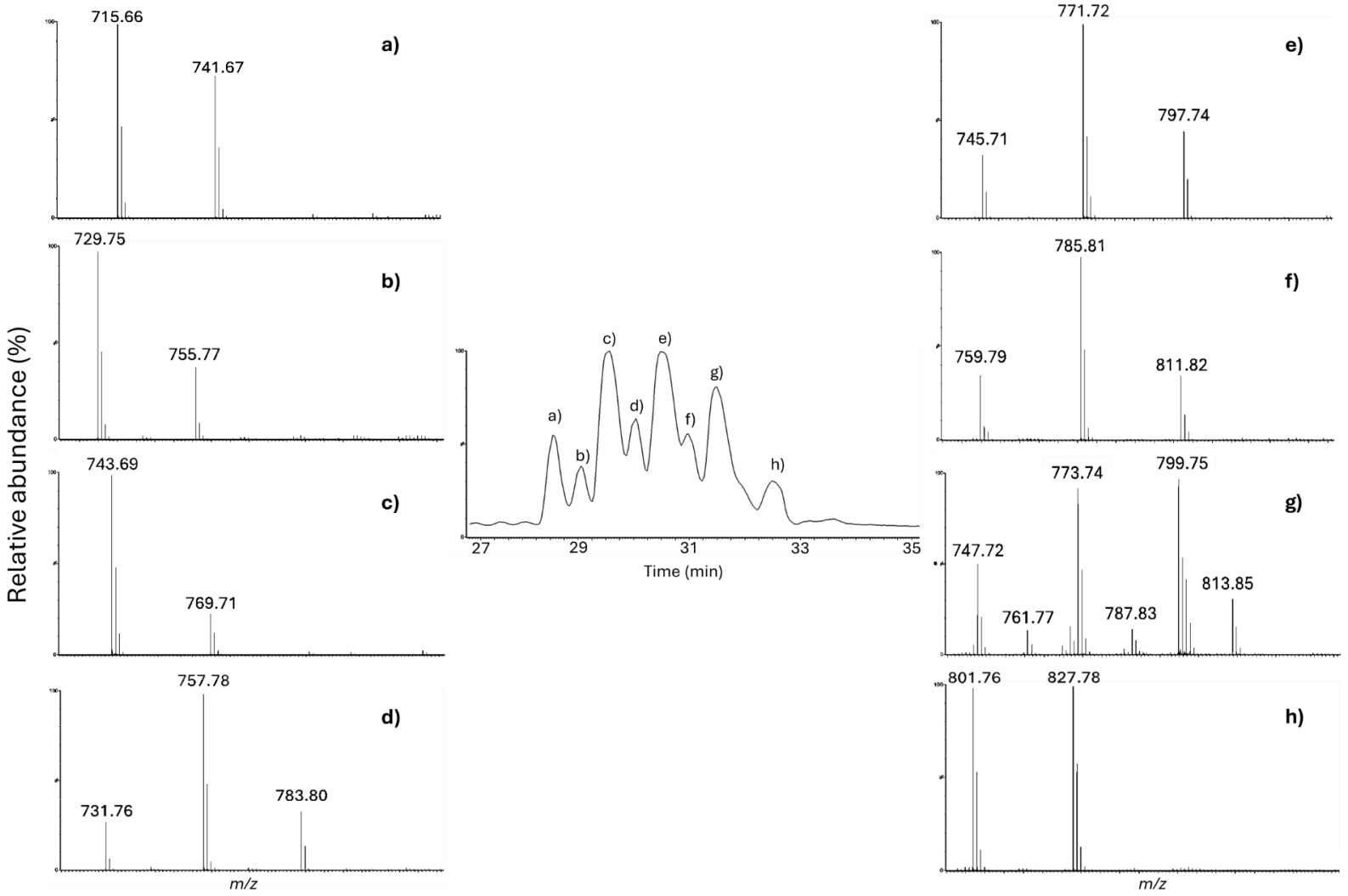

Figure 4.5: *Chromatogram for polarity-extractable and saponified MA mix from Gordonia amarae culture at the end of its growth curve in nutrient broth (middle), showing 4 major peaks eluting after approximately a) 28.5 , c) 29.5, e) 30.5, and g) 31.5 minutes, and 4 shorter peaks eluting after approximately b) 29, d) 30, f) 31 and h) 32.5 minutes, and mass spectrums for each eluted peak.*

Since different growth conditions have been reported to produce changes in bacterial lipid profiles (165), (166), lipids from different cultures of *Gordonia amarae* at the end of its growth curve, in nutrient rich media and minimal media containing 1% n-hexadecane, 1% olive oil, and 1% n-hexadecane + 0.5% acetate were extracted. Polarity-extractable and saponified mycolic acids were analysed separately by UPLC-MS to observe any possible variation in its lipidomic profile.

Polarity-extractable MA from *Gordonia amarae* cultures were consistently eluted between 28 and 35 minutes across all tested media (Fig. 4.6). The chromatogram from nutrient broth culture exhibited the highest number of distinct peaks, characterized by four major and four minor peaks, suggesting a more diverse profile of mycolic acid species (Fig. 4.6 a). In contrast, cultures grown with hydrophobic carbon sources showed three dominant peaks. Among these, olive oil culture displayed a notably higher baseline noise, probably due to the presence of other fatty acids present in olive oil (Fig. 4.6 d).

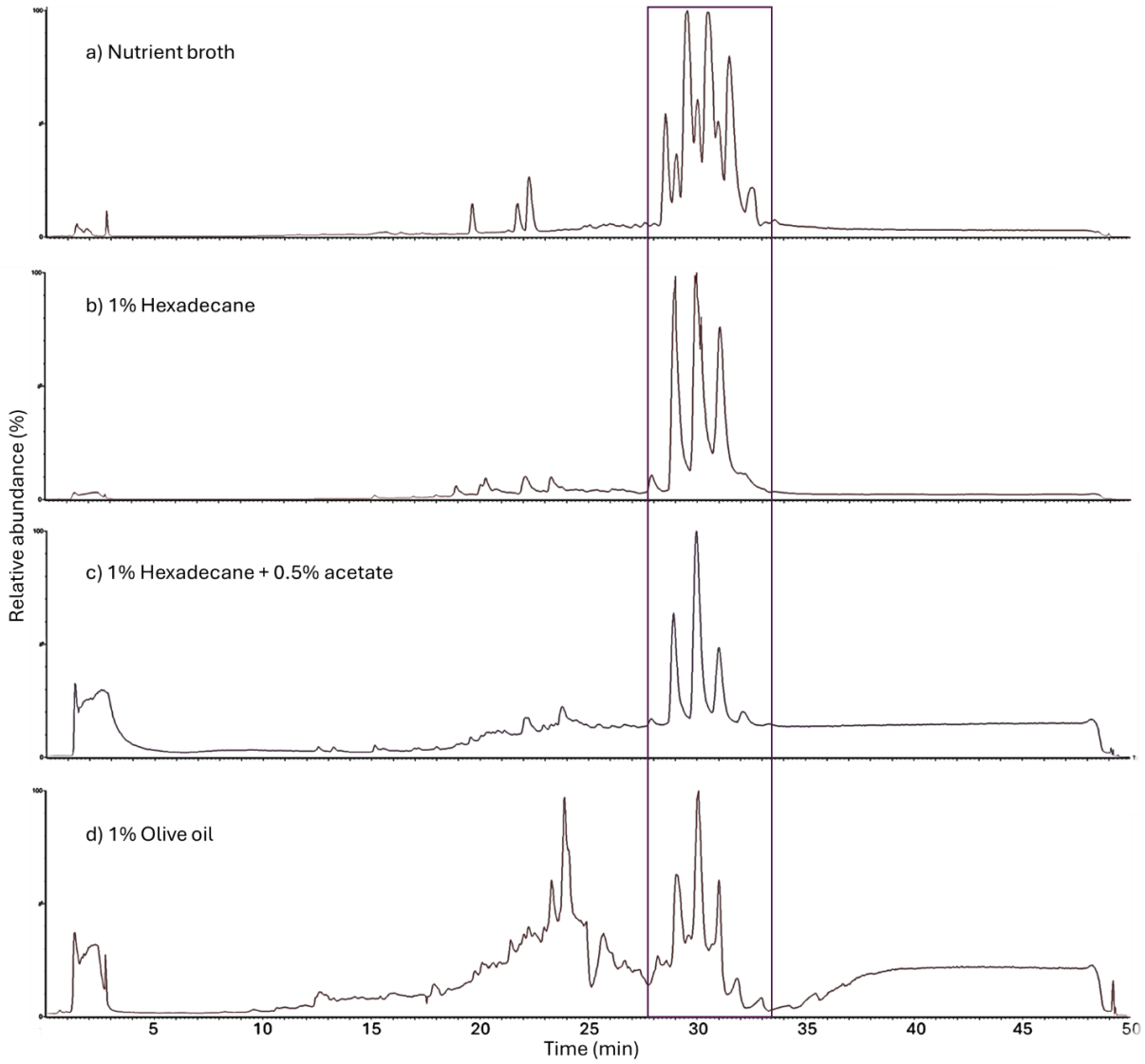

Figure 4.6: *Chromatograms for polarity-extractable MA from Gordonia amarae cultures at the end of its growth curve in a) nutrient broth, b) 1% n-hexadecane, c) 1% n-hexadecane + 0.5% acetate and d) 1% olive oil. MA eluted between 28 and 35 minutes (purple box).*

Mass spectra analysis of polarity-extractable MA from *Gordonia amarae* cultures revealed consistent clustering of lipid ions into distinct sets within the m/z range of 715 to 860 Da across all tested media (Fig. 4.7). This aligns with previous reports of *Gordonia amarae* strains that produced MA ranging from C_{31}–C_{54} (*m/z* 550–880 Da) under specific culture conditions (67).

Six main sets of MA ions were observed under all tested growth conditions, each characterized by a single most abundant ion; *m/z* of 715.66, 743.49, 771.72, 799.75, 827.82, and 853.83 Da in nutrient broth cultures and *m/z* of 715.66, 743.49, 769.71, 797.76, 825.80, and 851.82 Da in all cultures containing hydrophobic carbon sources. Lipid spectra were compared between nutrient conditions to assess: 1) diversity of lipid species, 2) unsaturations in abundant peaks, and 3) structural shifts in peaks from less-

abundant sets. These were then compared between polarity-extractable MA and saponified MA.

Cultures grown in nutrient broth displayed the greatest diversity of lipid species, including the six mentioned sets and an additional four minor sets. This broader lipidomic profile matches the more complex chromatographic pattern observed in Fig. 4.6, where a larger number of peaks were observed in *Gordonia amarae* cultured in nutrient broth compared to hydrophobic carbon sources. Specifically, the lipid ions sets present in the nutrient broth sample that seemed to have very low abundance in minimal media correspond to the lipid ions eluting in minor chromatographic peaks (Fig. 4.5).

Closer inspection of the lipid ions *m/*z sets revealed systematic shift to the left of 2 Da in the relative abundance of the most abundant ion in those *m/*z sets with a *m/z* greater than 769 Da. In particular, nutrient broth culture displayed several lipid *m/*z sets (highlighted in Fig. 4.7) where the most abundant ions (*m/z* of 771.72, 799.75, 827.82, and 853.83 Da) were systematically replaced in minimal media by ions with a *m/z* of 769.71, 797.76, 825.80, and 851.82, respectively. These 2 Da difference could correspond to the presence of an additional unsaturation, suggesting that the conditions of the hydrophobic carbon sources for growth may induce changes in the unsaturation levels of the mycolic acid backbone. These ion shifts were observed in triplicate cultures.

Such alterations in lipid composition indicate that *Gordonia amarae* modulates its MA synthesis in response to environmental nutrient availability. The enrichment of more unsaturated species in minimal media may reflect an adaptive strategy of membrane remodelling.

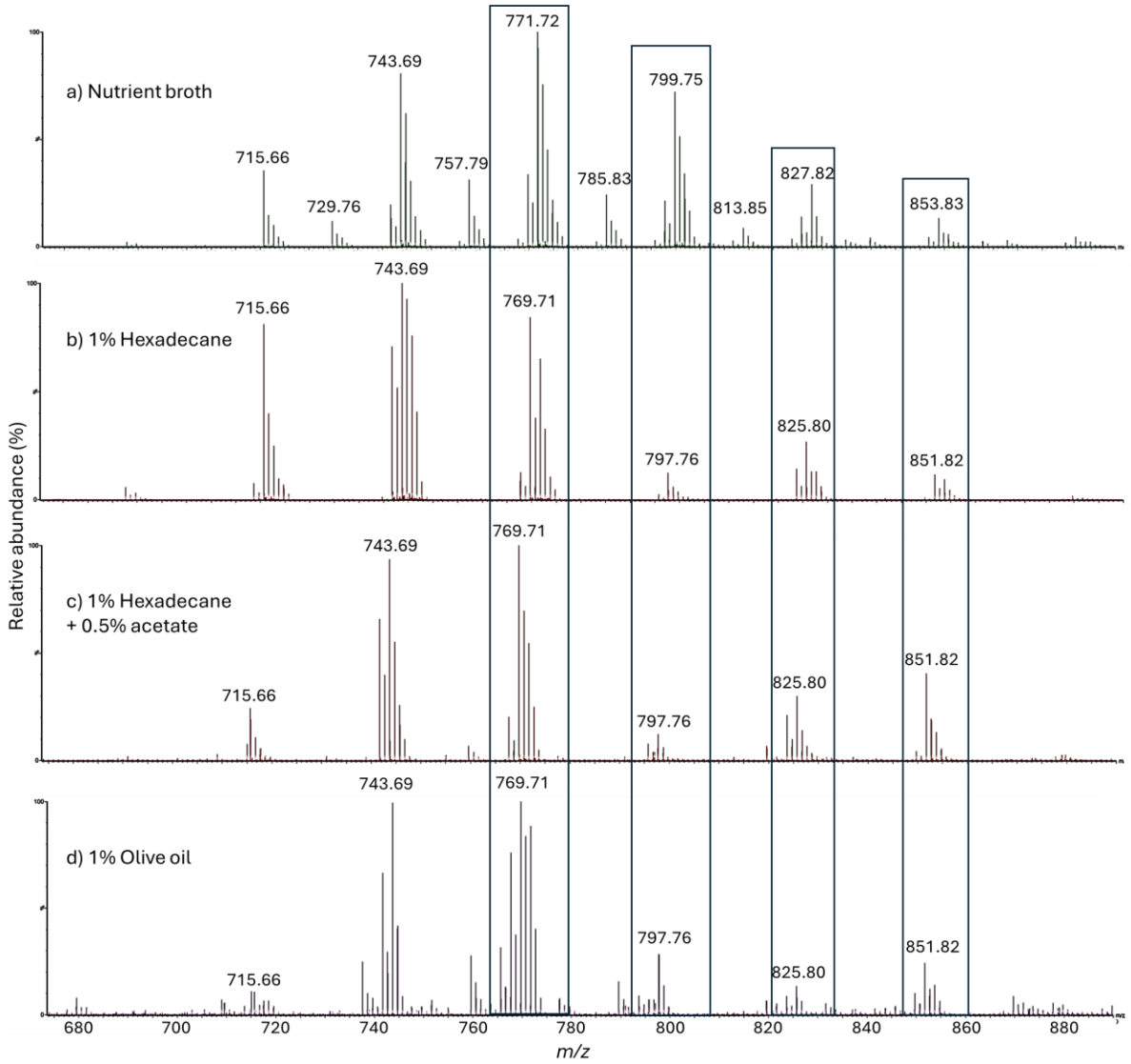

Figure 4.7: *Mass spectra (between 28 - 35 minutes) for polarity-extractable MA from Gordonia amarae at the end of its growth curve in a) nutrient broth, b) 1% n-hexadecane, c) 1% n-hexadecane + 0.5% acetate and d) 1% olive oil. Showing difference in MA profiles in nutrient broth compared to minimal media.*

Similarly, saponified mycolic acids from *Gordonia amarae* cultures at the end of its growth curve eluted between 28 and 35 minutes across all tested media (Fig. 4.8). Nutrient broth culture chromatogram exhibited the highest number of distinct peaks, consistent with the polarity-extractable MA profile shown previously (Fig. 4.6). Although a lower background was observed for saponified MA from all tested media, especially 1% olive oil minimal media, no significant differences in peak patterns were observed compared to the polarity-extractable MA profiles.

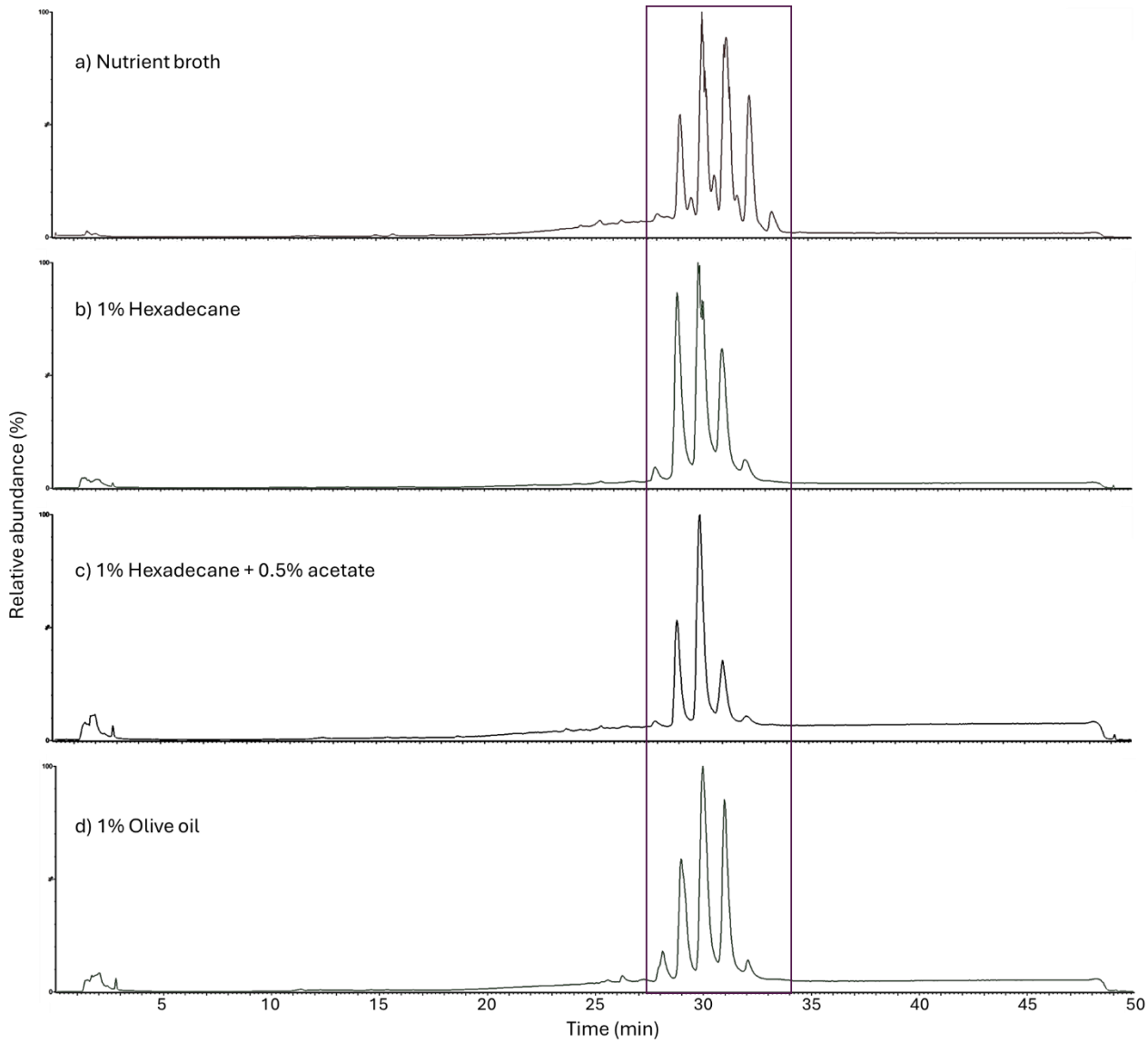

Figure 4.8: *Chromatograms for saponified MA from Gordonia amarae cultures at the end of its growth curve in a) nutrient broth, b) 1% n-hexadecane, c) 1% n-hexadecane + 0.5% acetate and d) 1% olive oil. MA elution occurred between 28 and 35 minutes.*

Mass spectra analysis of saponified MA from *Gordonia amarae* cultures (Fig. 4.9) revealed slight differences compared to polarity-extractable MA profiles (Fig. 4.7). A reduction of lipid ions *m/*z sets was noted in nutrient broth culture, with a marked decrease in the relative abundance of the high-mass *m/*z sets with a *m/z* of 813.85, 827.85, and 853.83 Da. However, 827.85 and 853.83 Da *m/*z sets were visible in minimal media cultures.

Despite the lower abundance of these higher-mass lipid *m/*z sets, nutrient broth culture still exhibited the broadest overall lipidomic profile, consistent with the polarity-extractable MA results. This broader profile was characterised by the presence of the lipid ions sets corresponding to minor chromatographic peaks (Fig. 4.8). These sets were not visible in minimal media cultures due to their low relative abundance. Moreover, the consistent shift to the left of 2 Da in the *m/z* of the most abundant ions within several lipid

m/z sets, from cultures with hydrophobic carbon sources compared to nutrient broth, was also observed indicating a recurring pattern. Bacterial extracellular lipids, including biosurfactants, are typically secreted in response to environmental pressures such as hydrophobic substrate availability (167), whereas cell envelope-associated lipids play structural and permeability roles (118). The recurrence of these shared lipidomic features in both polarity-extractable and saponified fractions suggests that the observed differences are not only due to extracellular lipid secretion. Instead, they reflect intrinsic remodelling of the bacterial cell envelope, induced by the growing conditions. These findings point to physiological adaptation at the membrane level and support the potential use of lipid composition as biomarkers to predict and potentially prevent foaming events in WWTPs.

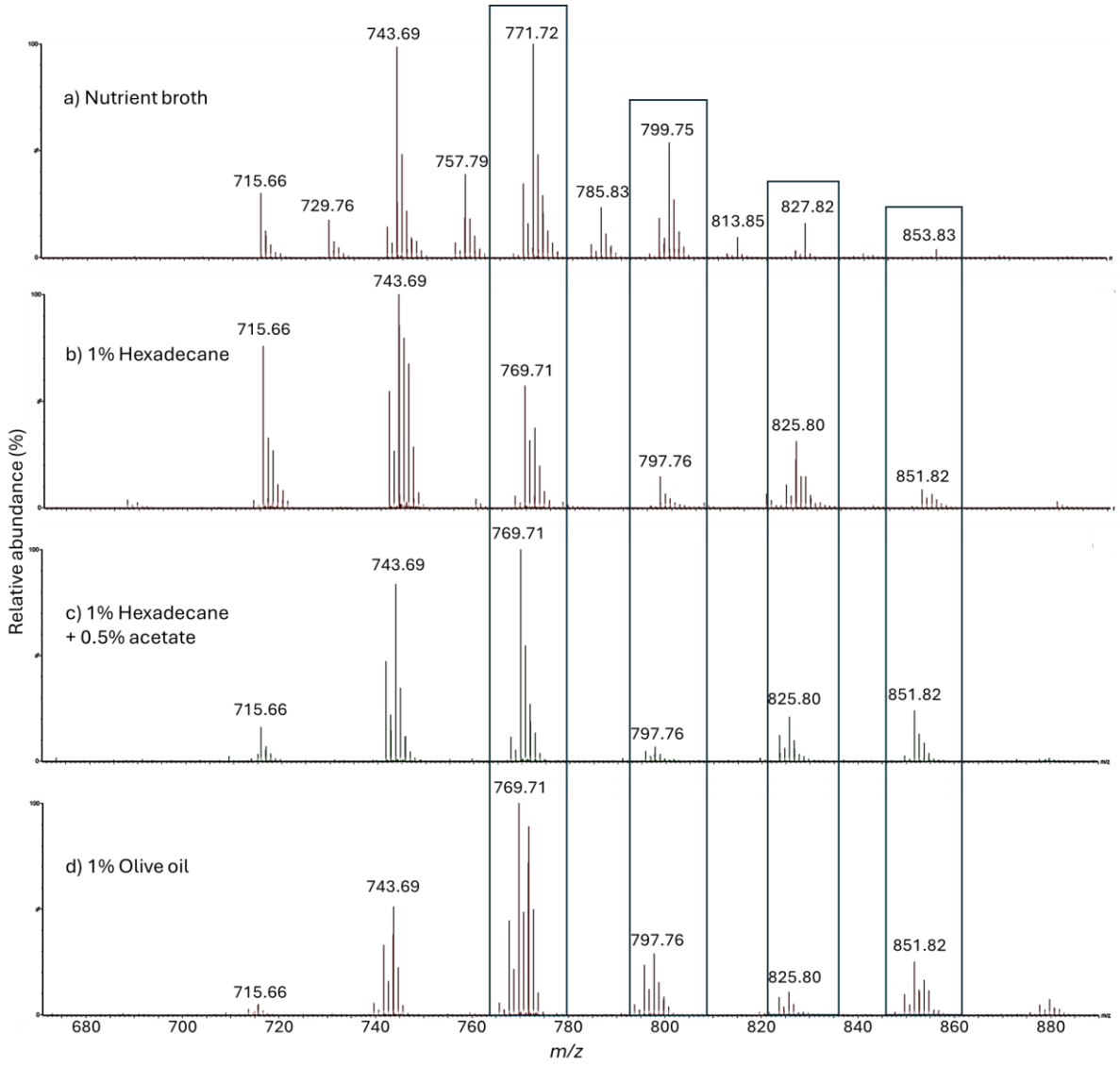

Figure 4.9: *Mass spectra (between 28 - 35 minutes) for saponified MA from Gordonia amarae cultures at the end of its growth curve in a) nutrient broth, b) 1% n-hexadecane, c) 1% n-hexadecane + 0.5% acetate and d) 1% olive oil. Showing difference in MA profiles in nutrient broth compared to minimal media.*

Changes were also found in the composition of minor lipid ions *m/z* sets on both polarity-extracted and saponified samples. Lipids with *m/z* of 759.79, 783.80 and 813.85 Da, abundant in *Gordonia amarae* grown in nutrient broth, were found to decrease significantly in cultures grown with hydrophobic carbon sources (Fig. 4.7), and in some cases were below detection (ANOVA & t-test $p < 0.01$, Shapiro-Wilk test ($\alpha = 0.05$) did not indicate a significant deviation from normality). However, there was an increase in the abundance of lipids with similar *m/z* (759.76, 783.72, and 813.77 Da) in cultures grown with hydrophobic carbon sources (Fig. 4.10) (see appendix for lipid ions abundancy ratios when normalised to lipid ion with *m/z* of 743.69 Da).

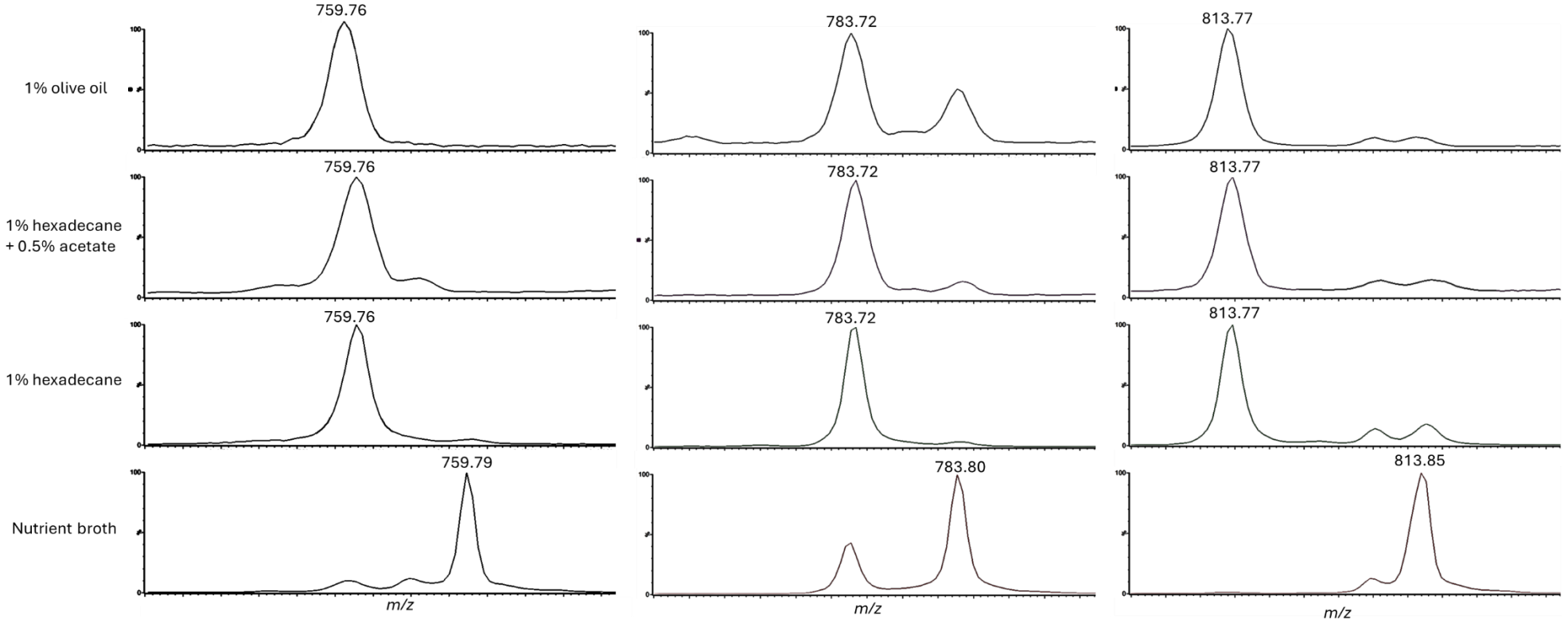

Figure 4.10: *Gordonia amarae mycolic acids changes observed cultures with hydrophobic carbon sources, when compared to nutrient broth culture. A shift of lipid ions with m/z of 759.79, 783.80 and 813.85 Da in nutrient broth cultures to lipid ions with m/z of 759.76, 783.72 and 813.77 Da, respectively, in minimal media cultures.*

To confirm these were distinct chemical species, their retention times were compared. When elution times were compared for lipid ions with *m/z* 783.80 and 783.72 in nutrient broth and 1% olive oil (where both ions were detected but at differing relative abundances), a retention time difference of approximately one minute was observed (Fig. 4.11). This elution separation supports the hypothesis that these ions represent distinct types of mycolic acids. Similar differences in elution times were also noted between ions *m/z* 759.79 and 813.85 (abundant in nutrient broth) when compared to *m/z* 759.76 and 813.77 (more abundant in minimal media). These retention time shifts further reinforce the likelihood of structural differences between these lipid species.

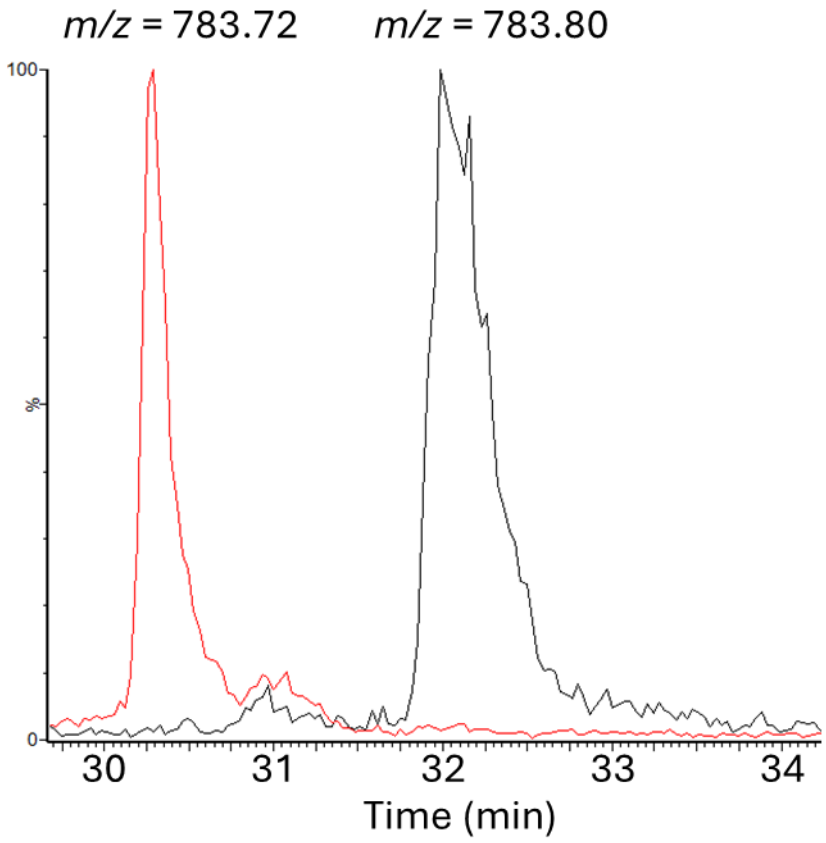

Figure 4.11: *Elution times for ions m/z 783.72 (left) and m/z 783.80 (right) showing a ~1 minute elution difference between them.*

Ions with *m/z* of 783.80 and 783.72 Da were present in both nutrient broth and 1% olive oil minimal media, but their relative abundancies differed, with 783.80 Da more abundant in nutrient broth and 783.72 Da dominant in 1% olive oil (Fig. 4.10). The presence of both lipid species across different media suggests that *Gordonia amarae* possesses the metabolic capacity to synthesize both forms, modulating their production in response to environmental conditions. This adaptive lipid regulation likely reflects a mechanism by which the bacteria optimises its membrane composition according to nutrient availability or stress factors associated with the growth medium (168).

The lipid ion with *m/z* of 759.79 Da, abundant in nutrient broth, could correspond to $C_{52}H_{103}O_2$ (1 double bond, -1.33 ppm mass accuracy), whereas the ion with *m/z* of 759.76 Da, observed in minimal media, could correspond to $C_{51}H_{99}O_3$ (2 double bonds, 3 ppm mass accuracy). These distinctions imply differences not only in unsaturation but also in number of carbons and oxygens. Teramoto *et al*. demonstrated the occurrence of α-type and oxygenated mycolic acids that differ only slightly in mass (169), due to the near-isobaric nature of CO and C_2H_4 units. The production of specific lipids by mycobacteria, in response to environmental conditions, has been previously documented by Smit *et al*. (126) who reported a distance-dependent lipid distribution at a natural gas seep, with the highest concentrations detected at the seep site. They identified previously unknown mycolic acids and high abundancies of unusual pentamethylated MAs, among other structural variants.

Predicted chemical formulas, mass accuracies, and number of double bonds are summarized in Table 4.5. Lipids predicted to contain only two oxygen atoms tend to decrease in abundance in minimal media, while others with three or more oxygen atoms appear to increase, suggesting a metabolic shift toward more oxidised lipid species under hydrophobic nutrient conditions.

Table 4.5: *Gordonia amarae mycolic acids changes observed in all minimal media cultures, when compared to nutrient broth culture.*

Media	Observed *m/z*	Predicted formula	Mass accuracy (ppm)	Number of double bonds
Minimal	759.7617	$C_{51}H_{99}O_3$	3.00	2
Nutrient	759.7948	$C_{52}H_{103}O_2$	-1.33	1
Minimal	783.7238	$C_{52}H_{95}O_4$	0.97	5
Nutrient	783.7985	$C_{54}H_{103}O_2$	3.44	3
Minimal	813.7737	$C_{54}H_{101}O_4$	4.56	4
Nutrient	813.8461	$C_{56}H_{109}O_2$	4.11	2

While *Gordonia amarae* is typically reported to produce MA with maximum chain lengths of 54 carbons (67), some work has reported *Gordonia amarae* is capable of synthesizing mycolic acids with chain lengths of up to 56 carbon atoms (66), aligning with the proposed molecular formula of $C_{56}H_{109}O_2$ for the lipid with *m/z* of 813.85 Da.

To the best of our knowledge, MA containing only two oxygen atoms have not been previously reported. However, exact mass-based molecular formula calculations suggest the presence of these structures. Confirmation through additional analysis techniques (e.g. NMR) would be necessary to definitively assign molecular formulas.

4.6. Conclusion

Growth monitoring and induction of biosurfactant and foam production by the foaming-associated mycobacteria *Gordonia amarae* were successfully achieved using minimal media supplemented with 1% n-hexadecane, 1% n-hexadecane + 0.5% acetate, and 1% olive oil. Quantification of surface-active substances (SAS) was carried out using polarography, revealing production levels of up to 502.37, 377.44, and 496.71 mg/L, respectively. Among these, 1% n-hexadecane induced the highest biosurfactant production and the most persistent foaming, which lasted over 24 hours. In contrast, nearly no SAS production or foam was observed in nutrient-rich media, indicating that biosurfactant synthesis is not constitutive, but rather induced under specific environmental conditions. These findings support the hypothesis that biosurfactant production by *Gordonia amarae* is tightly regulated by substrate availability, with hydrophobic carbon sources triggering biosurfactant synthesis to facilitate substrate uptake via emulsification. This regulatory mechanism highlights the metabolic adaptation of *Gordonia amarae* to environments with hydrophobic carbon sources present, and underlines its role in foam formation under wastewater treatment conditions.

Lipidomic profiling using UPLC-QToF-MS of both polarity-extractable and saponified mycolic acids revealed significant changes in lipid composition depending on the growth medium. *Gordonia amarae* cultures in nutrient-rich media displayed the most visibly diverse chromatographic lipid profile, including six main and four minor lipid sets, consistent with a more complex chromatographic pattern in this media. A constant 2 Da leftward shift in the *m/z* of the most abundant ions in several main lipid ions sets (*m/z* > 769 Da) was observed in all cultures with hydrophobic carbon sources. Specifically, most abundant ions with *m/z* of 771.72, 799.75, 827.82, and 853.83 Da in nutrient broth were replaced by 769.71, 797.76, 825.80, and 851.82 Da, respectively, in minimal media. This pattern suggests an increase in lipid unsaturation under nutrient-limited and stress conditions. In other bacteria, increased unsaturation has been reported as a mechanism to maintain membrane fluidity under stress conditions (170). Alternatively, this shift

could also represent a response aimed at enhancing the hydrophobicity of the bacterial cell wall, as demonstrated in other species (171).

Additional differences were observed in minor lipid ions sets. Lipid ions present in nutrient broth cultures, such as those at *m/z* 759.79, 783.80, and 813.85 Da, were reduced or undetectable in cultures containing hydrophobic carbon sources. Conversely, new ions at 759.76, 783.72, and 813.77 Da increased in abundance under these conditions. Accurate mass-based formula predictions suggest that lipids containing only two oxygen atoms decreased in minimal media, while those with three or more oxygen atoms became more prominent. These results appear to indicate a metabolic shift toward more oxidized lipid species under stress conditions. Additional structural elucidation techniques such as nuclear magnetic resonance (NMR), tandem mass spectrometry (MS/MS), or infrared (IR) spectroscopy would be required to confirm the identity these lipids.

In conclusion, the lipidomic shifts observed in *Gordonia amarae* under foaming related conditions, compared to nutrient-rich media, provide evidence that this bacterium modulates its lipid profile in response to environmental conditions. These findings establish a critical baseline for understanding lipid adaptations in foaming contexts and highlights the potential use of lipid biomarkers to monitor, possibly predict and prevent foaming events in activated sludge reactors of wastewater treatment plants. However, since these results were obtained from single-culture experiments, further investigation under more complex, mixed-community conditions representative of full-scale activated sludge reactors is required to determine whether similar lipidomic patterns can be observed in real-world systems.

Chapter 5: activated sludge characterisation under foaming and non-foaming related conditions

5.1. Introduction

The activated sludge (AS) process is designed to facilitate the aerobic biodegradation of organic matter within wastewater treatment plants (WWTPs). AS is one of the most widely employed biological methods for secondary wastewater treatment (172). In this process, microbial flocs are maintained in suspension within an aeration tank, where oxygen is supplied (typically as fine bubbles from the tank bottom) to promote efficient contact between microorganisms and the incoming wastewater and meet respiratory requirements of the microbial population (173). The microbial community within activated sludge is diverse, containing aerobic heterotrophic bacteria that degrade organic compounds, autotrophic nitrifiers and sulphur-oxidising bacteria, as well as denitrifying, sulphate-reducing, and phosphate-accumulating organisms (PAOs) the main responsible organisms for pollution reduction (174), (175).

The stability and efficiency of the AS process depend on the maintenance of an optimal microbial population density and activity. This is achieved by recycling a portion of the settled sludge from the secondary clarifier back into the aeration tank, ensuring nutrient availability thus continuous regeneration of active biomass and sustained pollutant degradation (173).

Filamentous bacteria within activated sludge are not primarily involved in pollutant removal but play a crucial structural role in the formation and stability of microbial aggregates, or flocs, which are essential for maintaining desirable sludge characteristics (174). The absence or low abundance of filamentous microorganisms can result in dispersed bacterial growth or the formation of small, weakly cohesive flocs, leading to poor settling properties and operational instability in aeration tanks and secondary clarifiers (174).

Conversely, excessive proliferation of filamentous bacteria can lead to increased biosurfactant production, causing the formation of stable foams on the surface of aeration tanks, negatively affecting plant performance and operations (176), and increasing maintenance and restoration costs (49). Such foams are often associated with significant microbial community shifts, typically characterised by the dominance of hydrophobic filamentous species such as *Actinobacteria* (e.g. *Gordonia*) and *Candidatus* Microthrix parvicella, compared with non-foaming activated sludge systems (24), (25).

The excessive proliferation of filamentous bacteria in WWTPs can be promoted by several operational and environmental factors, including low dissolved oxygen concentrations (< 2.0 mg/L), high sludge age (> 14 days) (177), as well as low food-to-microorganism ratios and the presence of hydrophobic substrates such as grease, oils (178), and long-chain fatty acids (179). Environmental factors such as temperature fluctuations, the presence of volatile fatty acids, and detergents have been shown to stimulate filamentous bacteria to form elongated chains and enhance biosurfactant production, thereby increasing the

likelihood of foaming events in AS systems. Although these factors are frequently associated with foaming episodes, the underlying mechanisms governing foam initiation and stabilisation are not fully understood. A more detailed understanding of the microbial community dynamics involved in these processes could provide valuable insights for the development of effective foam prevention and mitigation strategies.

High-throughput 16S rRNA gene sequencing has enabled detailed characterisation of microbial population dynamics within WWTPs (110), offering a powerful tool to investigate how operational and environmental factors influence community composition and function. This technique targets the 16S ribosomal RNA gene, a highly conserved genetic marker shared among all bacteria but containing hypervariable regions that allow for phylogenetic differentiation (180).

In this study, six one-month batch cultures of AS samples were established to evaluate how different growth conditions influence both microbial community dynamics and foam formation potential. Three cultures were grown in nutrient-rich media and three in minimal media supplemented with 1% n-hexadecane, a hydrophobic carbon source known to promote foaming-related conditions. To investigate the role of filamentous bacteria in shaping community behaviour, the foam-forming species *Gordonia amarae* (commonly associated with stable foams in wastewater treatment plants) was introduced in selected cultures using two distinct inoculation strategies.

Foaming potential was first assessed experimentally by inducing foam formation in 10 mL of each culture, simulating aeration conditions typical of AS reactors. Following this, high-throughput 16S rRNA gene sequencing was conducted to characterise shifts in microbial community composition over the one-month incubation period. This combined experimental design allowed us to examine how growth media, hydrophobic substrates, and the presence or absence of *Gordonia amarae* influence both foaming behaviour and microbial community under conditions representative of foaming and non-foaming environments. Microbial community shifts could be used as a marker to predict foaming events in wastewater treatment plants.

5.2. Aims

The aim of this study was to investigate how microbial community dynamics are shaped when activated sludge is exposed to foaming and non-foaming conditions, and how these dynamics are further influenced by the presence or absence of the foam-associated filamentous mycobacteria *Gordonia amarae*. Understanding these interactions is essential for identifying early microbial indicators of foam development and for improving strategies to predict and mitigate foaming events in wastewater treatment plants.

5.3. Objectives

This study was undertaken to elucidate how different culture conditions influence microbial community dynamics and foam formation potential in activated sludge samples. To achieve this, six one-month batch cultures were established; three grown in nutrient-rich media and three in foaming-related media. The filamentous foam-forming bacteria *Gordonia amarae*, frequently implicated in foaming events in wastewater treatment plants, was introduced using two distinct inoculation strategies to determine its role in shaping community structure and in aiding foaming formation under these contrasting conditions.

The first objective was to experimentally quantify foam formation capacity in each culture by inducing and measuring foam volume under simulating activated sludge aeration reactor conditions. The second objective was to characterise changes in microbial community composition using high-throughput 16S rRNA gene sequencing over the one-month incubation period in order to identify microbial patterns or indicators that could support the prediction and prevention of foaming events in wastewater treatment plants.

5.4. Experimental

5.4.1. Materials

Citric acid and magnesium sulphate heptahydrate were obtained from Sigma-Aldrich®. M9 salts and n-hexadecane were obtained from MP Biomedicals. Calcium chloride and sodium bicarbonate were obtained from Fisher Scientific™. Nutrient broth was obtained from Oxoid Ltd. 18.2 MΩ cm, Milli-Q, Millipore System Inc., USA. Casamino acids were obtained from VWR.

Gordonia amarae (NCIB 11222 strain) was purchased from NCIMB LTD.

5.4.2. Activated sludge collection and storage

Activated sludge samples were collected in August 2023 from Dunfermline wastewater treatment plant (Scotland, UK) after a foaming event. 1 mL of activated sludge was mixed with 0.5 mL of glycerol/water (50:50; v:v) solution and stored at -80 °C until use.

5.4.3. Bacterial growth in different media

Nutrient-rich media was prepared by dissolving 13 g of nutrient broth in 1L of MilliQ water. The solution was sterilized via autoclave at 120 °C for 15 minutes. 1 L of minimal media was prepared by adding 200 mL of minimal salts solution (56.4 g of M9 minimal salts in 1 L of water for 1 L stock) to 600 mL of MilliQ water. The mixture was supplemented with 2

mL of 1 M magnesium sulphate and 0.1 mL of 1 M calcium chloride. A 100 mL solution containing 10% (v/v) carbon source (n-hexadecane) in MilliQ water was added to the media. The solution was sterilized via autoclave at 120 °C for 15 minutes. A separate 100 mL solution containing 0.1 g/mL of casamino acids in MilliQ water was filter-sterilized and added to the sterile media.

Three different inoculation processes were used for nutrient-rich and minimal media. For inoculation process (A), a single colony of *Gordonia amarae* was aseptically transferred from an agar plate to 20 mL of nutrient broth and incubated at 30 °C for one week. Aliquots of this culture were used to inoculate 400 mL of fresh nutrient-rich or minimal media until an optical density (OD_{600}) of 0.08 AU was reached. These cultures were incubated at 30 °C and 150 rpm for one week. After this period, 200 µL of activated sludge samples (preserved in a 50:50 v/v glycerol:water solution) were added to the cultures. Cultures were then incubated at 30 °C and 150 rpm. Aliquots were collected for 16S rRNA and lipidomic analyses at the following time points: immediately after activated sludge inoculation (t_0), and at 3 days (t_1), 7 days (t_2), 10 days (t_3), 21 days (t_4), and 31 days (t_5) post-inoculation.

For inoculation process (B) a single colony of *Gordonia amarae* was aseptically transferred from an agar plate to 20 mL of nutrient broth and incubated at 30 °C for one week. Aliquots of this culture were used to inoculate 400 mL of fresh nutrient-rich or minimal media together with 200 µL of activated sludge samples (in 50:50 v/v glycerol:water). Cultures were incubated directly at 30 °C and 150 rpm. Aliquots were collected for 16S rRNA and lipidomic analyses at the same time points as Process (A): immediately after activated sludge inoculation (t_0), and at 3 days (t_1), 7 days (t_2), 10 days (t_3), 21 days (t_4), and 31 days (t_5) post-inoculation.

Inoculation process (C), 200 µL of activated sludge samples (in 50:50 v/v glycerol:water) were inoculated to 400 mL of nutrient-rich and minimal media. Cultures were then incubated at 30 °C and 150 rpm. Aliquots were collected for 16S rRNA and lipidomic analyses at the following time points: immediately after activated sludge inoculation (t_0), and at 3 days (t_1), 7 days (t_2), 10 days (t_3), 21 days (t_4), and 31 days (t_5) post-inoculation.

5.4.4. Foaming measurement

Foaming induction was achieved by adding a mixture of 0.38 g of citric acid and 0.72 g of sodium bicarbonate to 10 mL of liquid bacterial culture in a 25 mL measuring cylinder (2.5 cm internal diameter and 18 cm length). The reaction was left for 20 seconds before measuring the amount of foam produced.

5.4.5. Statistical analysis

Data normality was assessed using the Shapiro–Wilk test at a significance level of α = 0.05 prior to subsequent statistical analyses. The test was performed using the Stats Kingdom online platform (160).

Significant differences between experimental conditions were assessed through one-way and two-way analysis of variance (ANOVA) using Microsoft Excel.

5.4.6. 16s rRNA analysis

The 16S rRNA gene sequencing was performed by GENEWIZ, Inc. (Suzhou, China) using the Illumina MiSeq platform. DNA concentrations were quantified using a Qubit 2.0 Fluorometer (Invitrogen, Carlsbad, CA, USA). For each sample, 30–50 ng of genomic DNA was used to generate amplicons with the MetaVx™ Library Preparation Kit (GENEWIZ, South Plainfield, NJ, USA).

Amplicons targeting the V3–V5 hypervariable regions of the prokaryotic 16S rRNA gene were generated for taxonomic analysis. GENEWIZ designed a proprietary primer set targeting conserved regions flanking the V3, V4, and V5 hypervariable regions of bacterial and archaeal 16S rRNA genes. For samples containing eukaryotic DNA, amplification was limited to the V3–V4 regions. V3–V4 regions were amplified using forward primer CCTACGGRRBGCASCAGKVRVGAAT and reverse primer GGACTACNVGGGTWTCTAATCC, while the V4–V5 regions were amplified using forward primer GTGYCAGCMGCCGCGGTAA and reverse primer CTTGTGCGGKCCCCCGYCAATTC. The initial PCR products served as templates for a second-round PCR, which enriched the amplicons and incorporated indexed adapters at both ends to produce uniquely barcoded libraries suitable for Illumina sequencing.

The resulting libraries were validated using an Agilent 2100 Bioanalyser (Agilent Technologies, Palo Alto, CA, USA) and quantified with a Qubit 2.0 Fluorometer. Libraries were pooled in equimolar ratios and sequenced on an Illumina MiSeq platform (Illumina, San Diego, CA, USA) following the manufacturer's instructions, using a 2 × 300 bp (or 2 × 250 bp) paired-end configuration. Image analysis and base calling were performed with the MiSeq Control Software.

5.4.7. Bioinformatics and sequence data processing

The 16S rRNA gene sequencing data were processed and analysed using the QIIME (1.9.1) software. Paired-end reads were merged, demultiplexed according to their unique barcodes, and trimmed to remove barcode and primer sequences. Quality filtering was performed to exclude low-quality reads using the following criteria: sequence length <

200 bp, no ambiguous bases, or mean quality score ≥ 20. Sequences were then compared with the reference database (RDP Gold database) using UCHIME algorithm to detect and later remove chimeric sequences.

Operational taxonomic units (OTUs) were clustered using VSEARCH (version 1.9.6) at a 97% sequence identity threshold against the SILVA 119 reference database. Taxonomic classification of representative OTU sequences was performed using the Ribosomal Database Project (RDP) Classifier with a confidence threshold of 0.8, based on the SILVA 119 taxonomy, which provided annotations down to the genus level.

5.5. Results and discussion

5.5.1. Foaming measurement

Foaming potential was assessed by inducing foam formation through the addition of a citric acid and sodium bicarbonate mixture to 10 mL of each culture in a 25 mL measuring cylinder. The reaction generated carbon dioxide gas, which formed bubbles within the liquid phase. Cultures tested included: *Gordonia amarae* pre-cultured for one week followed by MLSS inoculation in minimal media with 1% *n-hexadecane*; *Gordonia amarae* pre-cultured for one week followed by MLSS inoculation in nutrient broth; *Gordonia amarae* and MLSS inoculated simultaneously in 1% *n-hexadecane* minimal medium; *Gordonia amarae* and MLSS inoculated simultaneously in nutrient broth; MLSS alone in 1% *n-hexadecane* minimal medium; and MLSS alone in nutrient broth. In cultures containing biosurfactants, the reduced surface tension at the air–liquid interface facilitated bubble stabilisation, resulting in visible foam accumulation. The foam height was recorded 20 seconds after the addition of the citric acid and sodium bicarbonate mixture (Fig. 5.1), providing a comparative measure of foaming accumulation capacity among the cultures.

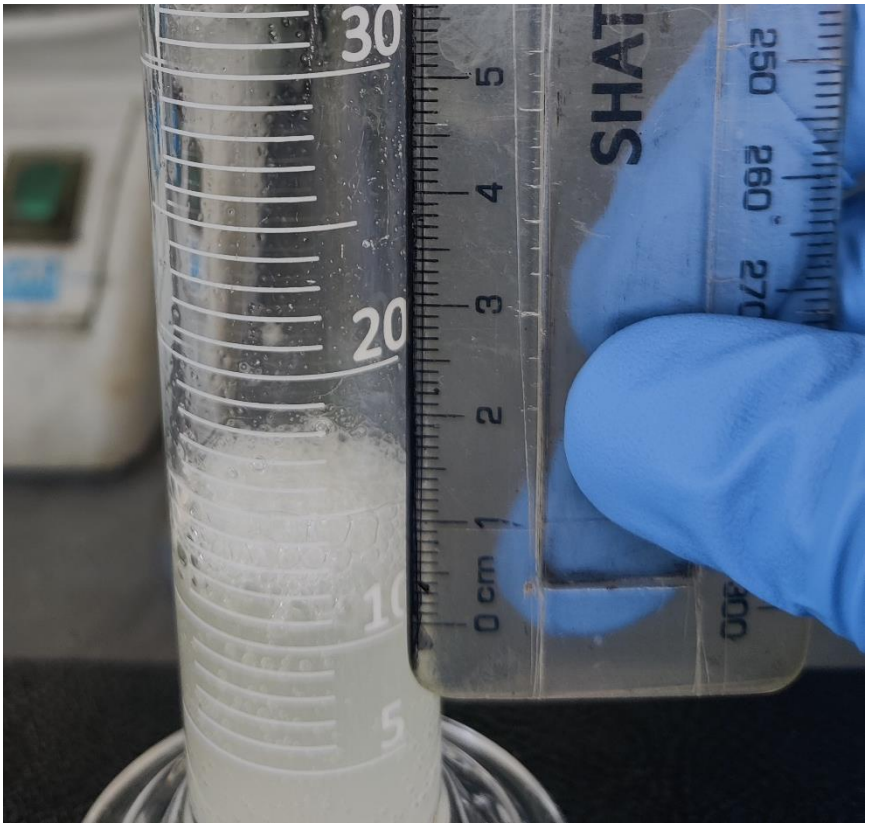

Figure 5.1: *Foaming potential of the experimental cultures, quantified as foam height measured 20 s after the addition of a citric acid–sodium bicarbonate mixture to 10 mL of culture.*

Distinct levels of foaming were observed among all cultures (Fig. 5.2). Cultures supplemented with 1% *n-hexadecane* as main carbon source exhibited the greatest foam formation in all cases. The highest foaming activity occurred when *Gordonia amarae* was pre-cultured for one week prior to the inoculation of activated sludge in minimal media with 1% *n-hexadecane* as main carbon source (average of 1.98 cm). This outcome was expected, as *Gordonia amarae* has been previously shown to produce substantial amounts of biosurfactants and foam under similar growth conditions (see Chapter 4). The accumulation of foam after 31 days of incubation indicates that the biosurfactants produced by *Gordonia amarae* remained stable throughout the culture period and were not degraded or utilised as an alternative carbon source, as previously suggested to be possible (181). Furthermore, this result also suggests that the overall biosurfactant concentration may have increased following the addition of activated sludge, potentially due to the proliferation of other foam-associated microorganisms.

The second highest foaming activity was observed in the culture where *Gordonia amarae* and activated sludge were inoculated simultaneously in minimal media with 1% *n-hexadecane* as main carbon source (average of 0.50 cm). This suggests that even at low abundance, the presence of *Gordonia amarae* in media containing hydrophobic carbon sources can contribute to foam accumulation and stabilisation, concordant to previous studies (50).

Finally, the MLSS culture itself also produced a small amount of foam (average of 0.28 cm), although it was the lowest among the cultures in minimal media with 1% *n-hexadecane* as main carbon source. This observation suggests that other foam-associated microorganisms were present within the AS community and could be stimulated to produce biosurfactants when exposed to hydrophobic carbon sources.

A low level of foaming was also detected in the culture where *Gordonia amarae* was pre-cultured for one week prior to MLSS inoculation in nutrient broth. This indicates that high cell densities of *Gordonia amarae* may create favourable conditions for the proliferation or activation of other foam-producing bacteria, thereby promoting foam formation even under conditions not typically associated with foaming. Interestingly, slight foaming was also observed in MLSS alone but not in the culture where MLSS and *Gordonia amarae* were inoculated simultaneously. This may indicate that competitive interactions between *Gordonia amarae* and native sludge microorganisms suppress the conditions required for foam formation when both communities are introduced concurrently and hydrophobic carbon sources are absent.

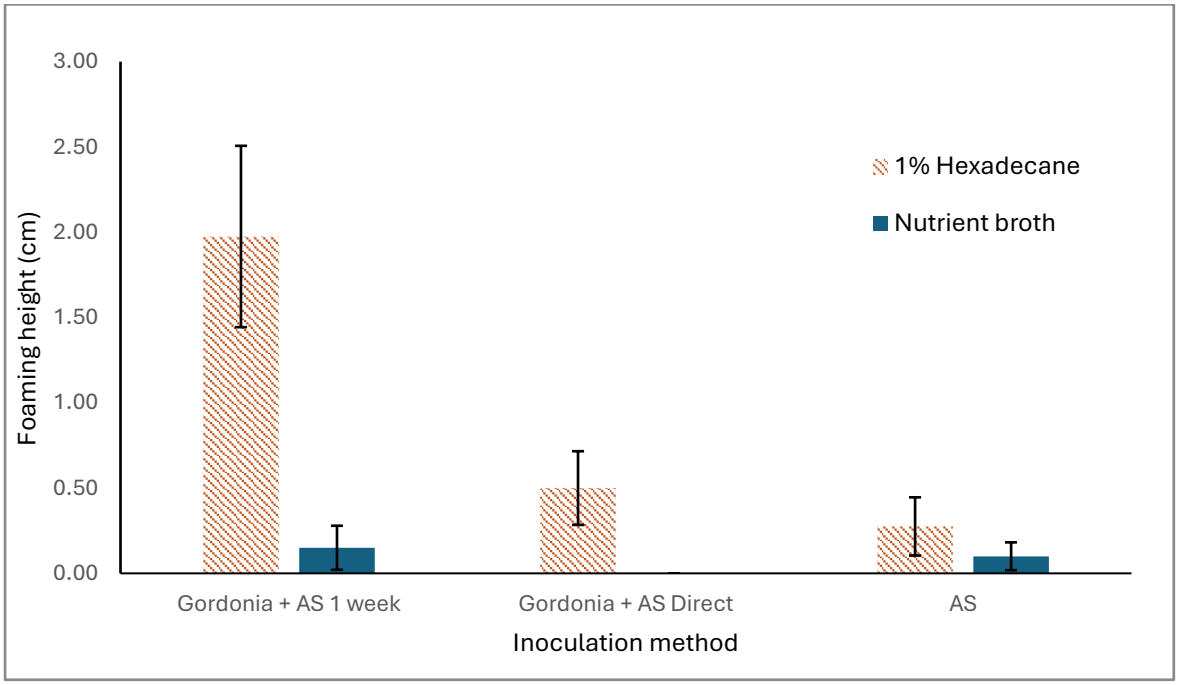

Figure 5.2: *Foam heights measured for each experimental culture following chemical foam induction. Cultures grown in minimal medium supplemented with 1% n-hexadecane exhibited substantially greater foam formation than nutrient-rich cultures. The highest foam levels were observed in cultures where Gordonia amarae was pre-cultured for one week prior to MLSS inoculation, highlighting the combined effect of hydrophobic substrate availability and inoculation strategy on foaming potential (Two-way ANOVA, $p < 0.05$).*

Two-way ANOVA with replication revealed that both the type of culture medium and the method of inoculating the microbial community had a significant effect on foam formation ($p < 0.05$). A significant interaction between these two factors ($p < 0.05$) indicated that the effect of microbial community inoculation on foam formation also

depended on the composition of the culture medium. Normality was assessed using the Shapiro-Wilk test (α = 0.05), which did not indicate a significant deviation from normality.

Together, these results highlight the complex ecological relationships between *Gordonia amarae* and activated sludge microorganisms in regulating biosurfactant-mediated foam formation. To get a better understanding of the real changes in microbial communities when all these growing conditions are applied, a 16s rRNA analysis was performed.

5.5.2. Microbial community profiles

High-throughput 16S rRNA gene sequencing was performed on all six culture conditions. Despite some limitations caused by the presence of suspended solids and residual organic matter in MLSS inoculums, taxonomic assignment down to the genus level was achieved, enabling a comparative assessment of community composition and temporal dynamics across the 30 most abundant genera (Fig. 5.3). Across all cultures and timepoints (excluding T0), genera *Phascolarctobacterium* and *Citrobacter* consistently emerged as dominant members of the community, reaching final relative abundances of approximately 10–20 % and 4–7 %, respectively. Their persistence across all experimental conditions suggests that these taxa are metabolically versatile under the presence of other bacteria and stress conditions.

In cultures where *Gordonia amarae* was pre-grown for one week prior to MLSS inoculation, *Gordonia* genus dominated the community at the initial timepoint (T0), representing approximately 87% of the total relative abundance in both media types. Although its relative abundance declined over the incubation period following MLSS addition, *Gordonia* remained detectable throughout the experiment, stabilising at ~3% in the n-hexadecane minimal media (Fig. 5.3 A) and ~4.6% in nutrient broth (Fig. 5.3 B) by the final sampling point. These findings underscore the importance of initial community composition in shaping long-term microbial dynamics, consistent with previous reports in complex microbial ecosystems (182).

In cultures in which *Gordonia amarae* and AS were inoculated simultaneously, *Gordonia* was also the most abundant genus at T0, accounting for 17–28 % of the community depending on the media. However, unlike the preculture condition, *Gordonia* declined rapidly in both media following incubation, reaching relative abundances below 0.5% at later timepoints. This pattern suggests that when *Gordonia amarae* is introduced at low initial density and in direct competition with the native MLSS community, it is quickly outcompeted and does not establish long-term dominance. Nevertheless, its presence could still have a significant impact in microbial population and foaming conditions.

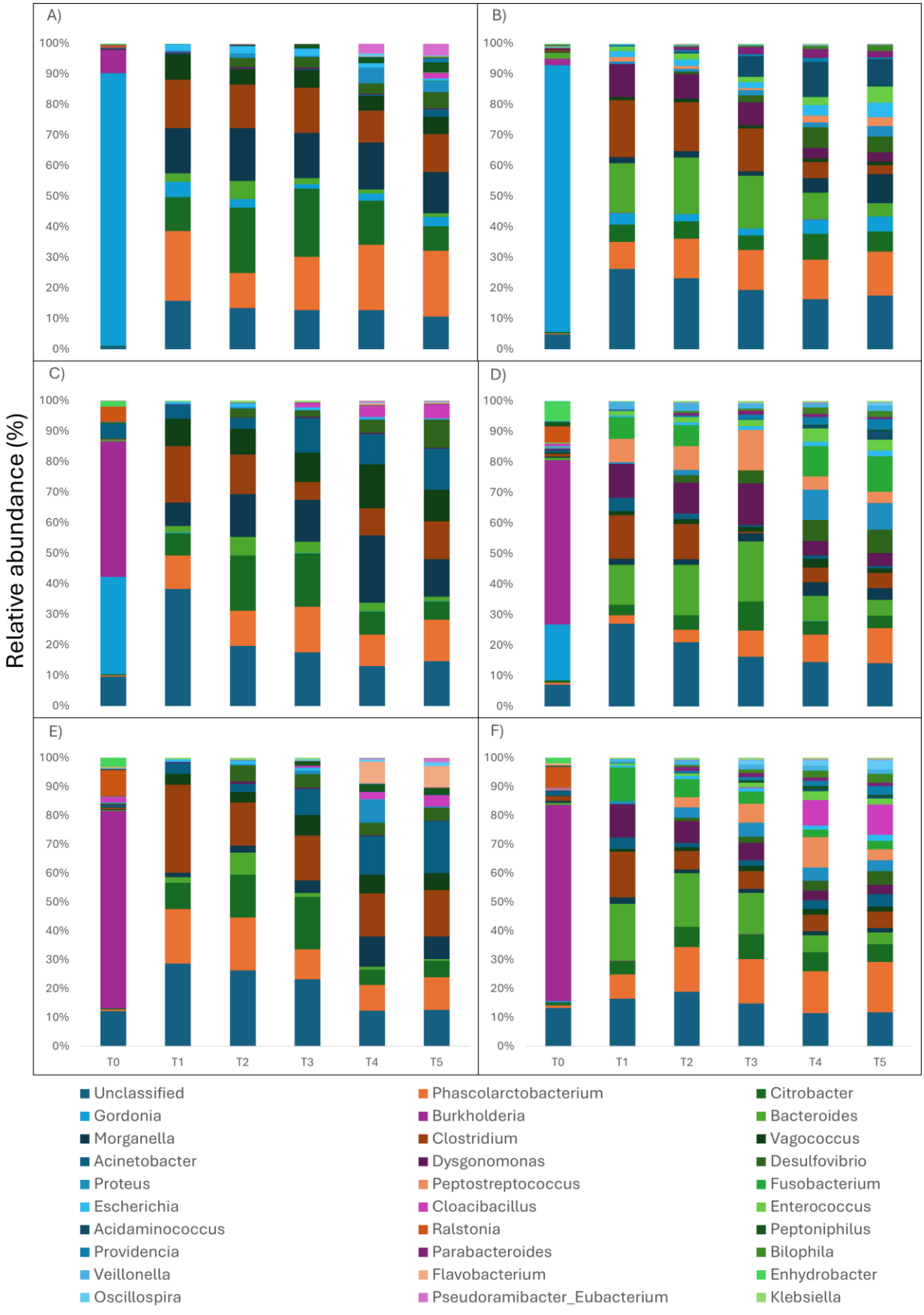

Figure 5.3: *Genus-level microbial community composition based on 16S rRNA gene sequencing for cultures grown under different media and inoculation strategies over the incubation period. Panels show: (A) foaming-related medium with Gordonia amarae pre-cultured for one week prior to MLSS inoculation; (B) nutrient-rich medium with Gordonia*

amarae pre-cultured for one week prior to MLSS inoculation; (C) foaming-related medium with simultaneous inoculation of Gordonia amarae and MLSS; (D) nutrient-rich medium with simultaneous inoculation of Gordonia amarae and MLSS; (E) foaming-related medium with MLSS inoculated alone; and (F) nutrient-rich medium with MLSS inoculated alone.

When community dynamics were examined with respect to growth medium (nutrient broth versus minimal medium supplemented with 1% *n-hexadecane*), clear medium-dependent shifts in genus-level composition were observed for several genera. *Morganella* (Fig. 5.4 A) and *Vagococcus* (Fig. 5.4 B) consistently exhibited higher relative abundances in the *n-hexadecane* cultures than in nutrient-rich media.

To statistically assess whether these differences were significant, one-way ANOVA was conducted across timepoints T1–T5 (T0 was excluded as it represents the inoculation baseline and does not reflect true community dynamics). Normality was assessed using the Shapiro-Wilk test ($\alpha = 0.05$), which did not indicate a significant deviation from normality. *Vagococcus* displayed a significant effect of growth media ($p < 0.05$) under all inoculation conditions, indicating that *n-hexadecane* consistently promoted its enrichment regardless inoculation method of *Gordonia amarae*. Although significant across all conditions, cultures containing *Gordonia amarae* showed a higher relative abundance of *Vagococcus* than in AS alone. Similarly, *Morganella* also showed significant media-associated differences ($p < 0.05$) in cultures where *Gordonia amarae* was pre-grown for one week prior to MLSS inoculation and where *Gordonia amarae* and MLSS were inoculated simultaneously. For the MLSS only cultures, an initial p-value of 0.056 (T1–T5) was obtained. However, significance was achieved ($p = 0.031$) when the earliest timepoint (T1) was removed, suggesting that the medium effect becomes more pronounced after initial community adaptation.

These findings indicate that foaming-related media containing hydrophobic carbon sources preferentially supports the growth of both *Morganella* and *Vagococcus* compared with nutrient-rich media. Although there is currently limited evidence that these genera include species capable of degrading hydrophobic substrates or producing biosurfactants, many bacteria (including *Gordonia amarae*) are known to synthesise surface-active compounds that enhance access to hydrophobic carbon sources (183). Such surface-active molecules enhance substrate bioavailability by lowering surface tensions and increasing solubilisation of hydrophobic molecules (184).

The accelerated and higher enrichment of *Morganella* in cultures containing *Gordonia amarae* further suggests a potential facilitative interaction. Even at low relative abundance, *Gordonia amarae* may create favourable physicochemical conditions (e.g., partial hydrocarbon degradation, biosurfactant production, or altered aqueous–organic interfacial properties) that indirectly promote the enrichment and accelerated proliferation of *Morganella* under hydrocarbon-based growth conditions.

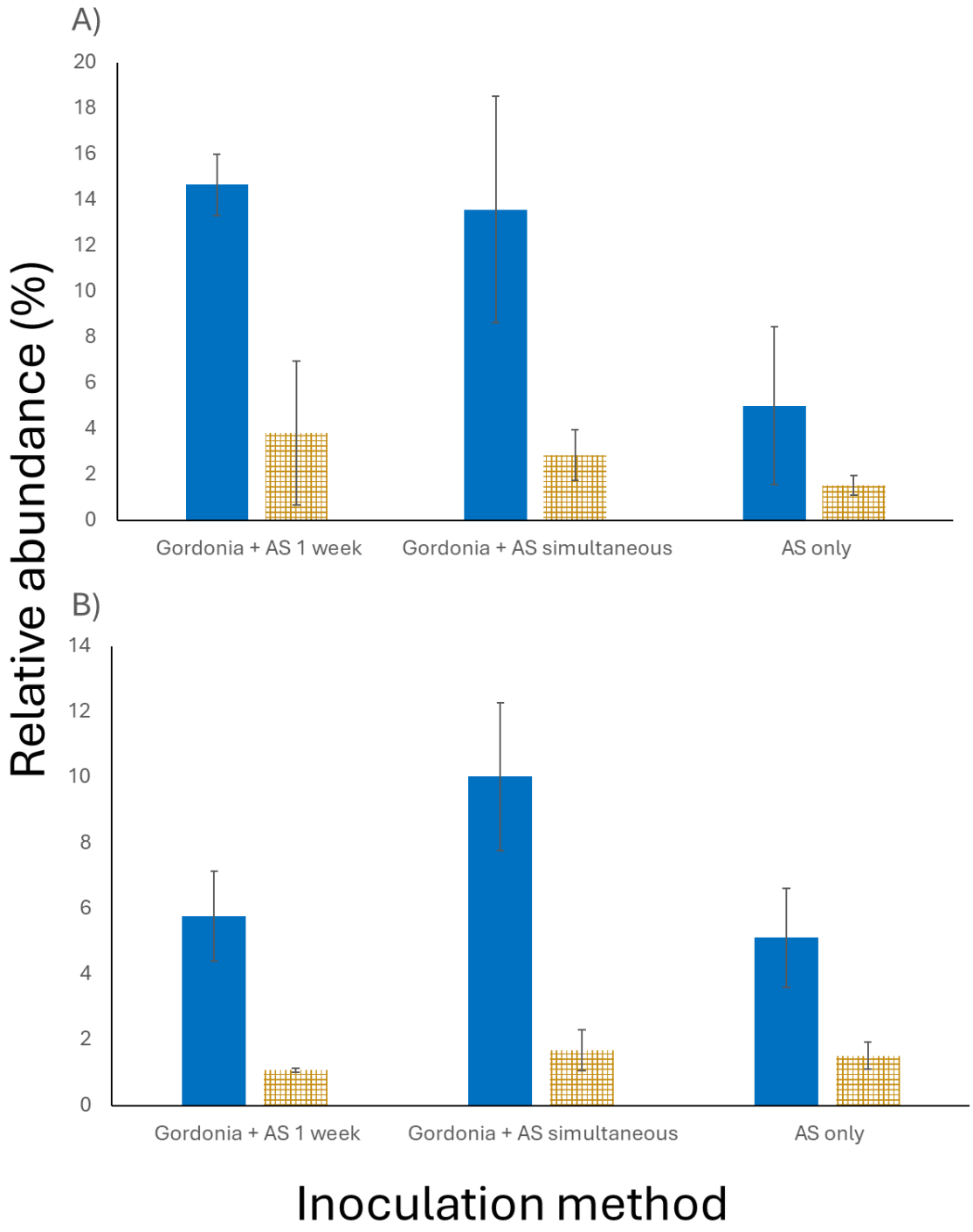

Figure 5.4: *Comparison of duplicate cultures average population relative abundance (%) of A) Morganella, B) Vagococcus in 1% n-hexadecane minimal media (straight blue) vs nutrient-rich media (pattern orange). Both genera exhibited significantly higher relative abundances under foaming-related conditions compared with nutrient-rich media (one-way ANOVA, $p < 0.05$). Error bars represent standard deviation of Morganella and Vagococcus relative abundancies across T1-T5.*

On the other hand, genera *Bacteroides*, *Dysgonomona* and *Peptostreptococcus* were consistently more abundant in nutrient-rich cultures compared with foaming associated cultures containing a hydrophobic carbon source (Fig 5.5). *Bacteroides* (dominant component of the human intestinal bacteriome, accounting for between 5 and 40% of all

anaerobes (185)) and *Dysgonomonas* have been associated with the degradation of complex biopolymers (186), while *Peptostreptococcus* species have been positively linked to protein and peptide degradation in WWTPs (187). One-way ANOVA performed across timepoints T1–T5 demonstrated a significant effect of growth medium for all three genera ($p < 0.05$), indicating that the presence of hydrophobic substrates and foaming-associated conditions suppressed their enrichment. Normality was assessed using the Shapiro-Wilk test ($\alpha = 0.05$), which did not indicate a significant deviation from normality.

Bacteroides (Fig. 5.5 A) and *Dysgonomona* (Fig. 5.5 B) exhibited relatively stable relative abundances across inoculation methods (~12 % and 6 – 8.5 %, respectively), suggesting that the presence of *Gordonia amarae* did not substantially influence their proliferation. In contrast, *Peptostreptococcus* (Fig. 5.5 C) displayed reduced relative abundance in cultures where *Gordonia amarae* was pre-grown for one week prior to MLSS inoculation, compared to the other inoculation methods. Although *Peptostreptococcus* still exhibited statistically significantly higher abundance in nutrient-rich cultures compared with minimal media, this reduction suggests that the presence of *Gordonia amarae* at high concentrations may produce a slight inhibitory effect on *Peptostreptococcus*, potentially due to competitive displacement.

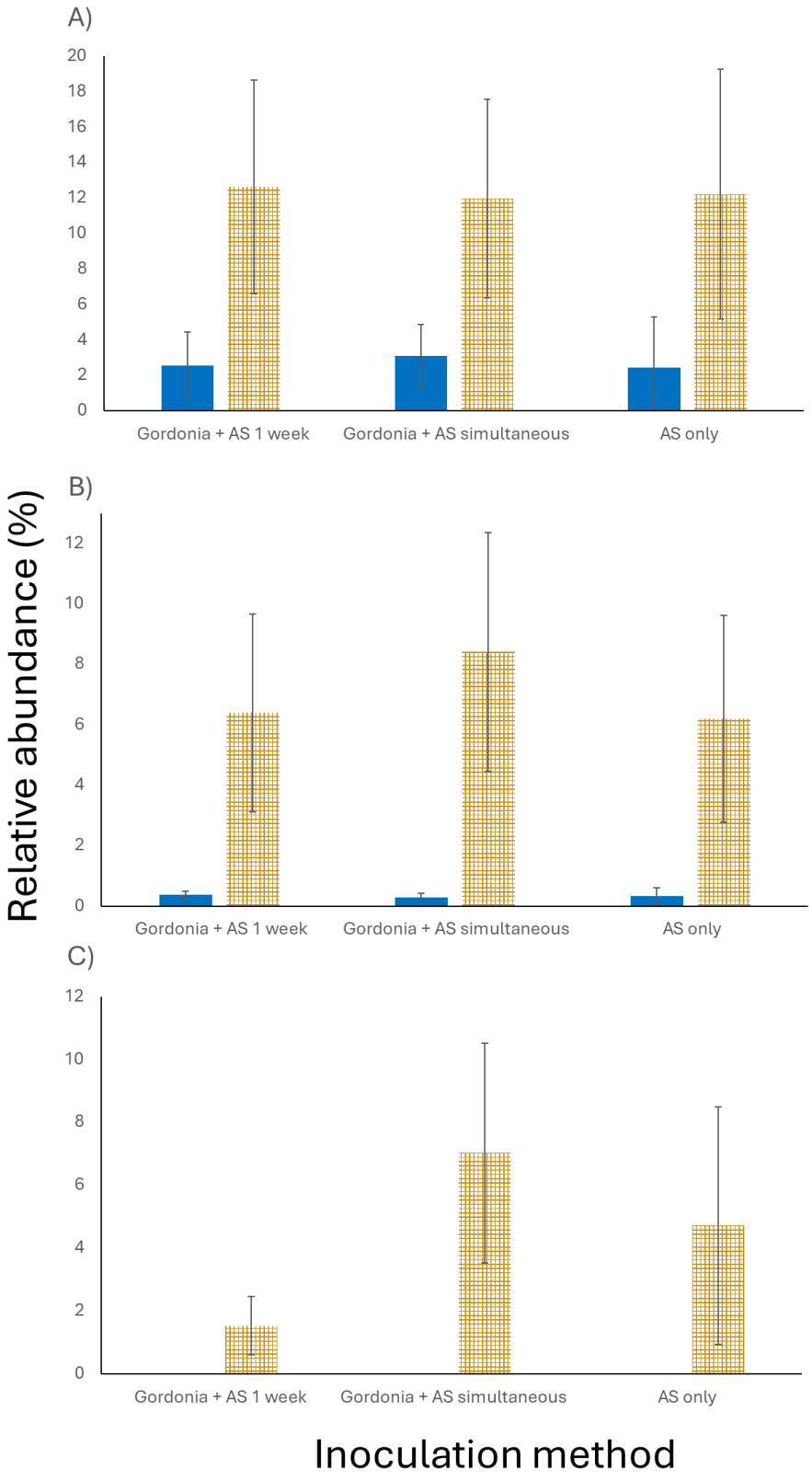

Figure 5.5: *Comparison of duplicate cultures average population relative abundance (%) of A) Bacteroides, B) Dysgonomonas and C) Peptostreptococcus in 1% n-hexadecane minimal media (straight blue) vs nutrient-rich media (pattern orange). These genera exhibited significantly higher relative abundances under nutrient-rich media compared with foaming-related conditions (one-way ANOVA, $p < 0.05$). Error bars represent standard deviation of Bacteroides, Dysgonomonas and Peptostreptococcus relative abundancies across T1-T5.*

When community dynamics were analysed with respect to inoculation method (*Gordonia amarae* pre-grown for one week prior to MLSS inoculation, simultaneous inoculation of *Gordonia amarae* and MLSS, and MLSS-only), several inoculation-dependent shifts in genus level composition were observed. Genus *Acinetobacter* (Fig. 5.6) exhibited comparable relative abundancies in cultures where *Gordonia amarae* and MLSS were inoculated simultaneously and in MLSS-only cultures, reaching average abundancies of 8–9% in foaming-related cultures (containing a hydrophobic carbon source) and 1.7–2.9% in nutrient-rich media. In contrast, cultures in which *Gordonia amarae* was pre-grown for one week prior to MLSS inoculation showed markedly lower average *Acinetobacter* abundancies, not exceeding 0.7% in foaming-related cultures or 0.03% in nutrient-rich media.

Statistical analysis demonstrated that the absence of *Gordonia amarae*, or its presence at low relative abundance, was associated with significantly higher *Acinetobacter* growth in foaming-related cultures compared with nutrient-rich cultures ($p < 0.05$). However, when *Gordonia amarae* was present at high relative abundance, *Acinetobacter* showed minimal growth and no significant difference between the two media types ($p = 0.16$). Normality was assessed using the Shapiro-Wilk test ($\alpha = 0.05$), which did not indicate a significant deviation from normality.

These findings indicate a strong antagonistic interaction between *Gordonia amarae* and *Acinetobacter* under the conditions tested, being opposite to previous reports by Kim et al (188), who described the competitive exclusion of *Gordonia* in co-cultures with *Acinetobacter* in controlled aerobic and anaerobic reactors. The apparent discrepancy likely reflects the increased ecological complexity of MLSS communities, where indirect interactions and multi-species feedback mechanisms can modify pairwise competitive outcomes observed in simplified co-culture systems (189). In complex microbial ecosystems, high initial dominance of a given taxon can lead to competitive exclusion of other strains while simultaneously enabling alternative stable states or bistable interactions among community members (190). Accordingly, the dominance of *Gordonia amarae*, even at early stages only, when introduced simultaneously with MLSS, may have been sufficient to modulate *Acinetobacter* population trajectories, suppressing its enrichment even under conditions that would otherwise favour its proliferation.

Collectively, these results indicate that the presence and initial dominance of *Gordonia amarae* can substantially modulate *Acinetobacter* dynamics, potentially suppressing its enrichment even under conditions that would otherwise favour its growth.

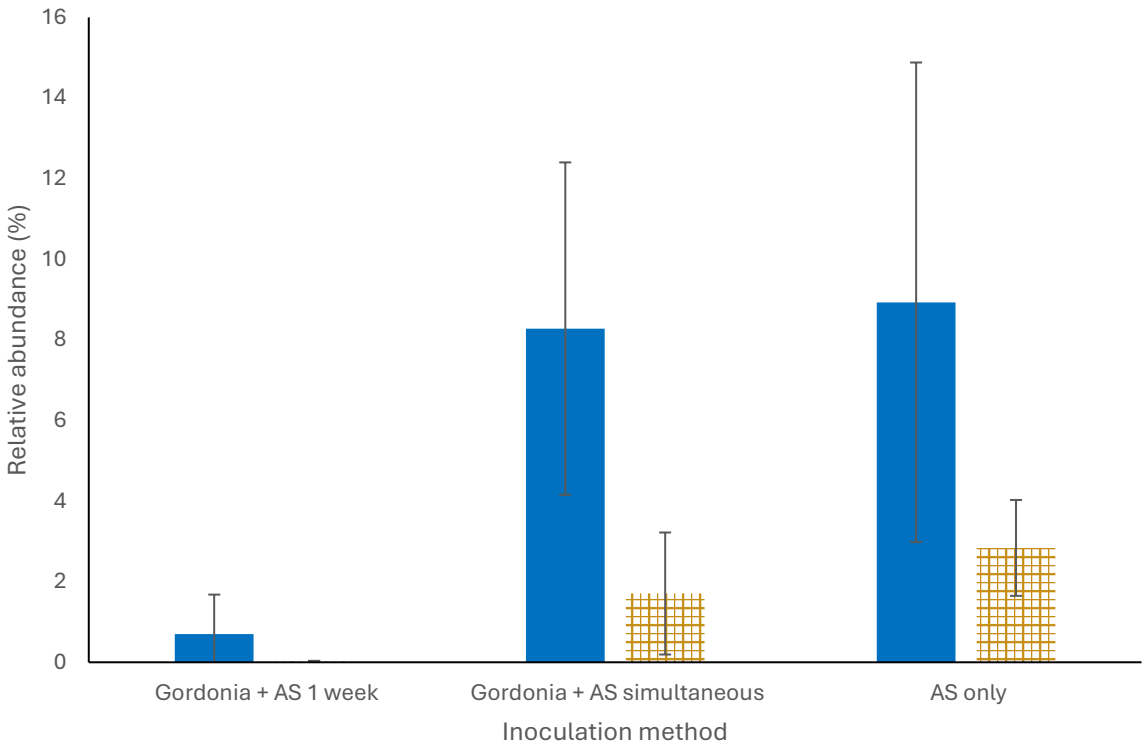

Figure 5.6: *Comparison of duplicate cultures average population relative abundance (%) of Acinetobacter genus in 1% n-hexadecane minimal media (straight blue) vs nutrient-rich media (pattern orange). This genus exhibited significantly higher relative abundances under foaming-related conditions compared with nutrient-rich media (one-way ANOVA, $p < 0.05$). Error bars represent standard deviation of Acinetobacter relative abundancies across T1-T5.*

Genus *VadinCA02* (Fig. 5.7) also displayed a clear inoculation-dependent pattern. In AS-only cultures, *VadinCA02* showed a pronounced increase in relative abundance during the final two sampling points (T4–T5), reaching ~7% in foaming-related cultures, while remaining undetectable in nutrient-rich media. In contrast, cultures containing *Gordonia amarae* exhibited markedly lower *VadinCA02* levels, which did not exceed 0.5% under any condition. These findings indicate that although *VadinCA02* is capable of proliferating under foaming-related, hydrocarbon-based conditions, its enrichment requires a prolonged adaptation period (~21 days). Moreover, the consistently low abundances observed in cultures where *Gordonia amarae* was present suggest that *Gordonia amarae* may exert an inhibitory effect on *VadinCA02* proliferation. Statistical analysis confirmed these observations, with the presence of *VadinCA02* being significant ($p < 0.05$) only in cultures where AS was inoculated alone in the foaming-related medium, and only after its extended adaptation period. Normality was assessed using the Shapiro-Wilk test ($\alpha = 0.05$), which did not indicate a significant deviation from normality.

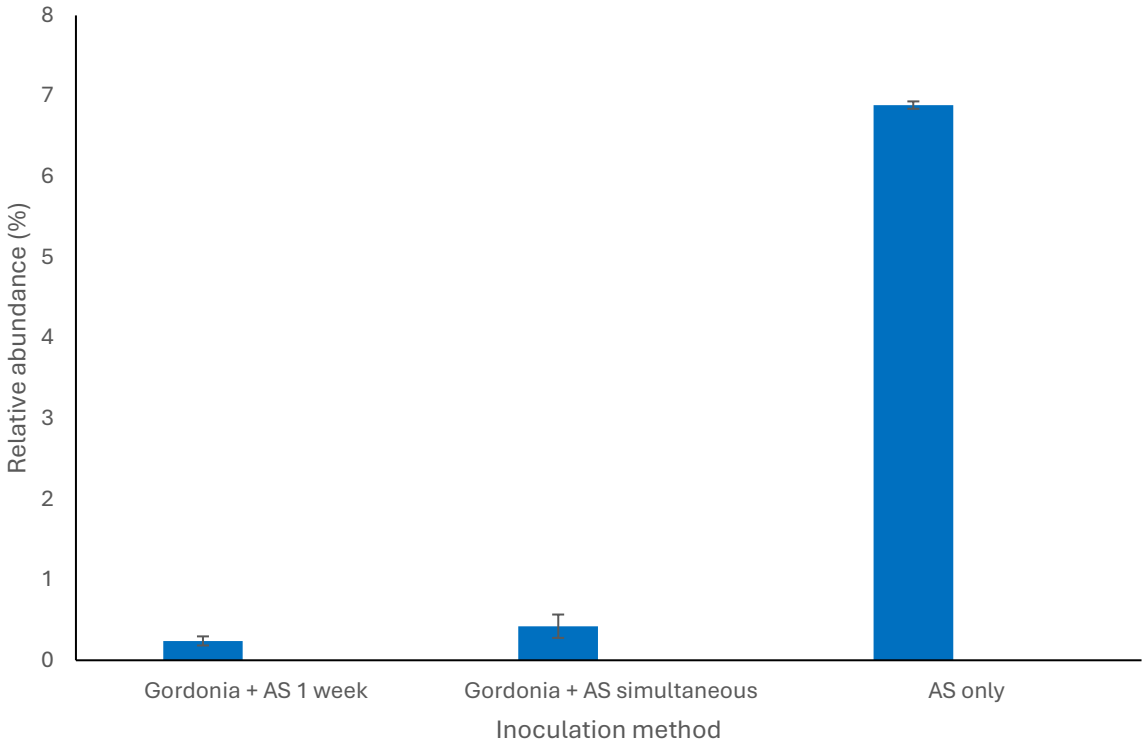

Figure 5.7: *Comparison of duplicate cultures average population relative abundance (%) of VadinCA02 genus in 1% n-hexadecane minimal media (straight blue) vs nutrient-rich media (pattern orange). This genus exhibited significantly higher relative abundances under foaming-related conditions compared with nutrient-rich media (one-way ANOVA, $p < 0.05$). Error bars represent standard deviation of VadinCA02 relative abundancies across T4-T5.*

Finally, genus *Acidaminococcus* (Fig. 5.8) exhibited a distinct inoculation-dependent response. Cultures in which *Gordonia amarae* was pre-grown for one week prior to MLSS inoculation showed a marked increase in *Acidaminococcus* relative abundance in nutrient-rich media after an extended adaptation period of approximately 10 days (T3-T5). Under these conditions, *Acidaminococcus* reached relative abundances of ~8.7%. In contrast, cultures inoculated simultaneously with *Gordonia amarae* and AS, as well as AS-only cultures, remained below 1.2% in nutrient-rich media and below 1% in all foaming-related media. Statistical analysis corroborated these trends; *Acidaminococcus* overgrowth was significant ($p < 0.05$) only in the nutrient-rich cultures where *Gordonia amarae* was pre-grown for one week prior to MLSS inoculation, and only between T3-T5. Normality was assessed using the Shapiro-Wilk test ($\alpha = 0.05$), which did not indicate a significant deviation from normality. These findings indicate that inoculation method and strongly influence *Acidaminococcus* proliferation, with pre-established *Gordonia amarae* populations facilitating its later-stage enrichment.

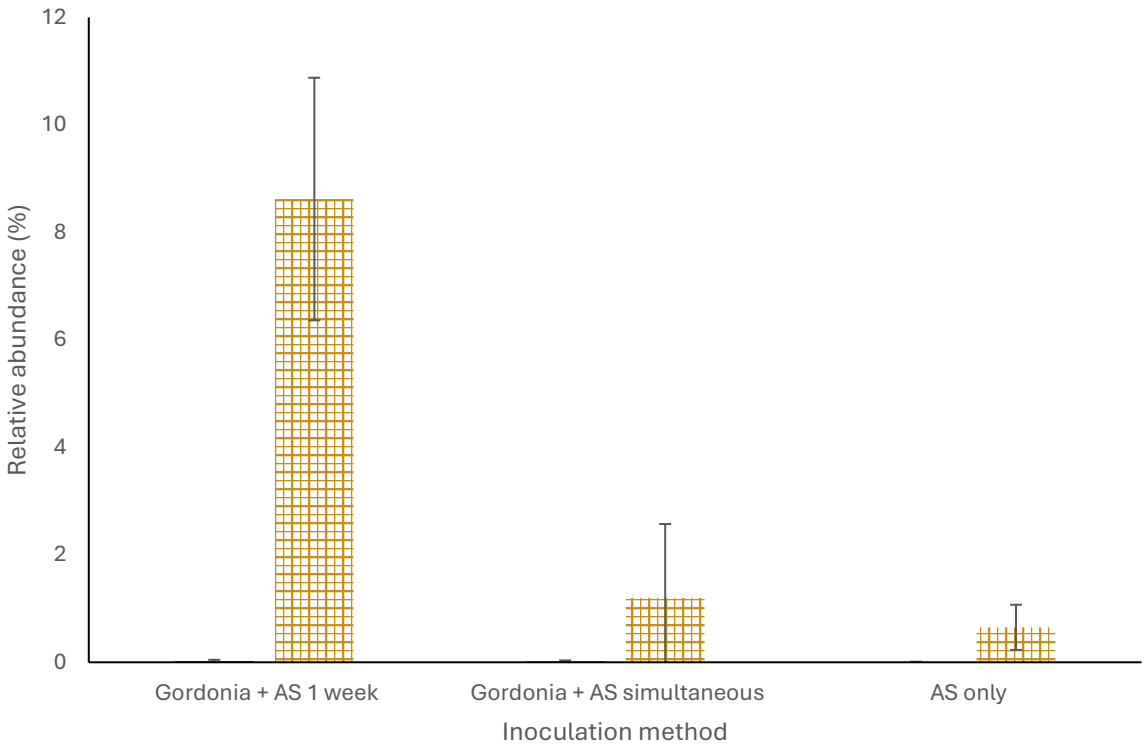

Figure 5.8: *Comparison of duplicate cultures average population relative abundance (%) of Acidaminococcus genus in 1% n-hexadecane minimal media (straight blue) vs nutrient-rich media (pattern orange). This genus exhibited significantly higher relative abundances under nutrient-rich media compared with foaming-related conditions (one-way ANOVA, $p < 0.05$). Error bars represent standard deviation of Acidaminococcus relative abundancies across T3-T5.*

Surprisingly, and despite all samples originating from an aerobic AS reactor, many of the genera exhibiting the strongest media- or inoculation-dependent shifts were taxa typically classified as anaerobic. This was unexpected because cultures were opened and exposed to air regularly throughout the experiment. *Bacteroides*, *Acidaminococcus* and *Peptostreptococcus* are obligate or strict anaerobes (191), (192), (193); these microorganisms can be inhibited by the presence of oxygen (194). *Dysgonomonas*, Vagococcus have been reported to be facultative anaerobes (195), (196). *VadinCA02* has also been associated with fermentative metabolism in anaerobic digestion systems (197). Conversely, *Morganella* is reported to grow under both aerobic and facultative anaerobic conditions (198), *Acinetobacter* is strictly aerobic (199).

The possibility of simultaneous coculturing and proliferation of strictly anaerobic and aerobic bacteria has been reported previously (200). However, the unexpected proliferation of anaerobic taxa suggests that the complex MLSS microbiome can rapidly modify microenvironmental conditions, even in nominally aerobic batch cultures. Initially, aerobic genera, mainly *Burkholderia* (201), dominated all cultures in which *Gordonia amarae* was not pre-grown for one week before MLSS addition (40–60% relative abundance at T0) and also appeared as the second most abundant genus (after *Gordonia* itself) in cultures where *Gordonia amarae* was pre-grown for one week prior to MLSS inoculation. They likely consumed a substantial proportion of the available oxygen.

Burkholderia is known for its metabolic versatility, biosurfactant production, and capacity to degrade hydrophobic substrates (202), traits that would provide a competitive advantage during the early stages of incubation. However, its relative abundance declined in all cultures over time, which could be consistent with a transition toward oxygen-limited or microanaerobic niches created by the broader microbial community.

Although cultures were intermittently opened, the formation of anoxic zones within deeper layers of sludge flocs or at the oil–water interface (particularly in the 1% n-hexadecane cultures) could have facilitated the survival and subsequent proliferation of facultative and strict anaerobes. Such microhabitats have been documented in aerobic sludge; Tay *et al*. (203) reported the presence of anaerobic genus *Bacteroides* in aerobically grown microbial granules.

5.6. Conclusion

This study examined the effects of growth conditions and inoculation strategy on foaming potential and microbial community dynamics in activated sludge (AS) mixed liquor suspended solids (MLSS). Foaming-related conditions were simulated using minimal medium supplemented with 1% n-hexadecane, and the filamentous foam-forming bacterium *Gordonia amarae* was introduced using two inoculation strategies (pre-cultivation or simultaneous inoculation), resulting in six experimental cultures.

Foaming was significantly enhanced in n-hexadecane-containing cultures compared with nutrient-rich media, and was further influenced by inoculation strategy (two-way ANOVA, $p < 0.05$). Normality was assessed using the Shapiro-Wilk test ($\alpha = 0.05$), which did not indicate a significant deviation from normality. The highest foam formation occurred when *Gordonia amarae* was pre-grown prior to MLSS inoculation, followed by simultaneous inoculation of *Gordonia amarae* and MLSS, and MLSS-only cultures. Although minor bubbling was observed in nutrient-rich media, statistically significant foaming was confined to n-hexadecane-containing cultures. These findings are consistent with the known ability of *Gordonia amarae* to promote foam formation through biosurfactant production (22), and suggest that the presence of hydrophobic substrates further intensify this process (50). Detectable foaming in MLSS-only n-hexadecane cultures also indicates that additional members of the mixed community, such as other filamentous bacteria (204), may contribute to foam formation under foaming-favourable conditions.

Microbial community analysis revealed distinct shifts driven by medium composition and *Gordonia amarae* presence. *Phascolarctobacterium* and *Citrobacter* consistently dominated communities across all conditions, reflecting their metabolic flexibility (205) and diverse nutrient acquisition adaptability across different ecological niches (206), respectively. Growth medium strongly structured some of the remaining community:

Morganella and *Vagococcus* were enriched under foaming-related conditions, whereas *Bacteroides*, *Dysgonomonas*, and *Peptostreptococcus* were favoured in nutrient-rich media ($p < 0.05$). Normality was assessed using the Shapiro-Wilk test ($\alpha = 0.05$), which did not indicate a significant deviation from normali

Other genera also exhibited clear inoculation-dependent responses. *Morganella* was consistently enriched in cultures containing *Gordonia amarae*, suggesting a facilitative interaction. In contrast, *Peptostreptococcus* and *VadinCA02* were suppressed when *Gordonia amarae* was present at high abundance or present at all, respectively, potentially through competitive interactions, environmental modifications or segregation of substances that inhibits its growth. This phenomenon has been reported in wastewater treatment plants (207). Notably, *VadinCA02* proliferated only in foaming-related cultures lacking *Gordonia amarae*, and only after an extended adaptation period (~21 days), indicating both substrate-driven selection and inhibitory microbial interactions. *Acidaminococcus* displayed the opposite trend, with significant enrichment occurring exclusively in nutrient-rich cultures where *Gordonia amarae* had been pre-grown, after an extended adaptation period (~10 days), suggesting a context-dependent positive interaction.

A particularly strong antagonistic interaction was observed between *Gordonia amarae* and *Acinetobacter*. Although *Acinetobacter* generally grew better under foaming-related conditions, its proliferation was strongly suppressed when *Gordonia amarae* dominated the community, regardless of medium type. This contrasts with previous co-culture studies in which *Acinetobacter* outcompeted *Gordonia*, highlighting how community complexity in MLSS systems can fundamentally alter pairwise interactions (189).

Collectively, these results demonstrate that both foaming-related conditions and the presence and high abundance of foaming-associated bacteria such as *Gordonia amarae* can substantially reshape microbial community trajectories. Several taxa exhibited clear facilitative or inhibitory responses, indicating that community restructuring is driven not only by substrate availability but also by microbe–microbe interactions. Monitoring these population-level shifts may therefore provide a useful basis for predicting the onset of foaming events in wastewater treatment systems. Furthermore, integrating microbial dynamics with additional biomarkers (such as lipidomic profiles of key genera) may enhance the ability to assess foaming risk and inform the development of more effective foaming prevention and mitigation strategies.

Further work on these results will include the incorporation of α- and β-diversity analyses to further characterise microbial community structure and variability across conditions. These analyses will provide additional insight into within-sample (α-diversity) and between-sample (β-diversity) community diversity, enabling a more robust assessment of how foaming-related conditions and the presence of *Gordonia amarae* influence overall community diversity and stability. Integrating these analyses would strengthen the

interpretation of microbial dynamics made in this chapter and could support the identification of community-level patterns associated with foaming events.

Future work will focus on lipidomic analysis throughout the one-month MLSS culture period under both nutrient-rich and foaming-related conditions, using the same inoculation strategies. In addition, continuous or semi-continuous cultivation systems such as drip-flow reactors or constant depth film fermenters (CDFF) will be explored to better mimic the hydrodynamic and biomass retention conditions of full-scale wastewater treatment processes. Combining community-level lipidomic profiling with these long-term cultivation models will enable a more robust linkage between microbial population shifts, changes in lipid composition, and foam formation potential, thereby improving mechanistic understanding and enhancing the predictive capability for foaming events in wastewater treatment plants.

Chapter 6: overall conclusion and future work

6.1. Conclusion

The overall aim of this thesis was to investigate lipidomic profiles, biosurfactant production, and microbial communities in activated sludge in order to gain a better understanding of the biochemical changes associated with foaming events in activated sludge (AS) reactors of wastewater treatment plants (WWTPs). This aim was addressed through a sequence of complementary studies that progressed from analytical method development, to targeted lipid and biosurfactant analysis in pure cultures, and finally to investigation of microbial dynamics in complex activated sludge communities.

The first stage of the thesis focused on the development and optimisation of analytical and experimental methodologies required to investigate foaming-associated bacterial lipids. The primary objective was to establish optimal growth conditions and robust lipidomic workflows, combining liquid chromatography with multiple mass spectrometry techniques, for the analysis of mycobacteria, including foaming-associated species present in activated sludge systems. Reproducible growth conditions for the foaming-related mycobacteria *Gordonia amarae* were successfully established in minimal media cultures supplemented with 1% n-hexadecane, 1% olive oil, and a combination of 1% n-hexadecane with 0.5% acetate. All of these cultures supported optimal growth and enabled cultivation under foaming-relevant conditions. In parallel, liquid chromatography – mass spectrometry (LC–MS) method was developed to allow reliable detection of mycolic acids across different mycobacterial species, with mycolic acids from *Mycobacterium tuberculosis* and *Gordonia amarae* successfully detected across broad mass ranges of *m/z* 1090–1300 and 715–830, respectively, and with low background noise. Cyclic ion mobility spectrometry (cIMS) parameters were further refined to maximise mycolic acid isomer separation while avoiding wrap-around effects and fragmentation losses during isomer resolving processes. Together, these developments provided a robust analytical platform that underpinned all subsequent experimental chapters.

Building on this analytical framework, the second part of the thesis investigated the isomeric complexity of mycolic acids produced by foaming-associated and pathogenic mycobacteria. The main objective here was to analyse, separate, and fragment mycolic acids isomers from mycobacteria species *Gordonia amarae* and *Mycobacterium tuberculosis*. By selectively isolating MA ions of interests and subjecting them to multiple passes through the cyclic ion mobility device, lipid species that appeared as single peaks in full-scan mass spectra were resolved into multiple distinct conformations, showing up to 6 and 2 conformations from *Gordonia amarae* and *Mycobacterium tuberculosis* respectively. These results demonstrated the possibility of using advanced ion mobility approaches to enhance structural characterisation of complex bacterial lipids, opening the possibility of applying this technique to find possible lipid isomer biomarkers.

The third stage of this thesis investigated the relationship between environmental conditions, biosurfactant production, and lipid composition in *Gordonia amarae*, with the principal objective of quantifying biosurfactant production under foaming-related conditions and correlating these data with lipidomic changes. Growth monitoring and polarographic analysis demonstrated that biosurfactant production and stable foam formation were strongly induced in the presence of hydrophobic carbon sources, particularly *n-hexadecane*, which resulted in the highest concentrations of surface-active substances (SAS) and the most persistent foaming behaviour. In contrast, biosurfactant production was negligible in nutrient-rich media, confirming that biosurfactant synthesis in *Gordonia amarae* is not constitutive but is tightly regulated by the presence of hydrophobic carbon sources. Complementary lipidomic analyses further revealed that foaming-related growth conditions were associated with reproducible and systematic remodelling of the *Gordonia amarae* lipidome. Cultures grown under these conditions exhibited consistent 2 Da shifts in the most abundant lipid ions across several mycolic acid ion sets, suggesting an increase in lipid unsaturation under stress-associated conditions. Additional mass shifts were observed within lower-abundance mycolic acid populations, which may reflect a transition towards more highly oxygenated lipid species, hypothesised from accurate-mass-based formula predictions. These findings establish a link between environmental conditions, biosurfactant production, and lipidomic adaptation in the foaming-associated mycobacteria *Gordonia amarae*. They define a robust baseline for the identification of lipidomic signatures related with foaming-associated conditions and highlight the potential of mycolic acid profiles as biomarkers for assessing foaming risk in activated sludge systems.

The final experimental stage of this thesis extended the investigation from controlled single-organism systems to complex microbial communities representative of activated sludge, in order to assess how foaming-related conditions and the presence of *Gordonia amarae* influence both foaming behaviour and microbial community dynamics. The incorporation of AS mixed liquor suspended solids (MLSS) samples to foaming-related cultures demonstrated that these conditions promote foam formation even in the absence of *Gordonia amarae*, although its presence and high abundance significantly intensified foaming. Microbial community analysis revealed that both growth medium and *Gordonia amarae* inoculation strategy exerted strong and interacting effects on community trajectories. While certain taxa, including *Phascolarctobacterium* and *Citrobacter*, consistently dominated across all conditions, reflecting broad metabolic versatility, other genera responded selectively to foaming-related conditions or to the presence of mycobacteria *Gordonia amarae*. Several taxa exhibited clear facilitative or inhibitory responses, providing evidence for complex microbe–microbe interactions that shape community structure beyond substrate-driven selection alone. Notably, antagonistic interactions between *Gordonia amarae* and *Acinetobacter* contrasted with outcomes previously reported in simplified co-culture studies, highlighting the necessity

of studying foaming processes within realistic, multi-species environments. These results demonstrate that foaming in activated sludge systems emerges from the combined effects of environmental conditions, microbial community composition, and interspecies interactions. The observed population-level shifts suggest that monitoring changes in key microbial taxa, particularly in conjunction with complementary biochemical indicators such as lipidomic profiles, may provide a valuable framework for anticipating foaming events.

In summary, this thesis demonstrates that foaming in activated sludge systems arises from the combined effects of lipid adaptations, biosurfactant production, and dynamic microbial interactions, rather than from any single factor in isolation. The findings highlight the potential of combining lipid-based markers with microbial population dynamics to improve early detection, prediction, and management of foaming events.

6.2. Future and ongoing work

Future and ongoing work will extend the findings of this thesis through integrated lipidomic and microbial community analyses of activated sludge mixed liquor suspended solids (MLSS) cultured under both foaming-related and non-foaming conditions, with and without the presence of *Gordonia amarae*. These studies aim to directly correlate lipidomic changes with microbial population dynamics, with the objective of identifying lipid-based biomarkers that may provide early indication of foaming behaviour. A reliable and reproducible LC–MS method for lipidomic analysis of mixed microbial communities has already been developed during this thesis, and funding has been secured to support this work.

To enhance the environmental and operational relevance of these findings, future research will focus on the analysis of samples obtained from full-scale activated sludge reactors experiencing foaming events. Mixed liquor and foam samples from three wastewater treatment plants across Scotland have already been collected and will be analysed to determine whether lipidomic and microbial signatures identified under controlled laboratory conditions can be detected in real-world systems.

While this thesis successfully modelled foaming-related conditions using hydrophobic carbon sources such as n-hexadecane and olive oil, these represent simplified systems compared to the complexity of full-scale wastewater treatment plants. Future work will therefore expand the range of environmental conditions investigated, including variations in temperature, pH, oxygen availability, nutrient loading, and the presence of mixed or industrial influents. Such studies will help determine the robustness and transferability of the observed lipidomic and microbial trends under dynamic and realistic operating conditions.

From an analytical perspective, although the LC–MS and cIMS methods developed here proved highly effective for the analysis of MA in controlled systems, their applicability to more complex environmental matrices requires further evaluation. Future work will assess method performance in heterogeneous sludge samples, including potential matrix effects, ion suppression, and co-eluting species. Further optimisation towards higher throughput and routine applicability would also be considered for implementation in monitoring frameworks. In addition, cIMS will be used to investigate key lipid species identified in both laboratory and full-scale samples. High-resolution separation of lipid isomers will provide deeper insight into structural diversity and could reveal isomer-specific biomarkers associated with foaming behaviour.

Although this thesis demonstrated clear lipidomic adaptations in *Gordonia amarae*, these findings were primarily derived from single-organism experiments. Extending lipidomic analyses to mixed microbial communities, and integrating these with metagenomic approaches, could provide a more comprehensive understanding of the functional roles of lipids within complex systems. Similarly, the microbial community analysis presented here highlight the importance of interspecies interactions. However, the mechanisms linking microbial community structure, lipid composition, and foaming behaviour remain unclear. Future work involving controlled co-culture or synthetic community experiments would help to disentangle these interactions and establish causative links between microbial composition, lipid dynamics, and foaming behaviour.

Overall, these combined approaches will strengthen the mechanistic understanding of foaming in wastewater treatment systems and support the development of integrated, biomarker-based tools for predicting and managing foaming events under real operational conditions.

References

1. Preisner M, Neverova-Dziopak E, Kowalewski Z. Analysis of eutrophication potential of municipal wastewater. Water Sci Technol. 2020.

2. Adegoke AA, Amoah ID, Stenström TA, Verbyla ME, Mihelcic JR. Epidemiological Evidence and Health Risks Associated With Agricultural Reuse of Partially Treated and Untreated Wastewater: A Review. Front Public Health 2018.

3. Giraudo M, Colson TLL, Pilote M, Gagnon C, Gagnon P, Houde M. A major release of urban untreated wastewaters in the St. Lawrence River (Quebec, Canada) altered growth, reproduction, and redox status in experimentally exposed Daphnia magna. Ecotoxicology. 2019.

4. Hrubik J, Glisic B, Tubic A, Ivancev-Tumbas I, Kovacevic R, Samardzija D, et al. Toxicological and chemical investigation of untreated municipal wastewater: Fraction- and species-specific toxicity. Ecotoxicology and Environmental Safety. 2016.

5. Sonune A, Ghate R. Developments in wastewater treatment methods. Desalination. 2004.

6. United States Environmental Protection Agency (EPA). How wastewater treatment works: the basics. Washington (DC): EPA. Available from: https://www.epa.gov

7. Majumder S, Mustafa R, Poornesh P, M.B. R. A Review on Working, Treatment and Performance Evaluation of Sewage Treatment Plant. 2019.

8. Govil T, Rathinam NK, Salem DR, Sani RK. Taxonomical Diversity of Extremophiles in the Deep Biosphere. Microbial Diversity in the Genomic Era. 2019.

9. Liebetrau J, Sträuber H, Kretzschmar J, Denysenko V, Nelles M. Anaerobic Digestion. Springer International Publishing. 2019

10. Xi H, Zhou X, Arslan M, Luo Z, Wei J, Wu Z, et al. Heterotrophic nitrification and aerobic denitrification process: Promising but a long way to go in the wastewater treatment. Science of The Total Environment. 2022.

11. Wang H, Dai H, Jiang D, Cao X, Wang R, Dai Z, et al. Screening, identification, and application of anaerobic ammonia oxidizing bacteria in activated sludge systems: A comprehensive review. Journal of Environmental Management. 2025.

12. van Loosdrecht MCM, Smolders GJ, Kuba T, Heijnen JJ. Metabolism of micro-organisms responsible for enhanced biological phosphorus removal from wastewater, Use of dynamic enrichment cultures. Antonie Van Leeuwenhoek. 1997.

13. Fuhs GW, Chen M. Microbiological basis of phosphate removal in the activated sludge process for the treatment of wastewater. Microb Ecol. 1975.

14. Kallistova AYu, Pimenov NV, Kozlov MN, Nikolaev YuA, Dorofeev AG, Aseeva VG, et al. Microbial composition of the activated sludge of Moscow wastewater treatment plants. Microbiology. 2014.

15. Hug LA, Co R. It Takes a Village: Microbial Communities Thrive through Interactions and Metabolic Handoffs. mSystems. 2018.

16. Foods NRC (US) P on the A of B to TF. Mixed-Culture Fermentations. Applications of Biotechnology to Fermented Foods: Report of an Ad Hoc Panel of the Board on Science and Technology for International Development. National Academies Press (US); 1992.

17. An W, Guo F, Song Y, Gao N, Bai S, Dai J, et al. Comparative genomics analyses on EPS biosynthesis genes required for floc formation of *Zoogloea resiniphila* and other activated sludge bacteria. Water Research. 2016.

18. Wilén BM, Jin B, Lant P. Relationship between flocculation of activated sludge and composition of extracellular polymeric substances. Water Sci Technol. 2003.

19. Speirs LBM, Rice DTF, Petrovski S, Seviour RJ. The Phylogeny, Biodiversity, and Ecology of the Chloroflexi in Activated Sludge. Front Microbiology. 2019.

20. Burger W, Krysiak-Baltyn K, Scales PJ, Martin GJO, Stickland AD, Gras SL. The influence of protruding filamentous bacteria on floc stability and solid-liquid separation in the activated sludge process. Water Research. 2017.

21. Carr EL, Eales KL, Seviour RJ. Substrate uptake by Gordonia amarae in activated sludge foams by FISH-MAR. Water Sci Technol. 2006.

22. de los Reyes III FL, Raskin L. Role of filamentous microorganisms in activated sludge foaming: relationship of mycolata levels to foaming initiation and stability. Water Research. 2002.

23. Petrovski S, Batinovic S, Rose JJA, Seviour RJ. Biological control of problematic bacterial populations causing foaming in activated sludge wastewater treatment plants—phage therapy and beyond. Lett Appl Microbiol. 2022.

24. Wang P, Yu Z, Zhao J, Zhang H. Seasonal Changes in Bacterial Communities Cause Foaming in a Wastewater Treatment Plant. Microb Ecol. 2016.

25. Guo F, Wang ZP, Yu K, Zhang T. Detailed investigation of the microbial community in foaming activated sludge reveals novel foam formers. Sci Rep. 2015.

26. D'Antoni M, Iracà F, Romero M. Brief review on filamentous foaming and bulking in activated sludge treatments: Causes and mitigation actions. 2017.

27. Foladori P, Bruni L, Tamburini S, Ziglio G. Direct quantification of bacterial biomass in influent, effluent and activated sludge of wastewater treatment plants by using flow cytometry. Water Research. 2010.

28. Dias PA, Dunkel T, Fajado DAS, Gallegos E de L, Denecke M, Wiedemann P, et al. Image processing for identification and quantification of filamentous bacteria in in situ acquired images. BioMedical Engineering OnLine. 2016.

29. Mesquita DP, Amaral AL, Ferreira EC. Activated sludge characterization through microscopy: A review on quantitative image analysis and chemometric techniques. Analytica Chimica Acta. 2013.

30. Lindner BG, Gerhardt K, Feistel DJ, Rodriguez-R LM, Hatt JK, Konstantinidis KT. A user's guide to the bioinformatic analysis of shotgun metagenomic sequence data for bacterial pathogen detection. International Journal of Food Microbiology. 2024.

31. Vonk JE, van Dongen BE, Gustafsson Ö. Lipid biomarker investigation of the origin and diagenetic state of sub-arctic terrestrial organic matter presently exported into the northern Bothnian Bay. Marine Chemistry. 2008.

32. Bischoff J, Sparkes RB, Doğrul Selver A, Spencer RGM, Gustafsson Ö, Semiletov IP, et al. Source, transport and fate of soil organic matter inferred from microbial biomarker lipids on the East Siberian Arctic Shelf. Biogeosciences. 2016.

33. Mensah L, Cartmell E, Fletton M, Scrimshaw M, Campo P. Proactive monitoring of changes in the microbial community structure in wastewater treatment bioreactors using phospholipid fatty acid analysis. Engineering Microbiology. 2024.

34. Joyeux C, Fouchard S, Llopiz P, Neunlist S. Influence of the temperature and the growth phase on the hopanoids and fatty acids content of Frateuria aurantia (DSMZ 6220). FEMS Microbiol Ecol. 2004.

35. Findlay RH, Dobbs FC. Quantitative Description of Microbial Communities Using Lipid Analysis. In: Handbook of Methods in Aquatic Microbial Ecology. CRC Press; 1993.

36. Romero-Güiza M, Peces M, Asiain-Mira R, Palatsi J, Astals S. Microbial assessment of foaming dynamics in full-scale WWTP anaerobic digesters. Journal of Water Process Engineering. 2023.

37. Moeller L, Herbes C, Müller RA, Zehnsdorf A. Formation and removal of foam in the process of anaerobic digestion. Landtechnik. 2010.

38. Moeller L, Görsch K. Foam formation in full-scale biogas plants processing biogenic waste. Energy, Sustainability and Society. 2015.

39. Mamais D, Marneri M, Noutsopoulos C. Causes and control practices of filamentous foaming in wastewater treatment plants. Water Practice and Technology. 2012.

40. Mamais D, Kalaitzi E, Andreadakis AD. Foaming control in activated sludge treatment plants by coagulants addition. 2011.

41. Goodfellow M, Chun J, Stubbs S, Tobili AS. Transfer of Nocardia amarae Lechevalier and Lechevalier 1974 to the genus Gordona as Gordona amarae comb. nov. Letters in Applied Microbiology. 1994.

42. Goodfellow M, Alderson G, Chun J. Rhodococcal systematics: problems and developments. Antonie Van Leeuwenhoek. 1998.

43. Jenkins D, Richard MG, Daigger GT. Manual on the Causes and Control of Activated Sludge Bulking, Foaming, and Other Solids Separation Problems. 3rd edn. Boca Raton: CRC Press; 2003.

44. Tsukamura M. Proposal of a New Genus, Gordona, for Slightly Acid-fast Organisms Occurring in Sputa of Patients With Pulmonary Disease and in Soil. Microbiology. 1971.

45. Tamura T, Saito S, Hamada M, Kang Y, Hoshino Y, Gonoi T, et al. Gordonia crocea sp. nov. and Gordonia spumicola sp. nov. isolated from sludge of a wastewater treatment plant. International Journal of Systematic and Evolutionary Microbiology. Microbiology Society. 2020.

46. Kageyama A, Iida S, Yazawa K, Kudo T, Suzuki S ichi, Koga T, et al. Gordonia araii sp. nov. and Gordonia effusa sp. nov., isolated from patients in Japan. International Journal of Systematic and Evolutionary Microbiology. Microbiology Society. 2006.

47. Iida S, Taniguchi H, Kageyama A, Yazawa K, Chibana H, Murata S, et al. Gordonia otitidis sp. nov., isolated from a patient with external otitis. International Journal of Systematic and Evolutionary Microbiology. Microbiology Society. 2005.

48. Arenskötter M, Bröker D, Steinbüchel A. Biology of the Metabolically Diverse Genus Gordonia. Appl Environ Microbiol. 2004.

49. Ganidi N, Tyrrel S, Cartmell E. Anaerobic digestion foaming causes--a review. Bioresour Technol. 2009.

50. Pagilla KR, Sood A, Kim H. Gordonia (nocardia) amarae foaming due to biosurfactant production. Water Sci Technol. 2002.

51. Gray(Gabb) DMD, De Lange VP, Chien MH, Esquer MA, Shao Y j. Investigating the Fundamental Basis for Selectors to Improve Activated Sludge Settling. Water Environment Research. 2010.

52. Madigan MT. Brock biology of microorganisms. Fourteenth global edition. Boston: Pearson. 2015.

53. Desai JD, Banat IM. Microbial production of surfactants and their commercial potential. Microbiol Mol Biol Rev. 1997.

54. Franzetti A, Caredda P, La Colla P, Pintus M, Tamburini E, Papacchini M, et al. Cultural factors affecting biosurfactant production by *Gordonia* sp. BS29. International Biodeterioration & Biodegradation. 2009.

55. Qi P, Zhang G, Sun D, Wu T, Li Y. Enhanced separation of emulsified oil from alkaline-surfactant-polymer flooding produced water by *Gordonia* sp. TD-4: From interactions to mitigation strategies and bio-demulsifying mechanisms. Journal of Cleaner Production. 2022.

56. Franzetti A, Bestetti G, Caredda P, La Colla P, Tamburini E. Surface-active compounds and their role in the access to hydrocarbons in Gordonia strains. FEMS Microbiology Ecology. 2008.

57. Zargar AN, Mishra S, Kumar M, Srivastava P. Isolation and chemical characterization of the biosurfactant produced by Gordonia sp. IITR100. PLoS ONE. 2022.

58. Harland CW, Botyanszki Z, Rabuka D, Bertozzi CR, Parthasarathy R. Synthetic Trehalose Glycolipids Confer Desiccation Resistance to Supported Lipid Monolayers. Langmuir : the ACS journal of surfaces and colloids. 2009.

59. Marrakchi H, Lanéelle MA, Daffé M. Mycolic Acids: Structures, Biosynthesis, and Beyond. Chemistry & Biology. 2014.

60. Nataraj V, Varela C, Javid A, Singh A, Besra GS, Bhatt A. Mycolic acids: deciphering and targeting the Achilles' heel of the tubercle bacillus. Mol Microbiol. 2015.

61. Dulberger CL, Rubin EJ, Boutte CC. The mycobacterial cell envelope - a moving target. Nat Rev Microbiol. 2020.

62. Zhao J, Siddiqui S, Shang S, Bian Y, Bagchi S, He Y, et al. Mycolic acid-specific T cells protect against Mycobacterium tuberculosis infection in a humanized transgenic mouse model. Colonna M, editor. eLife. 2015.

63. Naicker B. Identification of mycolic acid class ratios from Mycobacterium species using liquid chromatography-mass spectrometry. 2019.

64. Jackson M, McNeil MR, Brennan PJ. Progress in targeting cell envelope biogenesis in Mycobacterium tuberculosis. Future Microbiology. 2013.

65. Rose JJA, Johnson MD, Reyhani M, Batinovic S, Seviour RJ, Ghosal D, et al. Mutations in Gordonia amarae mycolic acid biosynthetic pathway confer resistance to Patescibacteria parasite Mycosynbacter amalyticus. Nat Commun. 2025.

66. Nishiuchi Y, Baba T, Yano I. Mycolic acids from Rhodococcus, Gordonia, and Dietzia. Journal of Microbiological Methods. 2000.

67. Stratton HM, Brooks PR, Seviour RJ. Analysis of the structural diversity of mycolic acids of Rhodococcus and Gordonla isolates from activated sludge foams by selective ion monitoring gas chromatography–mass spectrometry (SIM GC–MS). Journal of Microbiological Methods. 1999.

68. Hassan N, Anesio AM, Rafiq M, Holtvoeth J, Bull I, Haleem A, et al. Temperature Driven Membrane Lipid Adaptation in Glacial Psychrophilic Bacteria. Front Microbiol. 2020.

69. E H, S C, M SC, P V, C A, A K, et al. Membrane lipid adaptation of soil Bacteroidetes isolates to temperature and pH. Frontiers in microbiology. 2023.

70. Bayne S, Carlin M. Forensic Applications of High Performance Liquid Chromatography. 2017.

71. Badri S, G J, P D, D S, SK S, C V, et al. A review on different types of detectors used in chromatography techniques. UPI Journal of Pharmaceutical, Medical and Health Sciences. 2023.

72. Liu Y, Vailaya A. Normal-Phase HPLC. In: HPLC for Pharmaceutical Scientists. 2007.

73. Cajka T, Fiehn O. Comprehensive analysis of lipids in biological systems by liquid chromatography-mass spectrometry. Trends in analytical chemistry. 2014.

74. Z F, M C, G N, S H. Quantification of mycolic acids in different mycobacterial species by standard addition method through liquid chromatography mass spectrometry. Journal of chromatography B, Analytical technologies in the biomedical and life sciences. 2024.

75. Sakallioglu IT, Maroli AS, Liete ADL, Powers R. A Reversed Phase Ultra-High-Performance Liquid Chromatography-Data Independent Mass Spectrometry Method for the Rapid Identification of Mycobacterial Lipids. Journal of chromatography A. 2021.

76. Banerjee S, Mazumdar S. Electrospray ionization mass spectrometry: a technique to access the information beyond the molecular weight of the analyte. Int J Anal Chem. 2012.

77. Uchikawa H. 20 - Specialized Techniques. In: Ramachandran VS, Beaudoin JJ, editors. Handbook of Analytical Techniques in Concrete Science and Technology [Internet]. Norwich, NY: William Andrew Publishing. 2001.

78. Rayleigh, Lord. XX. On the equilibrium of liquid conducting masses charged with electricity. The London, Edinburgh, and Dublin Philosophical Magazine and Journal of Science. 1882.

79. Kebarle P, Tang L. From ions in solution to ions in the gas phase - the mechanism of electrospray mass spectrometry. Anal Chem. 1993.

80. Han X, Gross RW. Global analyses of cellular lipidomes directly from crude extracts of biological samples by ESI mass spectrometry: a bridge to lipidomics. Journal of Lipid Research. 2003.

81. Brügger B, Erben G, Sandhoff R, Wieland FT, Lehmann WD. Quantitative analysis of biological membrane lipids at the low picomole level by nano-electrospray ionization tandem mass spectrometry. Proceedings of the National Academy of Sciences. 1997.

82. Han X, Gross RW. Quantitative Analysis and Molecular Species Fingerprinting of Triacylglyceride Molecular Species Directly from Lipid Extracts of Biological Samples by Electrospray Ionization Tandem Mass Spectrometry. Analytical Biochemistry. 2001.

83. Anagnostopoulos AK, Tsangaris GTh. Proteomics advancements in fetomaternal medicine. Clinical Biochemistry. 2013.

84. Mellon FA. MASS SPECTROMETRY | Principles and Instrumentation. Encyclopedia of Food Sciences and Nutrition. Oxford: Academic Press; 2003.

85. Skrzydlewska E, Domingues P, García A, Medyczny (Białystok) U, Medyczny (Białystok) U. Advanced Analytical Chemistry for Life Sciences: AACLifeSci Course Companion Manual. Uniwersytet Medyczny; 2018.

86. Mamyrin BA. Time-of-flight mass spectrometry (concepts, achievements, and prospects). International Journal of Mass Spectrometry. 2001.

87. Holmes JL. Metastable Ions. Encyclopedia of Spectroscopy and Spectrometry. Oxford: Elsevier; 1999.

88. Liedl ER. Types of mass analysers – Time of flight (ToF). Bio-Analysis Centre. 2023.

89. Standing KG, Ens W. Time of Flight Mass Spectrometers. Encyclopedia of Spectroscopy and Spectrometry. Oxford: Elsevier; 1999.

90. Galindo Garcia A. Characterisation of a bacterial P450 system using surface mass spectrometry. 2016.

91. Dodds JN, Baker ES. Ion Mobility Spectrometry: Fundamental Concepts, Instrumentation, Applications, and the Road Ahead. J Am Soc Mass Spectrom. 2019.

92. Viehland LA, Mason EA. Gaseous lon mobility in electric fields of arbitrary strength. Annals of Physics. 1975.

93. May JC, Goodwin CR, Lareau NM, Leaptrot KL, Morris CB, Kurulugama RT, et al. Conformational Ordering of Biomolecules in the Gas Phase: Nitrogen Collision Cross Sections Measured on a Prototype High Resolution Drift Tube Ion Mobility-Mass Spectrometer. Anal Chem. 2014.

94. Cumeras R, Figueras E, Davis CE, Baumbach JI, Gràcia I. Review on Ion Mobility Spectrometry. Part 1: Current Instrumentation. The Analyst. 2015.

95. Cooper HJ. To What Extent is FAIMS Beneficial in the Analysis of Proteins? J Am Soc Mass Spectrom. 2016.

96. Kolakowski BM, Mester Z. Review of applications of high-field asymmetric waveform ion mobility spectrometry (FAIMS) and differential mobility spectrometry (DMS). Analyst. 2007.

97. Giles K, Ujma J, Wildgoose J, Pringle S, Richardson K, Langridge D, et al. A Cyclic Ion Mobility-Mass Spectrometry System. Anal Chem. 2019.

98. Giles K, Pringle SD, Worthington KR, Little D, Wildgoose JL, Bateman RH. Applications of a travelling wave-based radio-frequency-only stacked ring ion guide. Rapid Communications in Mass Spectrometry. 2004.

99. Riches E, Palmer ME. Application of a novel cyclic ion mobility-mass spectrometer to the analysis of synthetic polymers: A preliminary evaluation. Rapid Communications in Mass Spectrometry. 2020.

100. Cosović B, Vojvodić V. The application of ac polarography to the determination of surface-active substances in seawater. Limnology and Oceanography. 1982.

101. Ćosović B, Vojvodić V. Voltammetric Analysis of Surface Active Substances in Natural Seawater. Electroanalysis. 1998.

102. Rickard PC, Uher G, Upstill-Goddard RC, Frka S, Mustaffa NIH, Banko-Kubis HM, et al. Reconsideration of seawater surfactant activity analysis based on an inter-laboratory comparison study. Marine Chemistry. 2019.

103. Chemistry Glossary: Search results for ‘polarography’. Available from: https://glossary.periodni.com/dictionary.php?en=polarography

104. Hao Y, Pei Z, Brown SM. Chapter 1 - Bioinformatics in Microbiome Analysis. Methods in Microbiology. Academic Press; 2017.

105. Chakravorty S, Helb D, Burday M, Connell N, Alland D. A detailed analysis of 16S ribosomal RNA gene segments for the diagnosis of pathogenic bacteria. Journal of Microbiological Methods. 2007.

106. Bose N, Moore SD. Variable Region Sequences Influence 16S rRNA Performance. Microbiology Spectrum. 2023.

107. Christensen H, Andersson AJ, Jørgensen SL, Vogt JK. 16S rRNA Amplicon Sequencing for Metagenomics. Introduction to Bioinformatics in Microbiology. Springer International Publishing; 2018.

108. Clarridge JE. Impact of 16S rRNA Gene Sequence Analysis for Identification of Bacteria on Clinical Microbiology and Infectious Diseases. Clinical Microbiology Reviews. 2004.

109. Matsumoto T, Sugano M. 16S rRNA gene sequence analysis for bacterial identification in the clinical laboratory. Rinsho byori The Japanese journal of clinical pathology. 2013.

110. de Celis M, Belda I, Ortiz-Álvarez R, Arregui L, Marquina D, Serrano S, et al. Tuning up microbiome analysis to monitor WWTPs' biological reactors functioning. Sci Rep. 2020.

111. Johnston J, Behrens S. Seasonal Dynamics of the Activated Sludge Microbiome in Sequencing Batch Reactors, Assessed Using 16S rRNA Transcript Amplicon Sequencing. Applied and Environmental Microbiology. 2020.

112. Smets W, Leff JW, Bradford MA, McCulley RL, Lebeer S, Fierer N. A method for simultaneous measurement of soil bacterial abundances and community composition via 16S rRNA gene sequencing. Soil Biology and Biochemistry. 2016.

113. Yang C, Zhang W, Liu R, Li Q, Li B, Wang S, et al. Phylogenetic Diversity and Metabolic Potential of Activated Sludge Microbial Communities in Full-Scale Wastewater Treatment Plants. Environ Sci Technol. 2011.

114. Zhang L, Shen Z, Fang W, Gao G. Composition of bacterial communities in municipal wastewater treatment plant. Science of The Total Environment. 2019.

115. Chen H, Wang M, Chang S. Disentangling Community Structure of Ecological System in Activated Sludge: Core Communities, Functionality, and Functional Redundancy. Microb Ecol. 2020.

116. Kim TS, Kim HS, Kwon S, Park HD. Analysis of Bacterial Community Composition in Wastewater Treatment Bioreactors Using 16S rRNA Gene-Based Pyrosequencing. 2010.

117. Batt SM, Minnikin DE, Besra GS. The thick waxy coat of mycobacteria, a protective layer against antibiotics and the host's immune system. Biochem J. 2020.

118. Jackson M. The Mycobacterial Cell Envelope—Lipids. Cold Spring Harb Perspect Med. 2014.

119. Wang L, Slayden RA, Barry CE, Liu J. Cell Wall Structure of a Mutant of *Mycobacterium smegmatis* Defective in the Biosynthesis of Mycolic Acids*. Journal of Biological Chemistry. 2000.

120. Ratledge C, Dale JW. Mycobacteria: Molecular Biology and Virulence. John Wiley & Sons; 2009.

121. Rosso GE, Muday JA, Curran JF. Tools for Metagenomic Analysis at Wastewater Treatment Plants: Application to a Foaming Episode. Water Environment Research. 2018.

122. Shui G, Bendt AK, Jappar IA, Lim HM, Laneelle M, Hervé M, et al. Mycolic acids as diagnostic markers for tuberculosis case detection in humans and drug efficacy in mice. EMBO Molecular Medicine. 2012.

123. Rafał S, Magdalena D, Karol M, Bartłomiej S, Konrad K. Detection and accurate identification of Mycobacterium species by flow injection tandem mass spectrometry (FIA-MS/MS) analysis of mycolic acids. Sci Rep. 2025.

124. Pujol R, Duchene Ph, Schetrite S, Canler JP. Biological foams in activated sludge plants: Characterization and situation. Water Research. 1991.

125. Fu LM, Fu-Liu CS. Is Mycobacterium tuberculosis a closer relative to Gram-positive or Gram-negative bacterial pathogens? Tuberculosis (Edinb). 2002.

126. Smit NT, Villanueva L, Rush D, Grassa F, Witkowski CR, Holzheimer M, et al. Novel hydrocarbon-utilizing soil mycobacteria synthesize unique mycocerosic acids at a Sicilian everlasting fire. Biogeosciences. 2021.

127. Moussa T, Gaber A, Abdel-hamid S. Optimization of Cultural Conditions for Biosurfactant Production from Nocardia amarae. Journal of Applied Sciences Research. 2006.

128. Fatima Z, Chugh M, Nigam G, Hameed S. Quantification of mycolic acids in different mycobacterial species by standard addition method through liquid chromatography mass spectrometry. Journal of Chromatography B. 2024.

129. Butler WR, Guthertz LS. Mycolic Acid Analysis by High-Performance Liquid Chromatography for Identification of Mycobacterium Species. Clinical Microbiology Reviews. 2001.

130. Ndlandla FL, Ejoh V, Stoltz AC, Naicker B, Cromarty AD, van Wyngaardt S, et al. Standardization of natural mycolic acid antigen composition and production for use in biomarker antibody detection to diagnose active tuberculosis. Journal of Immunological Methods. 2016.

131. Koelmel JP, Ulmer CZ, Jones CM, Yost RA, Bowden JA. Common cases of improper lipid annotation using high-resolution tandem mass spectrometry data and corresponding limitations in biological interpretation. Biochimica et Biophysica Acta (BBA) - Molecular and Cell Biology of Lipids. 2017.

132. Hernández-Mesa M, Ropartz D, García-Campaña AM, Rogniaux H, Dervilly-Pinel G, Le Bizec B. Ion Mobility Spectrometry in Food Analysis: Principles, Current Applications and Future Trends. Molecules. 2019.

133. de Bruin CR, de Bruijn WJC, Hemelaar MA, Vincken JP, Hennebelle M. Separation of triacylglycerol (TAG) isomers by cyclic ion mobility mass spectrometry. Talanta. 2025.

134. Alshehry ZH, Barlow CK, Weir JM, Zhou Y, McConville MJ, Meikle PJ. An Efficient Single Phase Method for the Extraction of Plasma Lipids. Metabolites. 2015.

135. Vilchèze C, Jacobs WR. Isolation and Analysis of Mycobacterium tuberculosis Mycolic Acids. Current Protocols in Microbiology. 2007.

136. Baird R, Eaton AD, Rice EW, Bridgewater L, Association APH, Association AWW, et al. Standard Methods for the Examination of Water and Wastewater. American Public Health Association. 2017.

137. Stevenson K, McVey AF, Clark IBN, Swain PS, Pilizota T. General calibration of microbial growth in microplate readers. Sci Rep. 2016.

138. de Kok NAW, Exterkate M, Andringa RLH, Minnaard AJ, Driessen AJM. A versatile method to separate complex lipid mixtures using 1-butanol as eluent in a reverse-phase UHPLC-ESI-MS system. Chemistry and Physics of Lipids. 2021.

139. Teramoto K, Suga M, Sato T, Wada T, Yamamoto A, Fujiwara N. Characterization of Mycolic Acids in Total Fatty Acid Methyl Ester Fractions from Mycobacterium Species by High Resolution MALDI-TOFMS. Mass Spectrom (Tokyo). 2015.

140. Martin E. Palmer. Personal communication via email with Dr Martin E. Palmer. (Principal consulting scientist at Waters corporation). 2024.

141. Liu Y, Kaffah N, Pandor S, Sartain MJ, Larrouy-Maumus G. Ion mobility mass spectrometry for the study of mycobacterial mycolic acids. Sci Rep. 2023.

142. Pringle SD, Giles K, Wildgoose JL, Williams JP, Slade SE, Thalassinos K, et al. An investigation of the mobility separation of some peptide and protein ions using a new hybrid quadrupole/travelling wave IMS/oa-ToF instrument. International Journal of Mass Spectrometry. 2007.

143. Soddell J. Activated Sludge-Foaming. 2003.

144. Heard J, Harvey E, Johnson BB, Wells JD, Angove MJ. The effect of filamentous bacteria on foam production and stability. Colloids and Surfaces B: Biointerfaces. 2008.

145. Rosen MJ, Kunjappu JT. Surfactants and Interfacial Phenomena. John Wiley & Sons. 2012.

146. Marrengane Z, Kumar SKS, Pillay L, Bux F. Rapid quantification and analysis of genetic diversity among Gordonia populations in foaming activated sludge plants. Journal of Basic Microbiology. 2011.

147. Shen FT, Huang HR, Arun AB, Lu HL, Lin TC, Rekha PD, et al. Detection of filamentous genus Gordonia in foam samples using genus-specific primers combined with PCR – denaturing gradient gel electrophoresis analysis. Can J Microbiol. 2007.

148. Seviour R, Nielsen PH. Microbial Ecology of Activated Sludge. IWA Publishing; 2010.

149. Frigon D, Michael Guthrie R, Timothy Bachman G, Royer J, Bailey B, Raskin L. Long-term analysis of a full-scale activated sludge wastewater treatment system exhibiting seasonal biological foaming. Water Research. 2006.

150. Jiang XT, Guo F, Zhang T. Population Dynamics of Bulking and Foaming Bacteria in a Full-scale Wastewater Treatment Plant over Five Years. Sci Rep. 2016.

151. Krohn C, Khudur L, Biek SK, Elliott JA, Tabatabaei S, Jiang C, et al. Microbial population shifts during disturbance induced foaming in anaerobic digestion of primary and activated sludge. Water Research. 2025.

152. Collivignarelli MC, Baldi M, Abbà A, Caccamo FM, Carnevale Miino M, Rada EC, et al. Foams in Wastewater Treatment Plants: From Causes to Control Methods. Applied Sciences. 2020.

153. Iwahori K, Tokutomi T, Miyata N, Fujita M. Formation of stable foam by the cells and culture supernatant of *Gordonia* (*Nocardia*) *amarae*. Journal of Bioscience and Bioengineering. 2001.

154. Wörmer L, Lipp JS, Hinrichs KU. Comprehensive Analysis of Microbial Lipids in Environmental Samples Through HPLC-MS Protocols. Hydrocarbon and Lipid Microbiology Protocols: Petroleum, Hydrocarbon and Lipid Analysis. Springer; 2017.

155. Kolouchová I, Schreiberová O, Masák J, Sigler K, Řezanka T. Structural analysis of mycolic acids from phenol-degrading strain of Rhodococcus erythropolis by liquid chromatography–tandem mass spectrometry. Folia Microbiol. 2012.

156. Banat IM. Biosurfactants production and possible uses in microbial enhanced oil recovery and oil pollution remediation: A review. Bioresource Technology. 1995.

157. Ćosović B, Vojvodić V, Bošković N, Plavšić M, Lee C. Characterization of natural and synthetic humic substances (melanoidins) by chemical composition and adsorption measurements. Organic Geochemistry. 2010.

158. Avranas A, Papadopoulos N. Adsorption of surfactants: differential capacitance studies using phase-sensitive alternating current voltammetry. Langmuir. 1992.

159. Grahame DC. The Electrical Double Layer and the Theory of Electrocapillarity. Chem Rev. 1947.

160. Shapiro-Wilk test calculator: normality calculator. Available from: https://www.statskingdom.com/shapiro-wilk-test-calculator.html

161. Zhao F, Han S, Zhang Y. Comparative studies on the structural composition, surface/interface activity and application potential of rhamnolipids produced by *Pseudomonas aeruginosa* using hydrophobic or hydrophilic substrates. Bioresource Technology. 2020.

162. Boskou D, Blekas G, Tsimidou M. 4 - Olive Oil Composition. AOCS Press; 2006.

163. Hamill PG, Stevenson A, McMullan PE, Williams JP, Lewis ADR, S S, et al. Microbial lag phase can be indicative of, or independent from, cellular stress. Sci Rep. 2020.

164. Harayama T, Antonny B. Beyond Fluidity: The Role of Lipid Unsaturation in Membrane Function. Cold Spring Harb Perspect Biol. 2023.

165. Mahto KK, Singh A, Khandelwal NK, Bhardwaj N, Jha J, Prasad R. An Assessment of Growth Media Enrichment on Lipid Metabolome and the Concurrent Phenotypic Properties of Candida albicans. PLoS One. 2014.

166. Sohlenkamp C, Geiger O. Bacterial membrane lipids: diversity in structures and pathways. FEMS Microbiol Rev. 2016.

167. Goutx M, Acquaviva M, Bertrand JC. Cellular and extracellular carbohydrates and lipids from marine bacteria during growth on soluble substrates and hydrocarbons. Marine Ecology Progress Series. 1990.

168. Mykytczuk NCS, Trevors JT, Leduc LG, Ferroni GD. Fluorescence polarization in studies of bacterial cytoplasmic membrane fluidity under environmental stress. Progress in Biophysics and Molecular Biology. 2007.

169. Teramoto K, Tamura T, Hanada S, Sato T, Kawasaki H, Suzuki K ichiro, et al. Simple and rapid characterization of mycolic acids from Dietzia strains by using MALDI spiral-TOFMS with ultra high mass-resolving power. J Antibiot. 2013.

170. Russell NJ, Sandercock SP. The regulation of bacterial membrane fluidity by modification of phospholipid fatty acyl chain length. Membrane Fluidity: Biophysical Techniques and Cellular Regulation. Totowa, NJ: Humana Press; 1980.

171. Subczynski WK, Wisniewska A, Yin JJ, Hyde JS, Kusumi A. Hydrophobic Barriers of Lipid Bilayer Membranes Formed by Reduction of Water Penetration by Alkyl Chain Unsaturation and Cholesterol. Biochemistry. 1994.

172. Stott R. 31 - Fate and behaviour of parasites in wastewater treatment systems. Handbook of Water and Wastewater Microbiology. London: Academic Press; 2003.

173. Englande AJ, Krenkel P, Shamas J. Wastewater Treatment &Water Reclamation. Reference Module in Earth Systems and Environmental Sciences. 2015.

174. Leal C, Amaral AL, Costa M de L. Microbial-based evaluation of foaming events in full-scale wastewater treatment plants by microscopy survey and quantitative image analysis. Environ Sci Pollut Res. 2016.

175. H. Eikelboom D. Process Control of Activated Sludge Plants by Microscopic Investigation. IWA Publishing. 2000.

176. Nielsen PH, Kragelund C, Seviour RJ, Nielsen JL. Identity and ecophysiology of filamentous bacteria in activated sludge. FEMS Microbiol Rev. 2009.

177. Adonadaga MG, Ampadu B, Martienssen M. Effect of Sludge Loading and Dissolved Oxygen Concentration on Proliferation of Thiothrix and Eikelboom Types 1851 and 0041 in Activated Sludge Wastewater Treatment Plants. 2016.

178. Tansel B. Morphology, composition and aggregation mechanisms of soft bioflocs in marine snow and activated sludge: A comparative review. Journal of Environmental Management. 2018.

179. Mamais D, Nikitopoulos G, Andronikou E, Gavalakis E, Andreadakis A, Giotakis C, et al. Influence of the presence of long chain fatty acids (LCFAs) in the sewage on the growth of M. Parvicella in activated sludge wastewater treatment plants. Global Nest Journal. 2006.

180. Yang B, Wang Y, Qian PY. Sensitivity and correlation of hypervariable regions in 16S rRNA genes in phylogenetic analysis. BMC Bioinformatics. 2016.

181. Markam SS, Raj A, Kumar A, Khan ML. Microbial biosurfactants: Green alternatives and sustainable solution for augmenting pesticide remediation and management of organic waste. Curr Res Microb Sci. 2024.

182. Dolinšek J, Ramoneda J, Johnson DR. Initial community composition determines the long-term dynamics of a microbial cross-feeding interaction by modulating niche availability. ISME Commun. 2022.

183. Perfumo A, Smyth TJP, Marchant R, Banat IM. Production and Roles of Biosurfactants and Bioemulsifiers in Accessing Hydrophobic Substrates. Springer. 2010.

184. Ron EZ, Rosenberg E. Natural roles of biosurfactants. Environmental Microbiology. 2001.

185. Gorvitovskaia A, Holmes SP, Huse SM. Interpreting Prevotella and Bacteroides as biomarkers of diet and lifestyle. Microbiome. 2016.

186. Duan J, Liang J, Wang Y, Du W, Wang D. Kraft Lignin Biodegradation by Dysgonomonas sp. WJDL-Y1, a New Anaerobic Bacterial Strain Isolated from Sludge of a Pulp and Paper Mill. J Microbiol Biotechnol. 2016.

187. Schneider I, Topalova Y. Kinetic parameters of protease activity of Peptostreptococcus sp. as a tool for regulation of dairy wastewater treatment. Bulgarian Journal of Agricultural Science. 2014.

188. Kim H, Pagilla KR. Competitive growth of *Gordonia* and *Acinetobacter* in continuous flow aerobic and anaerobic/aerobic reactors. Journal of Bioscience and Bioengineering. 2003.

189. Ross BN, Whiteley M. Ignoring social distancing: advances in understanding multi-species bacterial interactions. Fac Rev. 2020.

190. Wright ES, Vetsigian KH. Inhibitory interactions promote frequent bistability among competing bacteria. Nat Commun. 2016.

191. Zhu J. A review of microbiology in swine manure odor control. Agriculture, Ecosystems & Environment. 2000.

192. Rogosa M. Acidaminococcus gen. n., Acidaminococcus fermentans sp. n., Anaerobic Gram-negative Diplococci Using Amino Acids as the Sole Energy Source for Growth. Journal of Bacteriology. 1969.

193. Murphy EC, Frick IM. Gram-positive anaerobic cocci – commensals and opportunistic pathogens. FEMS Microbiol Rev. 2013.

194. Gillespie SH. 8 - Anaerobes. Medical Microbiology Illustrated. Butterworth-Heinemann; 1994.

195. Hofstad T, Olsen I, Eribe ER, Falsen E, Collins MD, Lawson PA. Dysgonomonas gen. nov. to accommodate Dysgonomonas gadei sp. nov., an organism isolated from a human gall bladder, and Dysgonomonas capnocytophagoides (formerly CDC group DF-3). International Journal of Systematic and Evolutionary Microbiology. 2000.

196. Wang L, Cui YS, Kwon CS, Lee ST, Lee JS, Im WT. Vagococcus acidifermentans sp. nov., isolated from an acidogenic fermentation bioreactor. International Journal of Systematic and Evolutionary Microbiology. 2011.

197. Faria CV, Costa FCR, Jorge AEL, Melo ALP, Silva UbianaCM, Santos VL, et al. Effects of pharmaceuticals compounds and calcium on granulation, microbiology, and performance of anaerobic granular sludge systems. Water Sci Technol. 2022.

198. Tilea B, Szekely E, Teches S, Tilea I. Acute community-acquired meningoencephalitis with Morganella morganii – a case report / Meningoencefalită acută comunitară cu Morganella morganii – prezentare de caz. Revista Romana de Medicina de Laborator. 2015.

199. Prashanth K, Vasanth T, Saranathan R, Makki AR, Pagal S, Prashanth K, et al. Antibiotic Resistance, Biofilms and Quorum Sensing in Acinetobacter Species.

Antibiotic Resistant Bacteria - A Continuous Challenge in the New Millennium. IntechOpen; 2012.

200. Salmela M, Lehtinen T, Efimova E, Santala S, Mangayil R. Metabolic pairing of aerobic and anaerobic production in a one-pot batch cultivation. Biotechnol Biofuels. 2018.

201. Belova SE, Pankratov TA, Dedysh SN. Bacteria of the genus Burkholderia as a typical component of the microbial community of Sphagnum peat bogs. Microbiology. 2006.

202. Cauduro GP, Leal AL, Marmitt M, de Ávila LG, Kern G, Quadros PD, et al. New benzo(a)pyrene-degrading strains of the Burkholderia cepacia complex prospected from activated sludge in a petrochemical wastewater treatment plant. Environ Monit Assess. 2021.

203. Tay STL, Ivanov V, Yi S, Zhuang WQ, Tay JH. Presence of Anaerobic Bacteroides in Aerobically Grown Microbial Granules. Microb Ecol. 2002.

204. Zhang X, Chen Y, Yu C, Lin L, Wang X, Wang Y, et al. Identifying Bacteria and Sludge Characteristics of Foaming Sludge in Four Full-Scale Wastewater Treatment Plants in Fujian Province, China. Processes. 2025.

205. Ikeyama N, Murakami T, Toyoda A, Mori H, Iino T, Ohkuma M, et al. Microbial interaction between the succinate-utilizing bacterium Phascolarctobacterium faecium and the gut commensal Bacteroides thetaiotaomicron. MicrobiologyOpen. 2020.

206. Liang Q, Vallance BA. What's for dinner? How *Citrobacter rodentium*'*s* metabolism helps it thrive in the competitive gut. Current Opinion in Microbiology. 2021.

207. Martins J, Peixe L, Vasconcelos VM. Unraveling Cyanobacteria Ecology in Wastewater Treatment Plants (WWTP). Microb Ecol. 2011.

Appendix

App table 5: *Average abundance ratios of lipids ions with m/z of 759.79, 783.80 and 813.85 Da, when compared to lipid ion with m/z of 743.69 Da, present at high abundance in all samples.*

Lipid *m/z*	Nutrient broth	1% N-hexadecane	1% N-hexadecane + 0.5% acetate	1% Olive oil
759.79	0.0560	0.0003	0.0004	0.0004
783.80	0.0164	0.0002	0.0034	0.0027
813.85	0.0454	0.0003	0.0007	0.0009

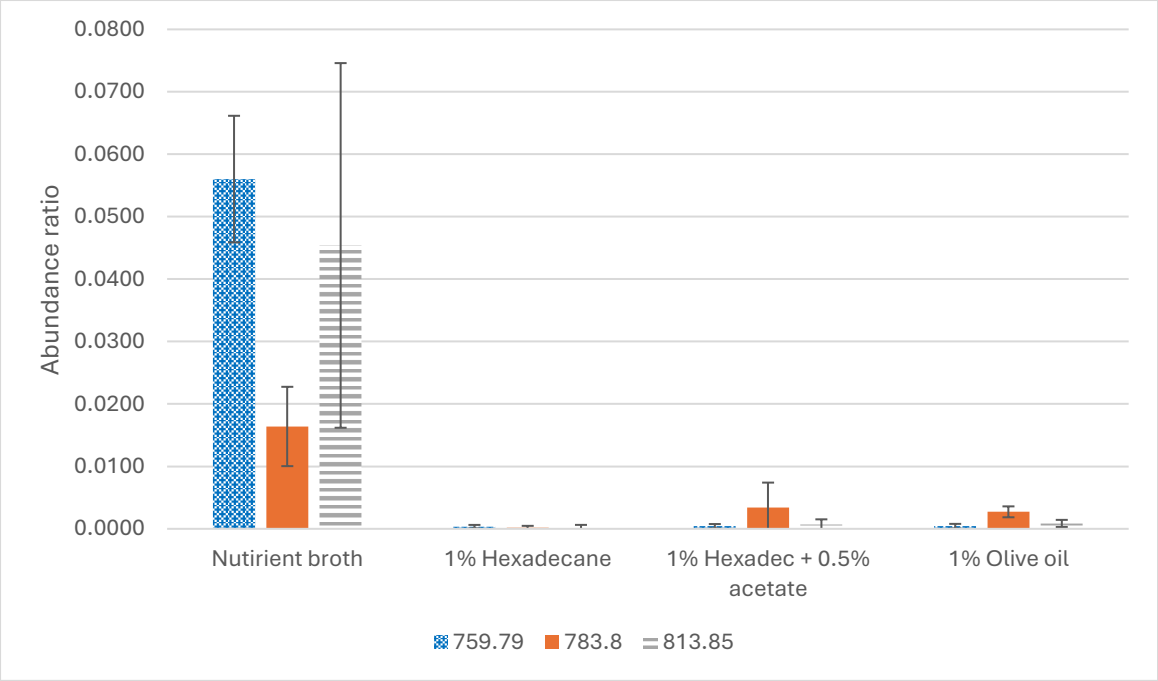

App figure 1: *Representation of average abundance ratios of lipids ions with m/z of 759.79, 783.80 and 813.85 Da, when compared to lipid ion with m/z of 743.69 Da, present at high abundance in all samples. Error bars represent relative abundance of triplicate measurements.*

App table 2: *Average abundance ratios of lipids ions with m/z of 759.76, 783.72 and 813.77 Da, when compared to lipid ion with m/z of 743.69 Da, present at high abundance in all samples.*

Lipid *m/z*	Nutrient broth	1% N-hexadecane	1% N-hexadecane + 0.5% acetate	1% Olive oil
759.76	0.0037	0.0318	0.0096	0.0281
783.72	0.0045	0.0171	0.0106	0.0095
813.77	0.0016	0.0205	0.0085	0.0057

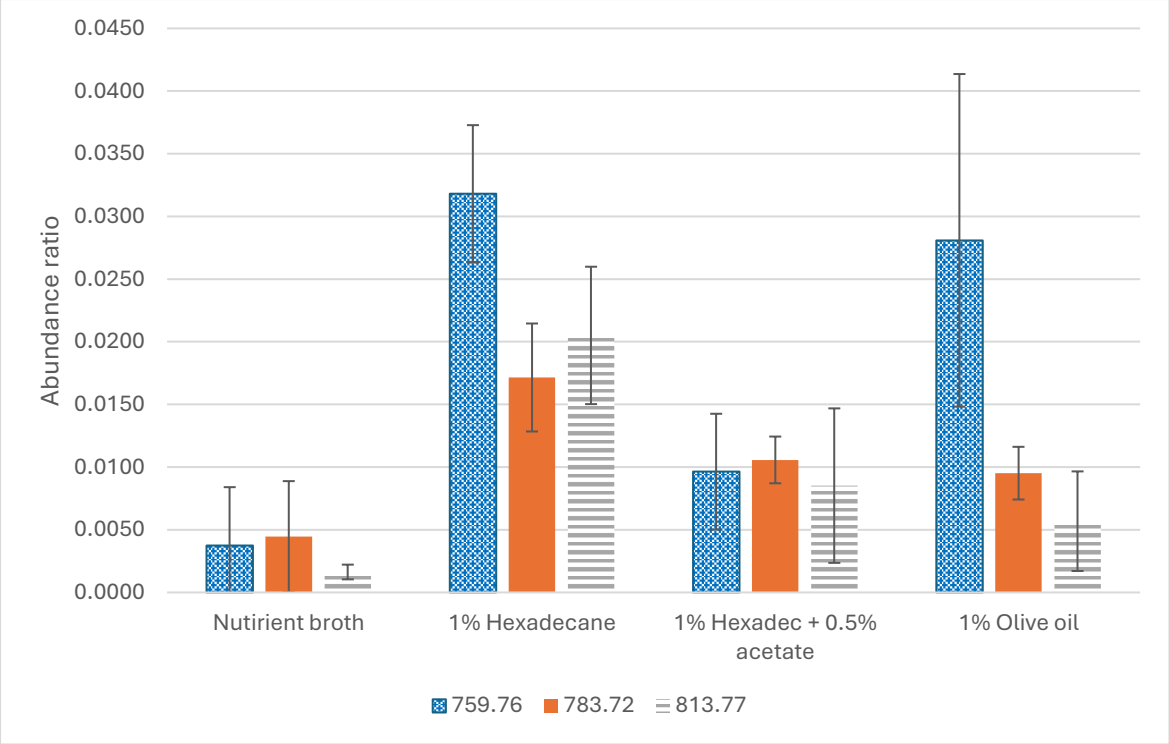

App figure 2: *Representation of average abundance ratios of lipids ions with m/z of 759.76, 783.72 and 813.77 Da, when compared to lipid ion with m/z of 743.69 Da, present at high abundance in all samples. Error bars represent relative abundance of triplicate measurements.*